Assessment of Viral Vaccine N-Glycosylation via Orthogonal Capillary Electrophoresis – Based Methods

By

Stewart Thomas Bigelow

A thesis submitted to the Faculty of Graduate and Postdoctoral Affairs in partial fulfillment of the requirements for the degree of

Master of Science

in

Chemistry

Carleton University
Ottawa, Ontario

Abstract

Despite global vaccination programs, seasonal influenza continues to pose a significant economic burden and strain on healthcare systems worldwide. Annual reformulation of influenza vaccines is required due to the high mutation rates of surface glycoproteins on influenza viruses. Although vaccination is the most effective preventative measure against influenza viruses, reduced vaccine efficacy in recent years has become an increasing concern. Egg-adaptations incurred through the manufacturing process of influenza vaccines result in antigenic mismatches, whereby vaccine strains differ from the wild-type circulating viruses. In 2017, low vaccine efficacy was attributed to altered glycosylation characteristics of the H3N2 vaccine strain whereby an egg-adaptation resulted in the deletion of a single N-glycosylation site. However, even with these implications on immunogenicity, influenza glycosylation is not a well-implemented critical quality attribute and therefore not optimally controlled or regulated during vaccine manufacturing due to assay limitations. Furthermore, current potency evaluation methods are not sensitive enough to capture differences in glycosylation. In this study, capillary zone electrophoresis with laser induced fluorescence (CZE-LIF) and sheathless capillary electrophoresis-mass spectrometry (CESI-MS) methods were developed for the assessment of influenza vaccine N-glycosylation. A magnetic bead-based sample preparation approach was adapted and modified for the fluorescent labeling and CZE-LIF analysis of enzymatically released N-glycans derived from three influenza vaccine monovalent bulk manufacturers. A filter-aided dual hydrazide labeling strategy was developed and elucidation of N-glycan structures was achieved using an untargeted sheathless CESI-MS/MS approach. There is currently a lack of standardized methods for analyzing N-glycosylation; therefore, this study highlights the utility of capillary electrophoresis-based methods for analysis of influenza vaccine N-glycosylation.

Acknowledgements

Firstly, I would like to express my sincere gratitude to my supervisor and defensive partner Dr. Jeff Smith for your guidance and overwhelming support throughout my studies. Whether it was meetings or friendly banter on the blue line, you always reassured me I was on the right track and for that, I am forever grateful. I would also like to thank the other members of the Smith Lab group and CMSC staff. Your questions during group meetings always kept me on my toes, which was key in the development of my scientific communication skills.

Next, I would like to thank my co-supervisor Dr. Simon Sauvé for the inspiration behind the project as well as your continued support through all of the troubleshooting and the experimental development process. To my colleagues in the Separation Science lab for keeping me sane and making sure everything kept running smoothly throughout my studies. I would also like to extend thanks to the remainder of the staff and students in RRD for their expertise and resources that were provided to me throughout the years.

To my parents and family, your unconditional love, never-ending words of encouragement and continued support throughout my life and university career has been paramount in shaping me into the man I am today.

Lastly, I would like to thank my amazing wife and best friend, Shannon. You have truly been my rock throughout this whole process. Your endless patience and understanding, positivity and love really made this possible and I could not have done it without you. I love you with all my heart.

Table of Contents

List of Abbreviations

IFV	Influenza virus
IAV	Influenza A virus
IBV	Influenza B virus
ssRNA	Single-stranded ribonucleic acid
PB1	Polymerase basic protein 1
PB2	Polymerase basic protein 2
PA	Polymerase acidic protein
HA	Hemagglutinin
NA	Neuraminidase
NP	Nucleoprotein
M1	Matrix protein 1
M2	Matrix protein 2
NS1	Non-structural protein 1
NS2	Non-structural protein 2
HA1	Hemagglutinin domain 1 (head)
HA2	Hemagglutinin domain 2 (stalk)
RBS	Receptor-binding site
PAMP	Pathogen-associated molecular pattern
PRR	Pattern recognition receptors
APC	Antigen-presenting cell
DC	Dendritic cell
NKC	Natural killer cell
ADCC	Antibody dependent cellular cytotoxicity
IIV	Inactivated influenza vaccine
BPL	β-propriolactone
FA	Formaldehyde
MDCK	Madin-Darby canine kidney
LAIV	Live-attenuated influenza vaccine
DNA	Deoxyribonucleic acid

mRNA	Messenger RNA
WHO	World Health Organization
GISRS	Global influenza surveillance and response system
SNDS	Supplemental new drug submissions
BRDD	Biologics and Radiopharmaceuticals Drug Directorate
SRID	Single radial immunodiffusion
PTM	Post-translational modification
GlcNAc	N-acetylglucosamine
mAb	Monoclonal antibody
FDA	Food and Drug Administration
IgG	Immunoglobulin G
Fc	Fragment crystallizable
CDC	Complement-dependent cytotoxicity
PK	Pharmacokinetic
PD	Pharmacodynamic
CQA	Critical quality attribute
Neu5Gc	N-glycolylneuraminic acid
ELISA	Enzyme-linked immunosorbent assay
HPLC	High-performance liquid chromatography
MS	Mass spectrometry
SPR	Surface plasmon resonance
RP-HPLC	Reversed-phase high performance liquid chromatography
cHA	Captured HA
ncHA	Non-captured HA
LC-MS/MS	Liquid chromatography tandem mass spectrometry
HILIC	Hydrophilic interaction chromatography
NP-HPLC	Normal-phase high performance liquid chromatography
HPAE-PAD	High-performance anion-exchange chromatography with pulsed amperometric detection
UV	Ultraviolet
2-AA	2-aminobenzoic acid

2-AB	2-aminobenzamide
ESI	Electrospray ionization
CE	Capillary electrophoresis
BGE	Background electrolyte
HVPS	High voltage power supply
μ_{ep}	Electrophoretic mobility
EOF	Electroosmotic flow
μ_{eof}	Electroosmotic mobility
μ_{app}	Apparent mobility
CZE	Capillary zone electrophoresis
CGE	Capillary gel electrophoresis
cIEF	Capillary isoelectric focusing
MEKC	Micellar electrokinetic capillary chromatography
CEC	Capillary electrochromatography
cITP	Capillary isotachophoresis
LOD	Limit of detection
LIF	Laser-induced fluorescence
m/z	Mass-to-charge ratio
MALDI	Matrix-assisted laser desorption ionization
RF	Radio frequency
DC	Direct current
TOF	Time-of-flight
MCP	Microchannel plate detector
QTOF-MS	Quadrupole time-of-flight mass spectrometer
CID	Collision-induced dissociation
NP-40	Nonidet P-40
SDS	Sodium dodecyl sulfate
IAA	Iodoacetamide
DTT	Dithiothreitol
ACN	Acetonitrile
MWCO	Molecular weight cut-off

AH	Acetohydrazide
HCl	Hydrochloric acid
EDC	1-ethyl-3-(3-dimethylaminopropyl) carbodiimide (EDC)
GT	Girard's reagent T
GP	Girard's reagent P
EtOH	Ethanol
PVA	Polyvinyl alcohol
MeOH	Methanol
FWHM	Full width at half maximum
TFA	Trifluoroacetic acid
IPA	Isopropanol
SPRI	Solid-phase reversible interaction
DP	Degree of polymerization
GU	Glucose unit
ƐACA	Ɛ-aminocaproic acid
HPMC	hydroxypropyl methylcellulose
AmOH	Ammonium hydroxide
EV	Extracellular vesicle
hBM-MSCs	Human bone marrow derived mesenchymal stromal cells
FASP	Filter-aided sample preparation
FASS	Field –amplified sample stacking
GISAID	Global Initiative on Sharing Avian Influenza Data
SARS-CoV-2	Severe acute respiratory syndrome coronavirus 2

List of Tables

List of Figures

Chapter 1: Introduction

1.1 Influenza

The emergence and spread of infectious diseases have been continuously occurring throughout human history. Occasionally, some diseases proliferate beyond isolated epidemics and spread between regions rapidly, leading to pandemics. Although communicable diseases would have affected even the earliest civilizations, it was not until the adoption of agrarian practices between 10,000 and 8,000 years ago that epidemics began to occur more frequently.[1-2] Diseases such as small pox, malaria, tuberculosis and influenza first appeared during this period but one in particular continues to be a major threat to public health and holds true pandemic potential – influenza.[3-4]

Influenza is a contagious viral respiratory infection caused by the influenza virus (IFV). IFVs cause seasonal influenza in roughly 10% of the world's population, 3 to 5 million of which are classified as severe cases, resulting in approximately 250,000 to 500,000 deaths annually.[5-6] IFVs cause enormous strain on health care systems worldwide; it is estimated that in the United States the average annual economic burden is $11.2 billion.[7] Despite global vaccination programs, which are currently the most effective preventative measure against IFV infection, seasonal influenza is and remains a major threat to public health.[8]

1.1.1 Influenza Viral Structure & Mechanism

IFVs belong to the family *Orthomyxoviridae* and they are classified as being either: A, B, C or D type viruses.[9] Influenza virus type A (IAV) and B (IBV) account for acute respiratory illness in humans.[10] IAV is also primarily responsible for seasonal epidemics as well as occasional pandemics.[10] IAV and IBV contain eight, negative-sense, single-stranded ribonucleic acid

(ssRNA) gene segments that encode for 10 essential viral proteins – Polymerase basic protein 1 (PB1), polymerase basic protein 2 (PB2), polymerase acidic protein (PA), hemagglutinin (HA), nucleoprotein (NP), neuraminidase (NA), matrix protein 1 (M1), matrix protein 2 (M2), non-structural protein 1 (NS1) and non-structural protein 2 (NS2)(Figure 1.1).[10-12] Upon host entry, commonly through aerosolized droplets, infection is triggered when HA proteins on the surface of the virion mediate binding and subsequent viral entry through receptors on epithelial cells within the respiratory tract.[13] Once entry is initiated and the viruses are trafficked to a late endosomal stage, the transition to a lower pH (~5.5) activates the M2 ion channel allowing the selective uptake of protons into the viral membrane, which triggers a conformational change in the HA proteins allowing fusion between the viral and endosomal membranes.[14-15] The release of the viral genome and subsequent transport to the nucleus enables viral replication using the machinery of the host cell. Newly assembled viral particles then bud from the cell surface at which point NA proteins cleave the sialic acid residues, releasing the viral particles so they can continue infecting neighbouring cells (Figure 1.2).[16]

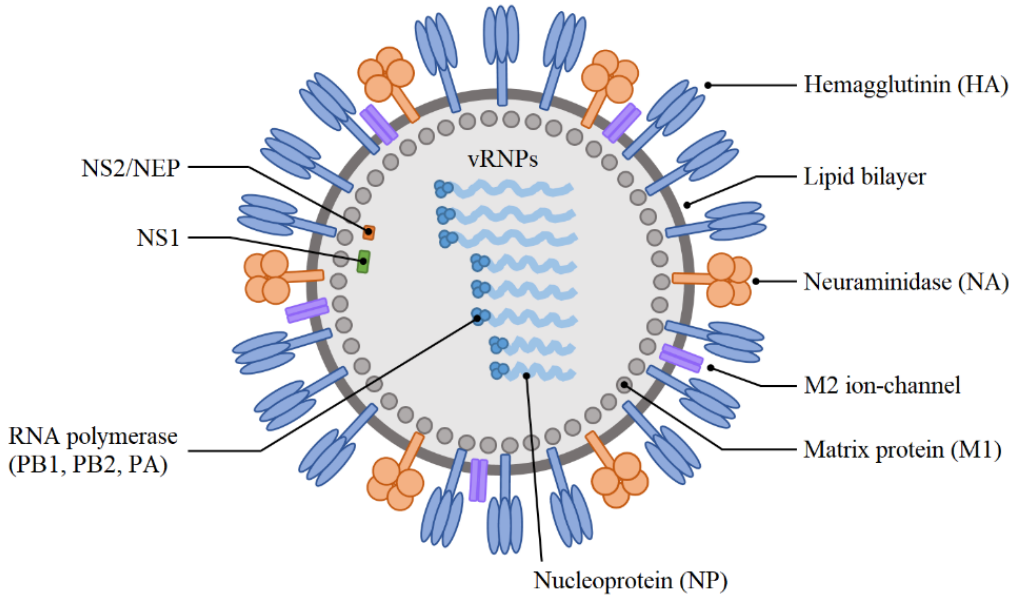

Figure 1.1. Structure of IAV/IBV viral particle

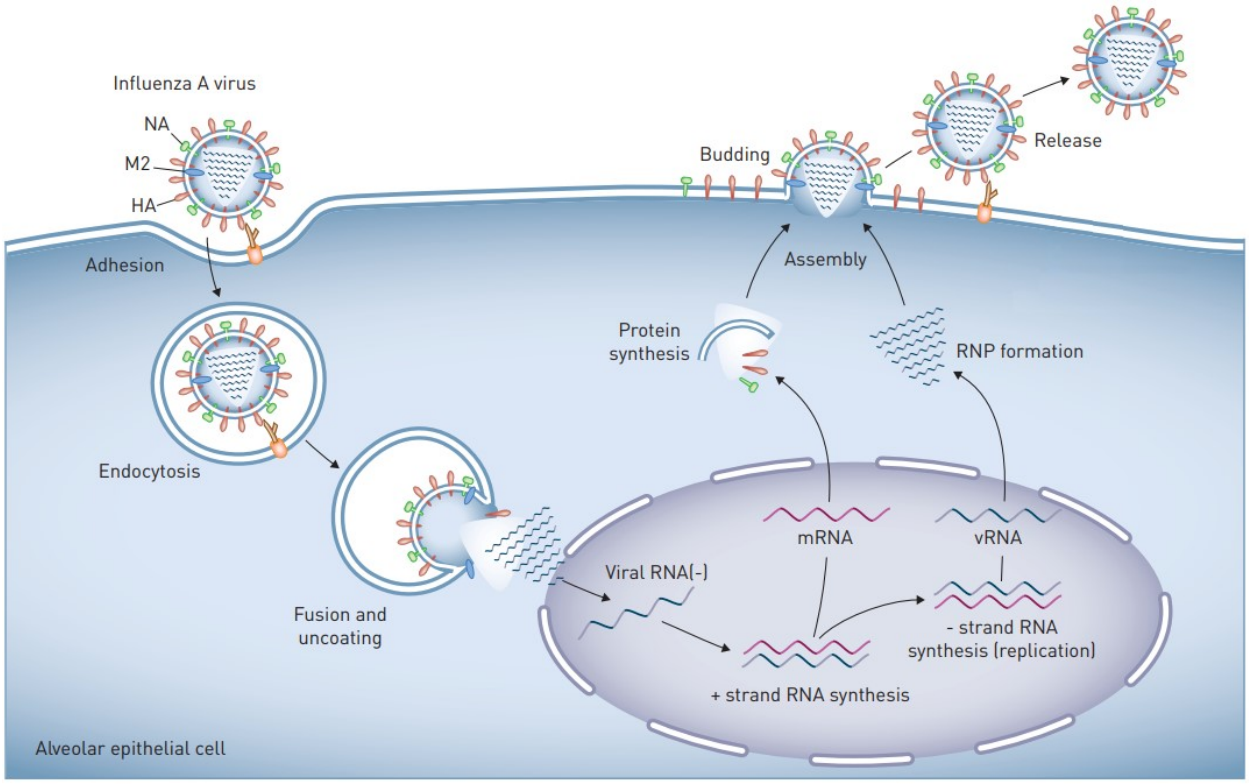

Figure 1.2. Influenza A virus life cycle. Adapted from Herold *et al.* (2015) [17]

1.1.2 Hemagglutinin & Neuraminidase

Two IAV/IBV proteins are particularly critical to viral replication, HA and NA. HA has two primary functions: mediating host cell entry by binding to α2,3- or α2,6-linked N-acetylneuraminic acid (Neu5Ac, sialic acid)-containing receptors on the cell surface (Figure 1.3c), and fusion of the viral and endosomal membranes facilitating the release of the viral genome.[13, 18] HA is a homotrimeric surface glycoprotein where each monomer contains two distinct subunits, the HA1 or head domain, and HA2 domain, typically referred to as the stalk or stem (Figure 1.3).[19] The HA1 domain is located at the distal tip of the molecule and is a highly variable region that contains the receptor-binding site (RBS) and many of the major antigenic sites.[20-21] In contrast, the HA2 domain is a conserved region containing the fusion peptide, which is embedded within

the viral envelope.[21] On the viral surface HA is expressed at a much higher degree than other glycoproteins, representing roughly 80% of the surface glycoproteome

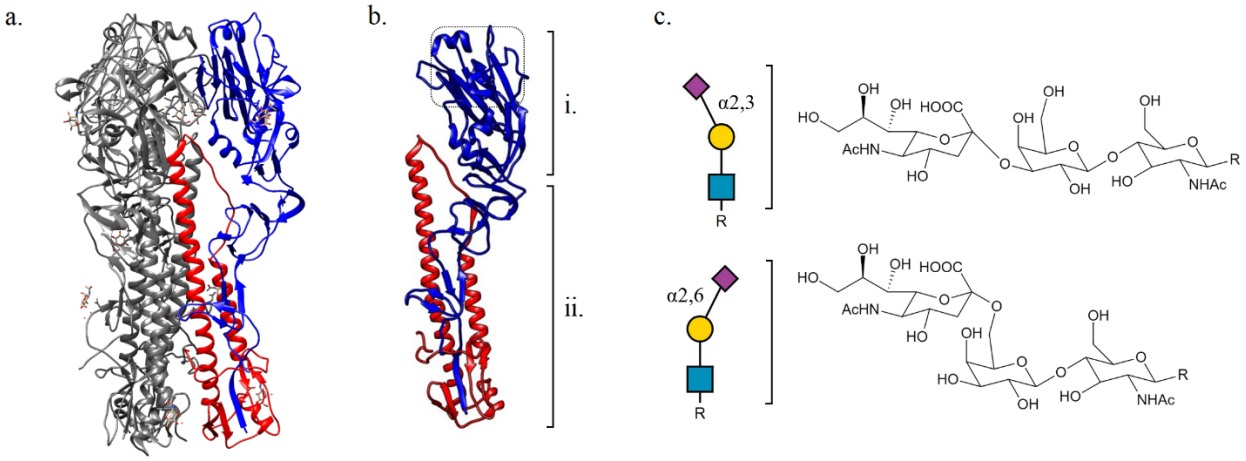

Figure 1.3. Influenza hemagglutinin (HA) structure. (a) Assembled trimer. (b) HA0 monomer. HA1 and HA2 subunits are represented in blue and red, respectively. (i) Globular head (RBS highlighted with dashed line) and (ii) stem region. (c) α2,3- and α2,6-linked N-acetylneuraminic acid HA receptor [Protein Data Bank (PDB) accession number 1RUZ]. Visualized with UCSF Chimera (version 1.10.2).

As a viral sialidase, the primary function of NA involves the enzymatic cleavage of α-ketosidic linked terminal sialic acid residues. Through this cleavage activity, NA prevents non-specific binding to sialylated mucins in the upper respiratory tract, facilitates the release of new budding virus particles and prevents their aggregation at the surface of host cells.[16, 22] NA is assembled as a homotetramer, and is also a glycoprotein accounting for the remaining 20% of the surface glycoproteome of influenza viruses.[23] Each monomer can be broken into four distinct regions: the cytoplasmic tail, the transmembrane region, the stalk, and the globular head (containing the enzyme active site) (Figure 1.4).[16, 24]

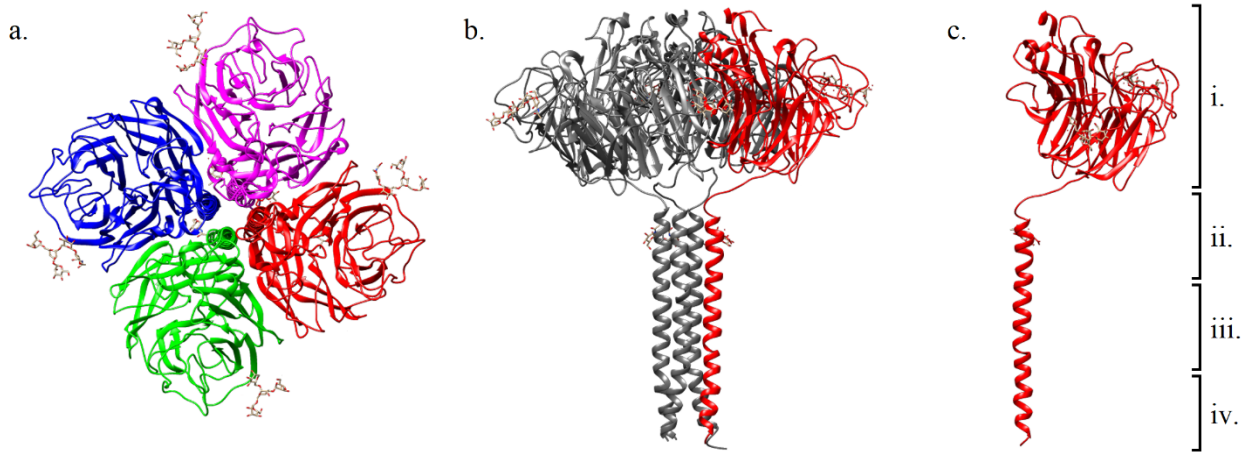

Figure 1.4. Influenza neuraminidase (NA) structure. Assembled tetramer top view (a) and side view (b). NA monomer (c) and (i) globular head, (ii) stalk, (iii) transmembrane and (iv) cytoplasmic tail regions. [PDB accession number 6CRD]. Visualized with UCSF Chimera (version 1.10.2).

IAVs have a broad host range and are categorized into subtypes based on the genetic sequences of HA and NA as well as their spatial and temporal distributions.[25] For example H1N1, where H1 and N1 are subtype 1 of the HA and NA surface proteins, respectively. Currently, there are 18 HA subtypes (H1-H18) and 11 for NA (N1-N11).[26] Contrarily, IBVs have no known natural host and are classified not as subtypes but as belonging to two distinct lineages which diverged in 1983, B/Victoria or B/Yamagata.[27-28] IAVs are mainly responsible for annual epidemics and occasional pandemics and although there are many HA and NA subtype combination possibilities, H1N1 and H3N2 typically circulate in humans.[29]

The immune response to natural influenza infection targets mainly HA, and to a lesser extent NA, due to their proximity to the surface of IFVs. Involvement from the innate and adaptive immune systems help control viral replication. The innate immune system provides the first line of protection against IFV infection and the response is triggered through the recognition of pathogen-associated molecular patterns (PAMPs) by pattern recognition receptors (PRRs) on host

cells.[30] The recognition of PAMPs including viral RNA induces the production of cytokines and antiviral molecules that limit viral replication by inhibiting protein synthesis within infected cells.[31] Additionally, recruitment of alveolar macrophages, antigen-presenting cells (APCs) like dendritic cells (DCs) and natural killer cells (NKCs), aid in preventing the progression of infection.[31-33] Along with the production of catalytic enzymes and pro-inflammatory cytokines, macrophages clear infectious particles through internalization (phagocytosis) followed by lysosomal degradation. DCs detect virions and apoptotic bodies from infected cells but as an APC, one their primary functions is to travel to the lymph nodes to initiate T cell activation, which is particularly important in the adaptive immune response.[34] NKCs recognize IFV infected cells and by binding through their cytotoxicity receptors, triggering cell lysis. Furthermore, the adaptive immune response induces the production of neutralizing antibodies targeted towards HA and NA. Antibodies targeting the major antigenic sites on the globular head of HA have potent neutralizing properties as they inhibit viral attachment and subsequent entry. In addition to their neutralizing properties, HA-specific antibodies promote the recruitment of more phagocytic cells as well as promote antibody dependent cellular cytotoxicity (ADCC) of infected cells.[35] NA specific antibodies also illicit protection by inhibiting NA activity thereby further reducing virus spread.

Due to immune selective pressure and the high mutational rates of influenza viral RNA, minor structural changes to the surface of HA and NA can occur through a process known as antigenic drift.[36] These structural changes usually present themselves as point mutations, in which a single amino acid residue is swapped for another.[37] In general, point mutations generate IFVs that have similar antigenic properties to the parent virus, therefore if there was previous exposure to the parent virus; it is likely that some level of cross-protection is achieved. However, as the virus replicates, these minor changes can accumulate over time and result in antigenically distinct

IFVs that are no longer recognized by humoral and cellular immune responses.[38] This phenomenon explains the requirement for annual vaccination programs. On the contrary, major changes to IFVs via antigenic shift can result in new HA and NA variants through genetic reassortment.[39] This occurs when two different viruses infect the same host (commonly pigs) and combine genetic information, resulting in a novel strain with pandemic potential.

Although, NA-specific antibodies have protective potential, the highly potent antibody response elicited towards the RBS of HA remains critical for the prevention of disease progression. Therefore, influenza vaccines are formulated to contain primarily the HA antigen.

1.1.3 Influenza Vaccines

Shortly after the successful isolation of IAVs in the early 1930's, the development of the first influenza vaccine came to fruition in 1938.[40] Jonas Salk and Thomas Francis developed the first inactivated influenza vaccine using embryonated chicken eggs that was approved for use in 1945.[41] Since then, a greater understanding of the properties of the influenza virus and its transmission have aided in the development of modern influenza vaccines. Current influenza vaccines primarily focus on the elicitation of an immune response towards HA and fall within one of three categories: inactivated, live attenuated and recombinant vaccines. Table 1.1 outlines the current licenced influenza vaccines on the Canadian market for the 2021-2022 season.

Table 1.1. Licenced IFV vaccines approved for Canadian market for the 2021-2022 Season.

Product Name	Vaccine Type	Formulation	Administration	Expression System	Age Recommendation
FluLaval Tetra	IIV	Standard-dose Quadrivalent	Intramuscular	Egg	≥ 6 months
Fluzone® Quadrivalent	IIV	Standard-dose Quadrivalent	Intramuscular	Egg	≥ 6 months
Flucelvax® Quad	IIV	Standard-dose Quadrivalent	Intramuscular	Cell	≥ 2 years
FluMist® Quadrivalent	LAIV	Standard-dose Quadrivalent	Intranasal	Egg	2-59 years
Afluria® Tetra	IIV	Standard-dose Quadrivalent	Intramuscular	Egg	≥ 5 years
Influvac® Tetra	IIV	Standard-dose Quadrivalent	Intramuscular or Subcutaneous	Egg	≥ 5 years
Fluzone® HD-Quadrivalent	IIV	High-dose Quadrivalent	Intramuscular	Egg	≥ 65 years
Fluad	A-IIV	Adjuvanted Trivalent	Intramuscular	Egg	≥ 65 years

Inactivated influenza vaccines (IIVs) contain whole-virus particles or parts of the virus (i.e. HA) that have been inactivated by chemical means either with β-propriolactone (BPL) or formaldehyde (FA).[42] Depending on the expression system, either egg-based or mammalian cell-based, the main component in IIVs (HA) is prepared by first propagating the seed virus in fertilized chicken eggs or Madin Darby Canine Kidney (MDCK) cells, respectively. After several days and sufficient replication has occurred (2-3 days) the virus is harvested, and chemically inactivated with FA or BPL followed by an initial clarification step (centrifugation or filtration) to remove large cellular debris.[43] The inactivated bulk is the further purified using sucrose gradient centrifugation in order to remove endogenous egg proteins and debris while isolating the inactivated virus particles. Although some IIVs are still manufactured to contain inactivated whole-viruses the majority of licensed IIVs are traditionally in the form of “split” or “subunit” vaccines and their classification is based on the purification and enrichment levels of the HA antigen. For split IIVs, the sucrose purified inactivated virus particles are disrupted or split by the addition of detergents (deoxycholate or Triton X-100) or diethyl ether, the former being the

common method of choice.[44] After disruption, purification steps to remove residual detergent are performed before a final sterile filtration step. For subunit IIVs, after disruption additional levels of purification and enrichment of the HA protein is performed, obtaining a much higher level of purity than its split IIV counterpart.

Live attenuated influenza vaccines (LAIVs) contain live viruses that have been attenuated or "weakened" to prevent the onset of infection. In this process, the seed strains are created through genetic reassortment to contain mutations that result in cold-adapted, temperature sensitive viruses.[45] Unlike, IIVs that are administered intramuscularly, LAIVs are administered via the intranasal route. Therefore, due to the temperature sensitive nature of the viruses in the vaccine, viral replication is restricted to the nasal cavity and cannot penetrate deeper to the lower respiratory tract where body temperatures are elevated. Although effective, there is infection risks associated with LAIVs, especially in immunocompromised individuals.[46]

Lastly, recombinant influenza vaccines use recombinant DNA technology to produce highly pure formulations of the HA protein. Currently there is only one approved recombinant influenza vaccine, FluBlok®, which uses a baculovirus expression vector system. In this system, insect cells (e.g. Sf21) are infected with a baculovirus, containing plasmid DNA that encodes for a protein of interest, in this case HA. The infected insect cells are cultured in a bioreactor, followed by mRNA transcription and subsequent protein translation. The cells are then separated from the media by centrifugation and the supernatant containing the overexpressed protein of interest is purified using several techniques such as filtration and column chromatography before final formulation.

Currently, influenza vaccines are manufactured as either trivalent or quadrivalent formulations, containing HA from three or four circulating influenza strains, respectively. Most

are of the quadrivalent type, containing two IAV strains (H1N1 & H3N2) and two IBV strains (one from each lineage; Yamagata & Victoria). However, due to the evolution of influenza viruses and the mutation rates of the surface glycoproteins, vaccines against influenza require annual updates and reformulation so that the vaccine strains are in agreement with the wild-type circulating virus.

1.1.4 IFV Regulation & Potency Evaluation

Reformulation of influenza vaccines is required annually to adapt to circulating strains. This process is extensive, requiring on average 6 months from the World Health Organization (WHO) recommendation and strain selection to vaccine release and distribution. The vaccine production timeline is summarized below in Table 1.2. For the Northern hemisphere, the process begins in February at the annual WHO information meeting. Along with members of the WHO Global Influenza Surveillance and Response System (GISRS), there is involvement from several other key stakeholders including representatives from regulatory agencies (i.e. Health Canada) and vaccine manufacturers.[47]

Table 1.2. IFV vaccine production timeline from WHO recommendation and strain selection to production and release.

Northern Hemisphere Southern Hemisphere	JAN JUL	FEB AUG	MAR SEP	APR OCT	MAY NOV	JUN DEC	JUL JAN	AUG FEB	SEP MAR	OCT APR	NOV MAY	DEC JUN
Surveillance												
WHO Recommendation/Strain Selection												
Reassortant Production												
Seed Production												
SRID Reagent Preparation												
Monovalent Bulk Production												
Formulate/Fill/Package												
Release/Distribution/Administration												

Based on global surveillance, viral strains to be included in vaccine formulations for that influenza season are selected. In Canada, vaccine manufacturers must file strain changes as Supplemental New Drug Submissions (SNDS) with the Biologics and Radiopharmaceuticals Drug Directorate (BRDD). Sponsors must provide quality data including qualification of reference antiserum reports, drug product accelerated stability data and real-time stability data for LAIV drug products.[48] Additionally, updated drug product labeling must also be submitted for review and approval. After submission, the updated vaccines are subjected to BRDD's lot release program. Vaccine manufacturers must provide samples from each lot intended for release in Canada. The BRDD lot release program performs consistency testing on each lot, and if requirements are met, a release letter approving sale of that specific lot on the Canadian market is issued.

Consistency testing and potency evaluation of IIVs involves numerous assays including the measurement of it's HA antigen content. This is accomplished using the single radial immunodiffusion (SRID) assay, which is the standard internationally accepted method for potency evaluation IIVs developed in the 1970's.[49] The SRID assay requires two primary reagents, (1) strain specific polyclonal antibodies and (2) reference antigens of known potency. The basic principle of the assay involves adding serial dilutions of vaccine sample to wells in an agarose gel slab containing a known concentration of antibody specific to the strain being assayed. The HA antigen in the vaccine sample then diffuses with the antibody and forms a precipitant ring, in which the diameter of the formed ring is directly proportional to the amount of HA in the sample (Figure 1.5).[50]

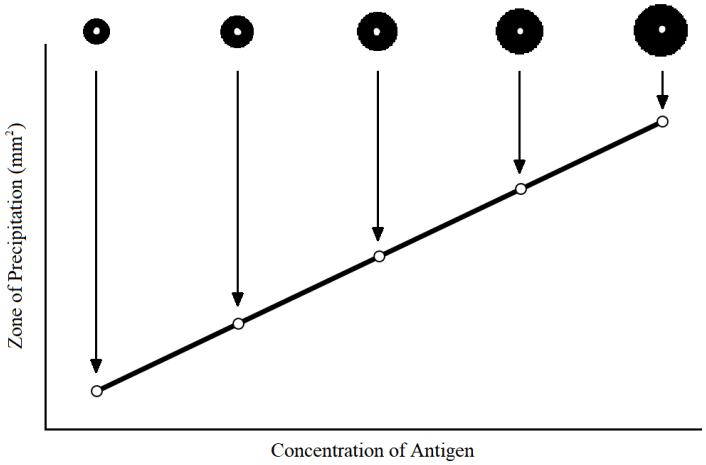

Figure 1.5. Principle of single radial immunodiffusion (SRID) assay used for IFV vaccine potency evaluation. The diameter of precipitant ring is directly proportional to [HA].

The SRID assay is widely accepted as the "gold standard" method for potency evaluation of IIVs and has some advantages that merit this classification. It is simple with respect to technical performance, robust and reproducible.[51] Additionally, it detects the HA antigen relevant from an immunological standpoint, that is HA in its native conformation capable of eliciting a neutralizing antibody response.[50, 52-54] Despite these advantages, there are some major drawbacks with SRID that need to be taken into consideration. The requirement of strain-specific and calibrated reference materials is a major limitation to the rapid regulation of vaccines as it can take up to 4 months before reagents become available to manufacturers and regulators. Additionally, the assay has a limited dynamic range and is not suitable for the potency evaluation of HA in novel vaccines, in which the HA content is derived recombinantly from plant or insect cell expression systems.[50-51] Furthermore, HA being a glycoprotein, the SRID assay is not sensitive enough to capture differences in glycosylation.[55]

1.2 Glycosylation

Glycosylation is the most common, yet complex post-translational modification (PTM) that occurs during protein biosynthesis via the ER-Golgi pathway.[56] It involves the covalent

attachment of oligosaccharide moieties, or glycans, to specific amino acid residues on the protein backbone. The two most common and extensively researched types of glycosylation are N- and O-linked glycosylation. O-linked glycans are attached to the protein backbone at serine or threonine residues. Whereas N-linked glycans are attached to asparagine residues with the consensus sequence asparagine-*X*-serine/threonine (N-*X*-S/T), where *X* can be any amino acid except proline. Although the biological relevance of O-glycosylation is undeniable, the remainder of this thesis will primarily focus on N-glycosylation.

N-glycans contain a conversed chitobiose core composed of two N-acetylglucosamine (GlcNAc) residues and three mannose residues.[57] Based on their structure extending from this conserved core, N-glycans are classified into three structural categories (Figure 1.6). High-mannose N-glycans, in which the glycan is composed primarily of mannose residues. Complex N-glycans, which are bi-, tri-, or tetra-antennary branched structures containing N-acetylglucosamine, galactose, and N-acetylneuraminic acid residues. Or hybrid N-glycans, which contain both high-mannose and complex branching.

Unlike protein biosynthesis, N-glycosylation is a non-template driven process that involves many players including glycolipid precursors, glycosyltransferases and glycosidases.[58] Being non-template driven, glycosylation site-occupancy (macroheterogeneity), monosaccharide composition, glycosidic linkage configurations and branching possibilities result in a high level of N-glycan diversity (microheterogeneity). Additionally, N-glycan biosynthesis is expression system specific, therefore depending on the organism, involvement of key processing enzymes differ giving rise to further structural diversity (Figure 1.7).

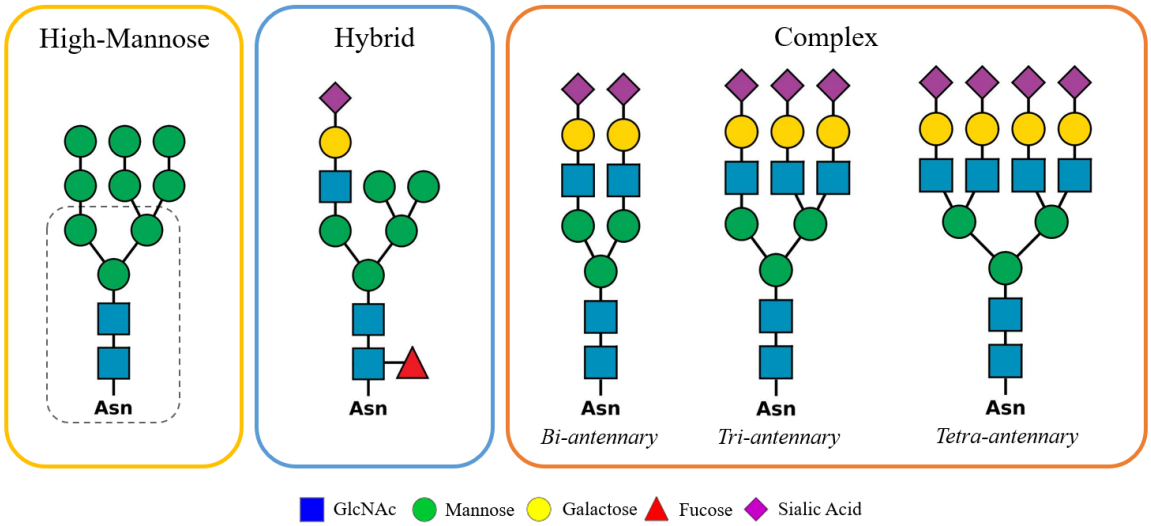

Figure 1.6. High mannose, hybrid and complex N-glycan subtypes. Conserved chitobiose core highlighted with a dashed box.

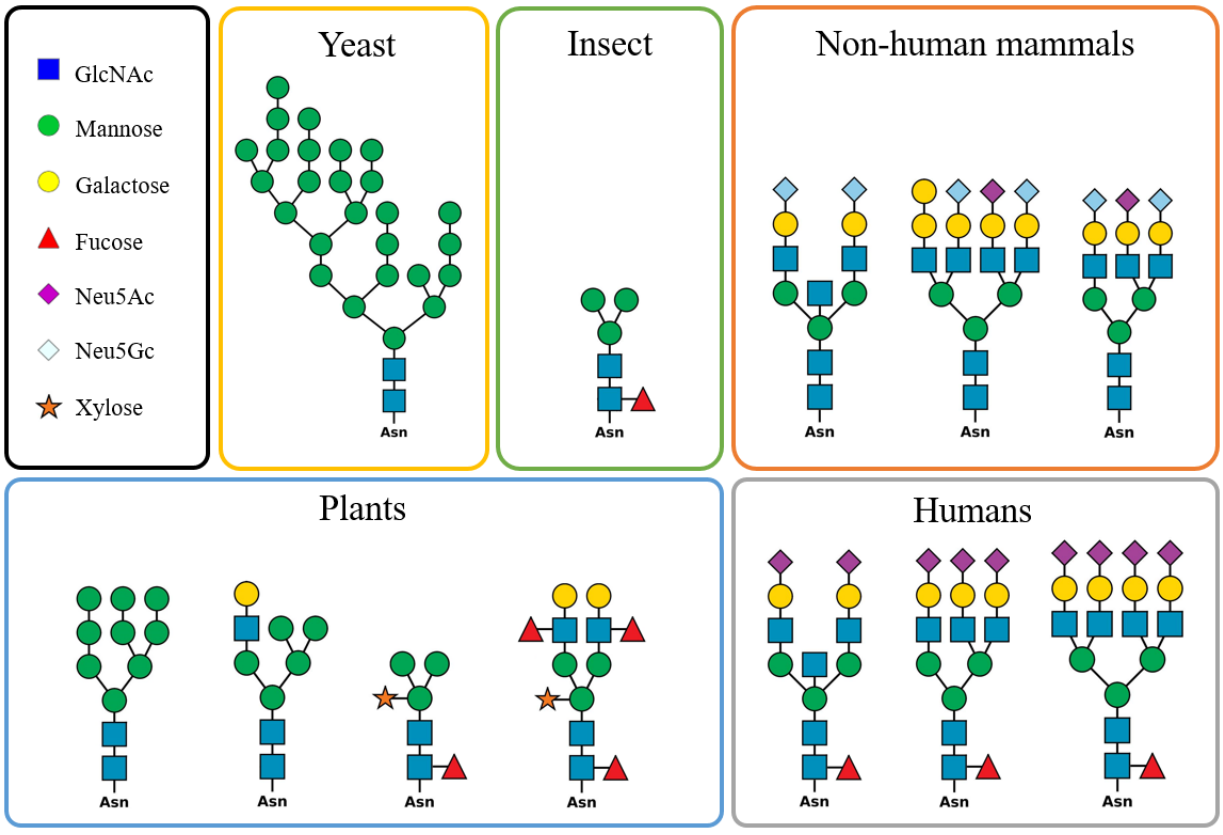

Figure 1.7. Typical N-glycan structures expressed by different organisms.

1.2.2 Glycosylation: Biological Context

N-glycans are involved in many biological processes, but in general, their specific roles can be broken down into four main categories. Structural and modulatory, intrinsic recognition, extrinsic recognition and molecular mimicry.[59-60]

Biologics including monoclonal antibodies (mAbs) are a class of therapeutic glycoproteins in which N-glycan involvement is critical for the proper function of these large biomolecules. Their therapeutic potential has been consistently demonstrated since the first mAb, OKT-3, an anti-rejection treatment given to patients after kidney transplantation, was approved by the Food and Drug Administration (FDA) in 1986.[61-62] Since then, the development of mAbs to treat various human aliments including cancers has been on a steady increase and is now one of the largest class of biotherapuetics with over 100 approved for use in the United States.

N-glycans play a major role in the proper folding of newly synthesized proteins, and subsequently help maintain biologically active conformation. They also have an effect on various physiochemical properties including thermostability and solubility. The majority of approved mAbs are Immunoglobulin G-type (IgG-type) antibodies. These mAbs contain a conserved N-glycosylation site at the asparagine-297 position on the fragment crystallizable (Fc) region of the heavy chain (Figure 1.8).[63] Therefore, in terms of glycosylation site occupancy, diversity on a macroheterogenity level is limited. However, the composition of the N-glycans attached to these sites (microheterogeneity) can have major implications on therapeutic efficacy.[63-65] For example, N-glycosylation on the Fc region regulates effector functions including antibody-dependent cellular cytotoxicity (ADCC) and complement-dependent cytotoxicity (CDC).[57] Additionally, glycan microheterogeneity can also affect immunogenicity as well as the pharmacokinetic (PK) and pharmacodynamic (PD) profiles of these therapeutic molecules.

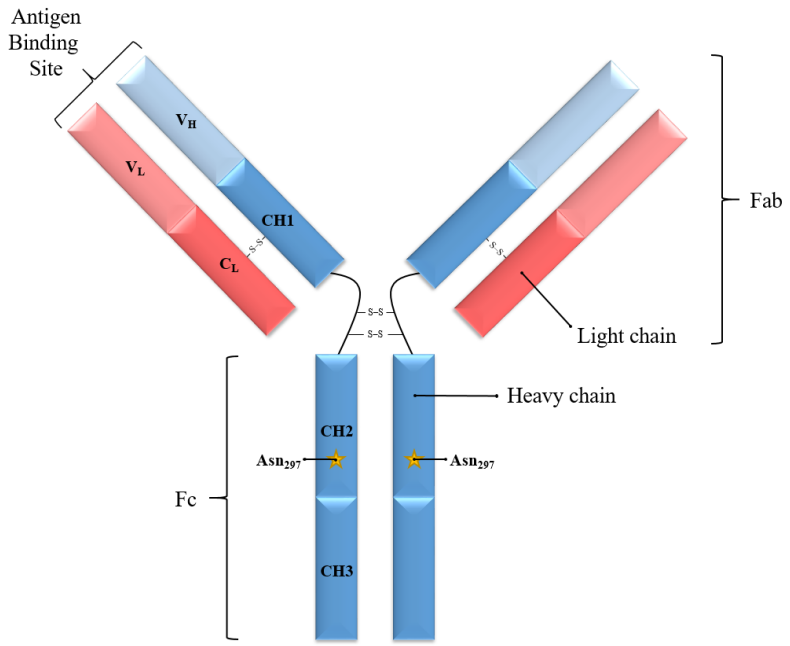

Figure 1.8. Structure of an Immunoglobulin G-Type (IgG) monoclonal antibody (mAb).

1.2.3 Glycosylation: Regulatory Implications

Unlike Small-molecule drugs, which are relatively simple (< 1 kDa), highly reproducible, chemically synthesized compounds, mAbs are large (≥ 150 kDa), extremely complex molecules requiring extensive production and purification processes. In process variables including temperature, culture pH, media supplementation ($MnCl_2$ & NH_4Cl) and O_2 concentration impact the resultant molecules N-glycan profile.[66] Therefore, upon submission for market approval, manufacturers must provide detailed information outlining the products critical quality attributes (CQAs).

Along with other PTMs including deamidation, oxidation and isomerization, N-glycosylation is one of the main CQAs of therapeutic mAbs. This is because core fucosylation, terminal galactosylation and sialyation, as well as degree of branching of Fc expressed N-glycans can impact product quality and efficacy. For example, the presence of core fucosylation decreases ADCC activity due to decreased binding affinity to FcγR receptors.[67] The degree of terminal

galactosylation can increase CDC activity whereas an increase in terminal sialylation of Fc N-glycans has been shown to affect ADCC activity and serum half-life.[63, 68-70] In addition to the reported implications on quality and efficacy, the safety of these drugs is also influenced by the structural characteristics of their Fc glycans. Adverse reactions through the induction of anti-drug antibodies have been linked to the presence of N-glycolylneuraminic acid (Neu5Gc) and α1,3-bound galactose residues.[71-72]

The above examples have major regulatory implications especially when processes are changed to meet market demands or if patent expiration requires approval of non-innovator drugs such as biosimilars. The main take away is that variation of a biologics glycosylation profile can impact efficacy. However, not all biologic products have the same level of quality control processes as mAbs when it comes to monitoring glycosylation.

1.2.4 IFV Glycosylation

As outlined in section 1.1.2, the surface glycoproteins of influenza viruses accumulate point mutations over time, in addition to structural changes these mutations can result in the addition or deletion of N-glycosylation sites, effectively altering their overall glycosylation profile. Like with most glycoproteins including mAbs, glycosylation of IFV glycoproteins is important for their proper folding and biological activity. In particular, studies have demonstrated that conserved glycosylation sites located on the stem region of HA is crucial for ensuring proper folding and pH stability.[73-74] IFV glycosylation can also dictate a variety of disease related properties including host-specificity, antigenicity, virulence and pathogenicity. For example, alteration of glycosylation characteristics near HA's RBS can affect receptor binding affinity as well as receptor-specificity, which could influence the zoonotic potential of IFVs.[75-76] Proteolytic cleavage of HA0 into its HA1 and HA2 subunits is affected by glycosylation, which has implications on IFV virulence and

pathogenicity.[77] The significance of IFV glycosylation is clearly evident, but their impact on immunogenicity and viral fitness are of particular interest. For instance, the location, occupancy, and size of N-glycans can enhance viral fitness by sterically blocking key antigenic sites targeted by neutralizing antibodies of the humoral immune response.[78-80]

1.2.5 Influenza Vaccine Glycosylation: Implications on Safety and Efficacy

Seasonal influenza vaccines on average exhibit a 60% effectiveness.[81] However in recent years, vaccine effectiveness has been as low as 43% and in some instances has been linked to glycosylation characteristics of the egg-adapted antigens present in IIVs.[82-84] In 2017, Zost *et al.* demonstrated that an egg-adaptive mutation of the H3N2 strain in the 2016-2017 season IIVs resulted in the deletion of a glycosylation site at antigenic site B.[57] Therefore, the neutralizing antibody responses elicited through vaccination were not protective against the wild-type circulating H3N2 virus, which retained this glycosylation site. However, is observed that higher neutralizing antibody titres towards the wild-type circulating H3N2 viruses were present in individuals primarily vaccinated with FluBlok, wherein the HA content is produced through recombinant DNA technology using a baculovirus-insect cell expression system. Interestingly, this recombinant-HA retained the glycosylation site at the antigenic site B similar to the wild-type circulating H3N2 virus. Their data suggests that glycosylation-site occupancy near major antigenic sites of HA may alter the elicitation of protective antibody responses, however further investigation is required. In addition to the cost effective and robust nature of insect cell expression systems the ability to avoid adaptive-mutations during vaccine production is a particularly attractive trait.[85]

Not only is site occupancy important but some studies suggest that the subtype, size and complexity of the N-glycans on influenza vaccine antigens can impact protective antibody

responses induced through vaccination. Several studies have demonstrated that altering N-glycosylation profiles with glycan processing inhibitors (kifunensine) and endo-glycosidases (Endo-H) prior to immunization can offer better cross-strain protection.[86-88] For example, Chen *et al.* (2014) evaluated that cross-strain protection capabilities of several HA antigen vaccine candidates with varying glycosylation profiles (fully-, mono-, and de-glycosylated).[86] The mono-glycosylated HA (A/Brisbane/59/2007) vaccine candidate antigens were produced and treated with Endoglycosidase H (EndoH), an enzyme that cleaves N-glycans between the two core-GlcNAc residues leaving behind a single GlcNAc covalently attached to each glycosylation site. Whereas the de-glycosylated and fully-glycosylated vaccine candidates were treated with PNGase F to remove N-glycans from all sites, and untreated, respectively. Interestingly, mice immunized with the mono-glycosylated candidate vaccine antigen produced neutralizing antibodies with better cross-strain protection when subjected to lethal viral challenges (A/California/07/2009, A/Wisconsin/1933, and A/Puerto Rico/8/1934). The cross-strain protection was also tested in ferrets and similar responses were observed further suggesting and that N-glycan size on HA antigens may impact immune responses elicited through vaccination. There is additional evidence suggesting that the complexity of N-glycans on recombinant HA vaccine antigens can impact the immune responses elicited through vaccination. de Vries *et al.* (2012) demonstrated that immunogenic potential of recombinant HA had a dependency on N-glycan complexity.[89] In this study, five recombinant H5 proteins were produced using several expression systems (mammalian and insect) and each carried distinct N-glycan signatures with varying degrees of complexity by controlling specific N-glycan processing enzymes or using endoglycosidases (i.e. EndoH). Their results demonstrated that recombinant HA carrying terminal mannose residues induced lower HA

inhibition titres in comparison to complex and mono-glycosylated (EndoH treated) counterparts. Other research groups have reported similar observations.[90-91]

Therefore, with the current implications on vaccine efficacy (i.e. deleterious egg-adaptive mutations), and the increasing evidence that N-glycan size and complexity impact immunogenicity, N-glycosylation of influenzas antigenic surface glycoproteins is something to be carefully considered during the production of these vaccines. Similar to mAbs, influenza glycosylation should be considered a CQA that is regulated and controlled.

1.2.6 Alternative Influenza Vaccine Potency Evaluation Strategies

Due to major limitations of the current potency evaluation method (Section 1.1.4), alternative approaches are consistently in development to aid in the regulation of influenza vaccines. Biochemical methods including enzyme-linked immunosorbent assays (ELISA) as well as chip-based immunoassay platforms have been developed and show advantages over the traditional SRID.[92-94] Analytical techniques including high-performance liquid chromatography (HPLC), mass spectrometry (MS) and surface plasmon resonance (SPR) have shown promising results with respect to their utility and quantitative capacity.

Physiochemical methods like HPLC for quantification of HA content in influenza vaccines offer some unique advantages over traditional biochemical assays. Reversed-phase HPLC (RP-HPLC) methods are robust and offer a high level of precision and selectively, enabling the separation, identification, and quantification of HA content in trivalent and quadrivalent vaccine formulations (Figure 1.10a).[95-96] However unlike the SRID assay, which can quantify conformationally active forms of HA, RP-HPLC alone lacks this capacity. To address this, Lorbetskie *et al.* (2019) combined a quantitative RP-HPLC assay with an initial conformationally selective receptor-binding step.[52] This was accomplished by coupling a synthetic biotinylated

sialic acid receptor to streptavidin coated magnetic beads (Figure 1.9). When added to a vaccine sample, the HA material capable of binding to its natural receptor (sialic acid), assumed to be in its well-folded conformationally active state, will be selectively captured (cHA) and separated from non-captured HA material (ncHA). The fraction containing ncHA can be separated using a magnet and removed, and the cHA content can be released from the receptor by the addition of a zwitterionic detergent (Zwittergent®). Both cHA and ncHA fractions can then be analyzed separately via quantitative RP-HPLC and compared to a maximal signal control.

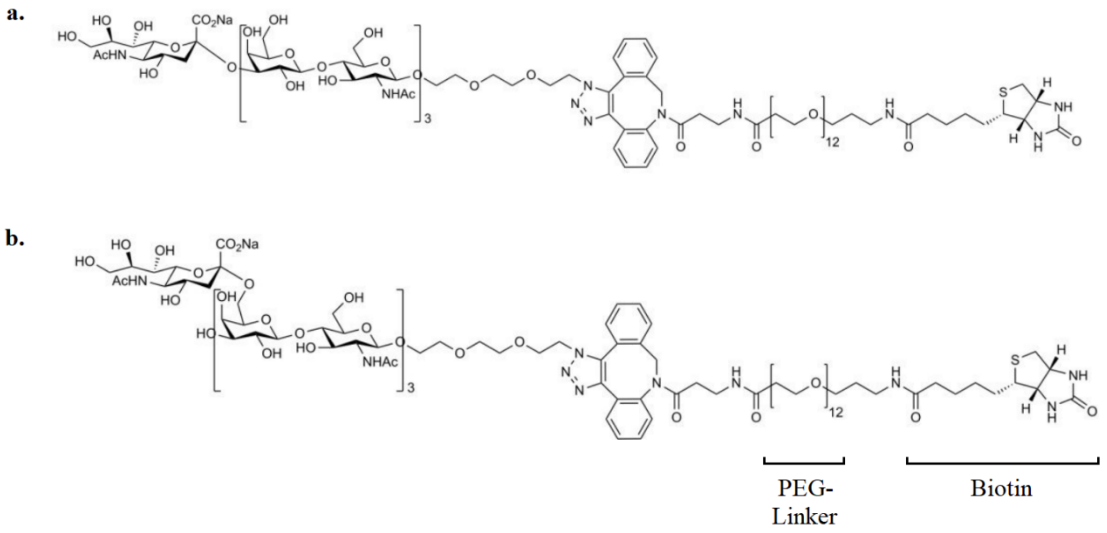

Figure 1.9. Biotinylated synthetic sialic acid receptor used for the selective capture of well folded HA in vaccine formulations. (a) α2,3-linked NeuAc avian receptor (b) α2,6-linked NeuAc human receptor. Adapted from Lorbetskie *et al.* (2019).[52]

This combined assay was used to evaluate the receptor binding capacity of H1N1 (A/California/07/2009) HA monovalent vaccine bulks from two manufacturers (Figure 1.10b,c). Interestingly, it was determined that the material present in manufacturer I's monovalent bulk was almost entirely in the cHA fraction, whereas the opposite was observed for manufacturer II, and only material in the ncHA fraction was detected. As a means of comparison, the potency of each sample was evaluated via SRID and the results suggested that SRID could not discriminate

between "structurally well folded" HA.[52] The differences in receptor binding affinity could be a result of manufacturer induced structural modifications, mutations in close proximity to the RBS, or increased glycosylation. Therefore, this combined assay may prove to be sensitive enough to capture differences in the degree of HA glycosylation within vaccine formulations, therefore meriting further investigation.

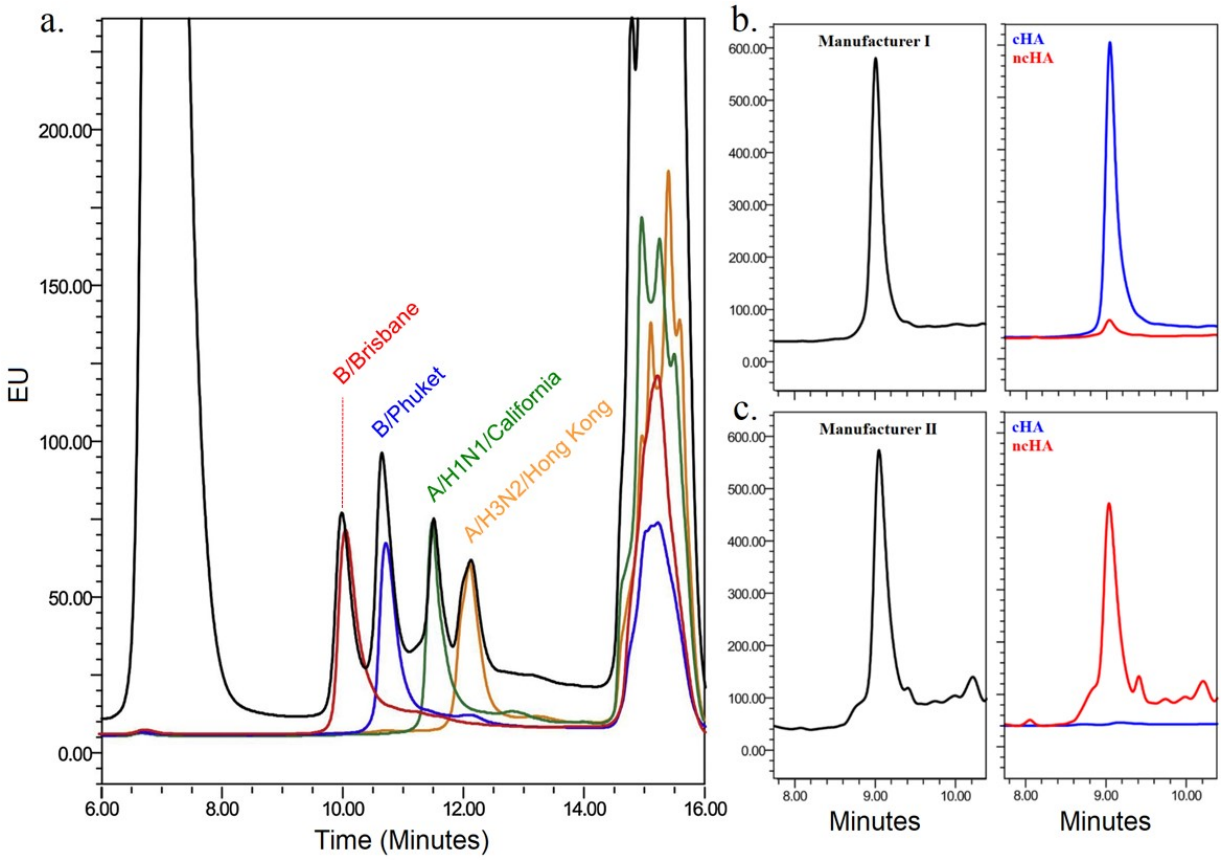

Figure 1.10. Representative RP-HPLC chromatogram of a commercial quadrivalent influenza vaccine (2016-2017 season) overlaid with respective reference antigens (a). RP-HPLC chromatograms of an H1N1 (A/California/07/2009) monovalent vaccine bulk after selective capture with synthetic sialic receptor (α2,6-linked NeuAc) from manufacturer I (b) and manufacturer II (c). Black traces represent maximal HA signal in a control sample. Blue and red traces represent cHA and ncHA, respectively. (b) Manufacturer I contained material entirely in the cHA fraction whereas, (c) Manufacturer II contained material entirely in the ncHA fraction. Adapted from Lorbetskie *et al.* (2017, 2019).[52, 96]

1.2.7 N-Glycosylation Analysis

Many techniques can be used for the analysis of protein N-glycosylation. Lectin microarrays which use immobilized lectins to bind glycans displaying specific structural characteristics may be used in conjunction with fluorescence detection.[97] Enzymatic treatments with various exoglycosidases may be employed in which glycans are sequentially degraded from their terminal ends in order to elucidate underlying structures. These techniques are useful; however, they lack the capacity for in-depth structural characterization and therefore physiochemical-based methods appear to a greater extent in the literature when it comes to the analysis of N-glycosylation.

The analysis of protein N-glycosylation by physiochemical methods is typically performed on either the macroheterogeneity level to determine site occupancy related information, or microheterogeneity level for structural determination. Site-specific glycosylation analysis is accomplished by enzymatically digesting glycoproteins into individual glycopeptide fragments with proteases like trypsin. The glycopeptides are analyzed as is or can be further purified (enriched) before analysis, which is commonly performed by MS-based methods (discussed further in Section 1.4.5). Glycopeptide analysis presents many analytical challenges, therefore to simplify analysis N-glycans can be cleaved from the protein backbone enzymatically using peptide-N4-(N-acetyl-beta-glucosaminyl) asparagine amidase (PNGase F). PNGase F has a broad specificity catalyzing the cleavage of N-glycans between the innermost GlcNAc and asparagine residue (expect if the core GlcNAc contains an α1,3-linked fucose residue) (Figure 1.11).

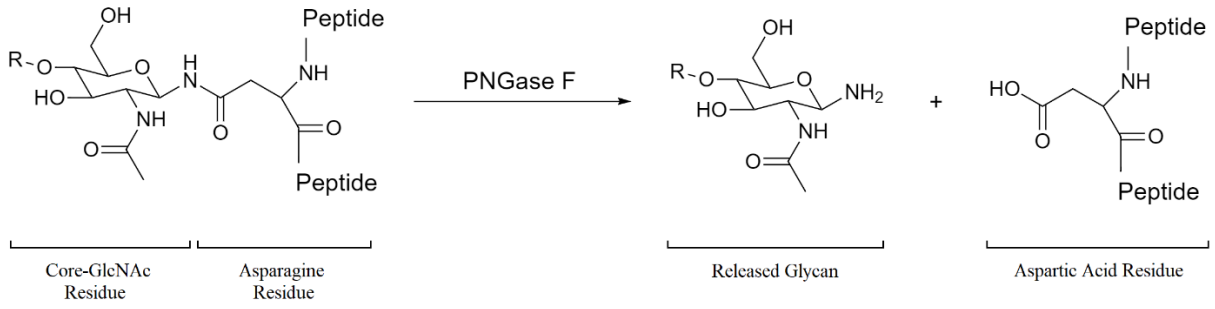

Figure 1.11. PNGase F N-glycan cleavage mechanism resulting in a released N-glycan and aspartic acid residue

Chromatographic methods including hydrophilic interaction chromatography (HILIC), normal-phase HPLC (NP-HPLC), and high-performance anion-exchange chromatography with pulsed amperometric detection (HPAEC-PAD) are all commonly used for profiling enzymatically released N-glycans.[98-99] The latter is able to detect N-glycans in their native state due to their electrochemical activity.[100] However, HILIC and NP-HPLC are not suitable for the analysis of released native N-glycans because these techniques are often coupled with optical detectors (UV), and N-glycans lack a chromophore or fluorophore required for detection. Therefore, derivatization of N-glycans is required prior to analysis when using optical detection methods. Enzymatic release of N-glycans (i.e. via PNGase F) yields a glycosylamine product that is non-enzymatically hydrolyzed into a reducing sugar (Figure 1.12). Various labeling strategies exist for the derivatization of the resulting glycosylamines, however, due to their tendency to spontaneously hydrolyze into their reducing sugar counterparts, derivatization of N-glycans reducing-end aldehyde moiety is most commonly performed.[101] This is accomplished through reductive amination whereby primary amine containing labels react with the aldehyde group of reducing N-glycans forming an intermediate imine (Schiff base) before reduction with a mild reducing agent like sodium cyanoborohydride.[102] The reaction is acid catalyzed and therefore when using sodium cyanoborohydride as a reducing agent a by-product is hydrogen cyanide which is acutely toxic,

but can be avoided by using non-toxic alternatives including 2-picoline borane. Many commercially available labels exist, however, 2-aminobenzoic acid (2-AA) and 2-aminobenzamide (2-AB), procainamide, and 8-aminopyrene-1,4,6-trisulfonic acid are the most commonly employed for physiochemical applications including liquid chromatography and capillary electrophoresis (Figure 1.13).

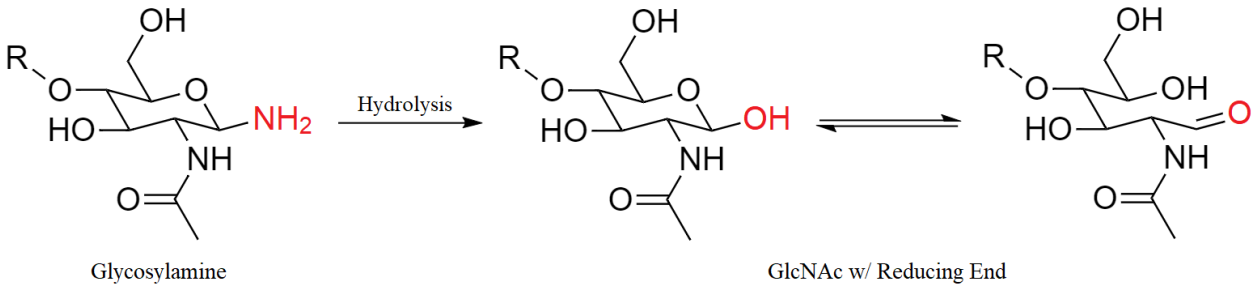

Figure 1.12. Hydrolysis of glycosylamine product after enzymatic released with PNGase F into a reducing sugar. The resulting reducing sugar co-exists in cyclic and acyclic forms.

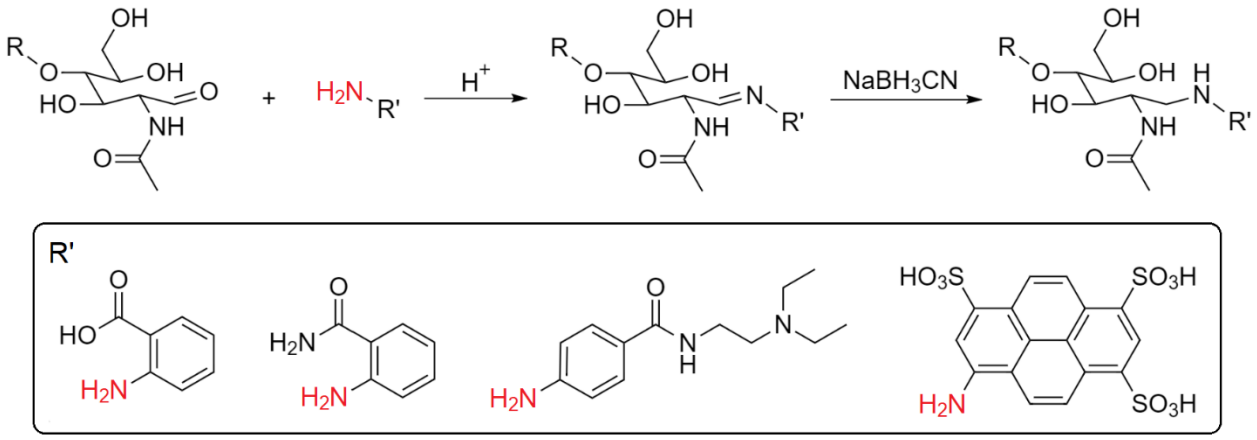

Figure 1.13. Reductive amination reaction mechanism for the reducing-end labeling of N-glycans via primary amine containing labels (APTS). R' = common commercially available N-glycan labels from left to right, 2-aminobenzoic acid (2-AA), 2-aminobenzamide (2-AB), procainamide, and 8-aminopyrene-1,4,6-trisulfonic acid (APTS)

Identification of derivatized N-glycans via LC with optical detection methods usually requires specific standards that allow for retention time comparison in addition to large

comprehensive databases. Unfortunately, pure chemically synthesized standards are expensive and due to the high level of structural diversity displayed by N-glycans, other means of identification are preferred, especially when dealing with highly complex glycoproteins. Therefore, for accurate identification as well as structural characterization, LC is commonly coupled to tandem MS with electrospray ionization (ESI).

Finally, a technique that has been recently emerging in the field of N-glycosylation analysis is capillary electrophoresis (CE). CE is the primary technique used in this study due to its high sensitivity and ability to obtain high-resolution separations. The theory, instrumentation and method details are explained in subsequent chapters.

1.3 Capillary Electrophoresis

Capillary electrophoresis (CE) is powerful analytical technique that involves the separation of charged molecules under the influence of an electric field. Separations are performed within a narrow-bore capillary filled with an electrolyte solution, commonly referred to as the background electrolyte (BGE). The basic schematic of CE instrumentation is depicted in Figure 1.14 and includes a fused silica capillary (25-100 μm inner diameter), a cathode and anode connected to a high voltage power supply (HVPS) and a detector. For sample injection, the BGE reservoir is temporarily replaced with the sample vial and sample is introduced into the capillary through either applied pressure (hydrodynamic) or voltage (electrokinetic). Once injected, the capillary is placed back into the BGE reservoir followed by the application of a high voltage (5-30 kV). Analyte migration is based on its charge-to-size ratio, defined as their electrophoretic mobility (μ_{ep}) (Equation [1]).[103]

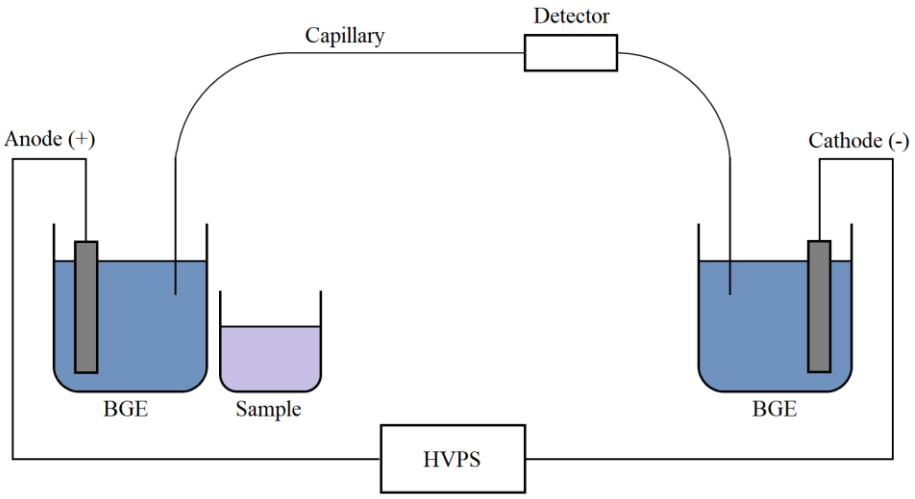

Figure 1.14. Principle components of capillary electrophoresis (CE) instrumentation

$$\mu_{ep} = \frac{q}{6\pi\eta r} \quad [1]$$

Where q is the analyte's net charge, η is the viscosity of the electrolyte and r is the hydrodynamic radius of the analyte. An additional factor that contributes to the overall migration of the analyte is a phenomenon known as electroosmotic flow (EOF). This occurs in bare-fused silica capillaries when operating at pH values greater than 3. Above pH 3, the weakly acidic silanol groups (pKa ~2) that populate the inner surface of the capillary become deprotonated.[104] Cations within the BGE are electrostatically attracted to the negatively charged capillary wall resulting in the formation of two layers, (1) the fixed or stern layer in which the cations are bound strongly to the capillary wall partially neutralizing the negative charges, and (2) the diffuse layer which is rich in cations are but not tightly bound to the capillary wall. When voltage is applied to the system, cations present in the diffuse layer will migrate to the cathode resulting in the movement of the bulk solution towards the cathode (Figure 1.15). The electroosmotic mobility (μ_{eof}) is defined in Equation [2]. In comparison to HPLC which generates parabolic flow profiles (Figure 1.16b), EOF

generates a flat-flow profile and primarily responsible for CEs high separation efficiencies, resulting in narrow peaks (Figure 1.16a).

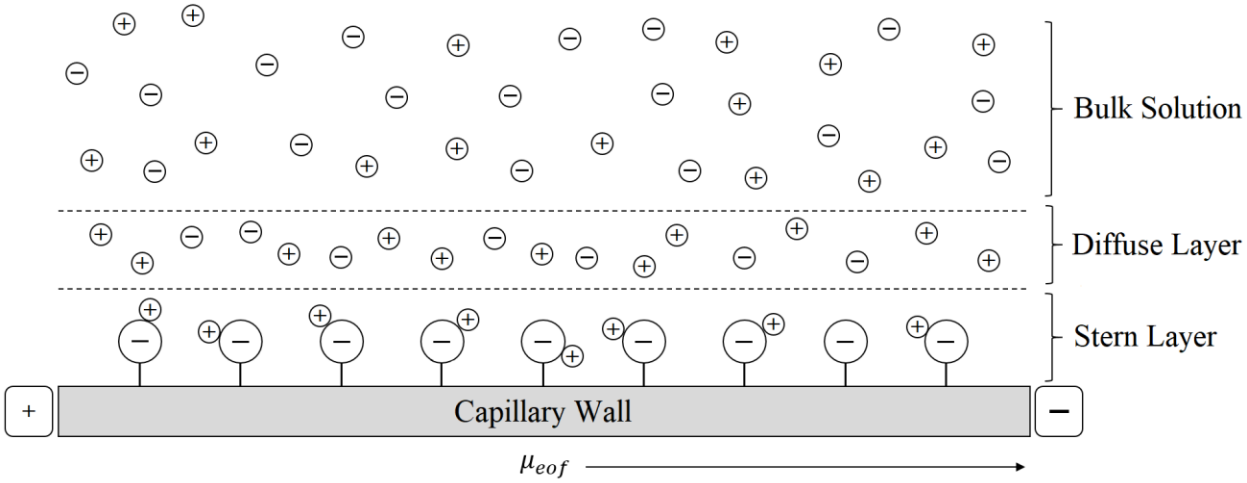

Figure 1.15. Depiction of EOF electric double layer

$$\mu_{eof} = \frac{\varepsilon\zeta}{4\pi\eta} \quad [2]$$

Where ε is the dielectric constant of the electrolyte, ζ is the zeta potential of the capillary wall, and η is the electrolyte viscosity. Therefore, with both μ_{ep} and μ_{eof} contributing to the overall migration of the analyte, the total or apparent mobility (μ_{app}) of the analyte is the sum of the two as defined in Equation [3].

$$\mu_{app} = \mu_{ep} + \mu_{eof} \quad [3]$$

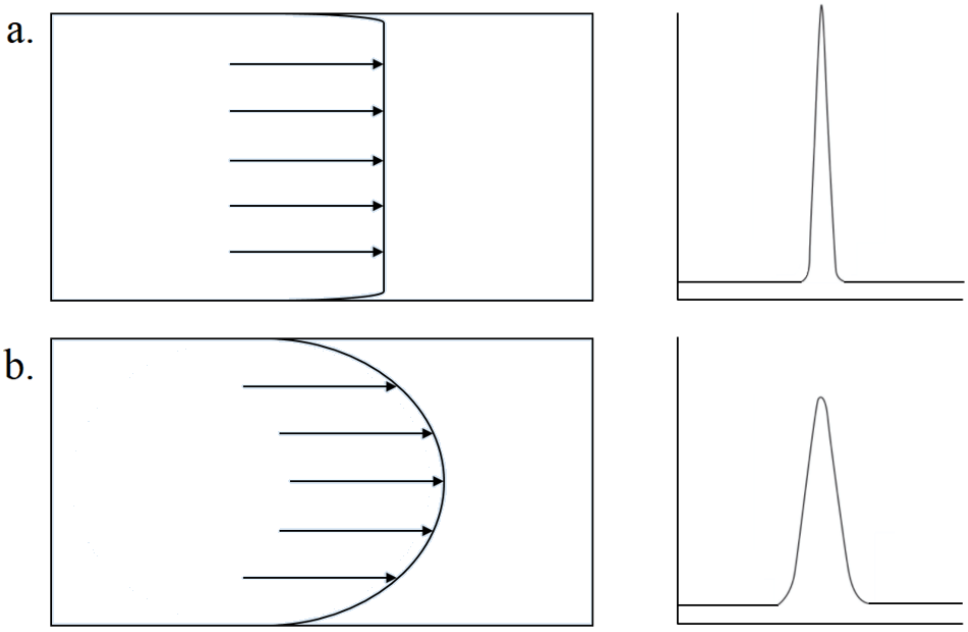

Figure 1.16. Depiction of EOF generated flat flow and resulting peak shape by CE (a) versus pumped generated parabolic flow and resulting peak shape by HPLC (b).

There are a variety of separation modes that can be used is CE applications including capillary zone electrophoresis (CZE), capillary gel electrophoresis (CGE), capillary isoelectric focusing (cIEF), micellar electrokinetic capillary chromatography (MEKC), capillary electrochromatography (CEC) and capillary isotachophoresis (cITP). CZE and CGE were used in this study. CZE is the most common separation mode of CE in which analyte molecules are separated according to their μ_{ep} (charge-to-size ratio). Contrarily, in CGE the gel-based BGE acts as a seizing matrix and separates analyte molecules primarily based off size.

1.3.1 CE Detection Modes

Analyte detection in CE-based applications can be achieved using various techniques. Due to their versatility, optical detection methods including UV absorbance and fluorescence are most commonly employed.[105] Since CE uses optically transparent silica-based capillaries, detection is performed on-column by first removing a small portion of the protective polyimide coating which

creates the detection "window". One of the main advantages of CE is the low injection volume requirements, typically in the nL range. However, this in combination with shortened path lengths due to narrow capillary diameters limits UV absorbance sensitivity.[106] Therefore, fluorescence detection can be used as it offers better limits of detection (LOD), (fM range).[107] However, unlike HPLC, the availability of native fluorescence detectors for commercial CE instrumentation is limited. Therefore, laser induced fluorescence (LIF) detection is typically used for CE applications, and was used accordingly in the following study.

In LIF detection, as the analyte molecules pass the capillary window they are irradiated with a laser resulting in the molecules transition from ground state to an excited electronic state. Upon transition back to the molecules ground state, light with a longer wavelength is emitted and subsequently detected. The main disadvantage with LIF detection is the need for pre-derivatization because many molecules do not contain fluorophores (i.e. N-glycans). However, depending on the analyte, many fluorophore derivatization reagents are available and when applied enable low LODs (fM).[108] Finally, another detection method that offers significant advantages with respect to detection limits is MS.

1.4 Mass Spectrometry (MS)

Since its invention in the late 1890's, major technological advancements and the development of highly sophisticated instrumentation has made Mass Spectrometry (MS) an invaluable analytical technique in many scientific fields. Mass spectrometers are used extensively in many fields of study and have a wide range of applications including forensics for the detection of illicit substances in complex biological matrices, identification of important biomarkers in cancer research, and for drug discovery in the pharmaceutical industry.[109-111] In general, MS involves the generation of ions from organic or inorganic mixtures followed by the separation of

these ions according to their mass-to-charge ratios (*m/z*) before their subsequent detection. Although complex, these instruments are generally composed of three main components: an ion source, mass analyzer, and a detector (Figure 1.17)

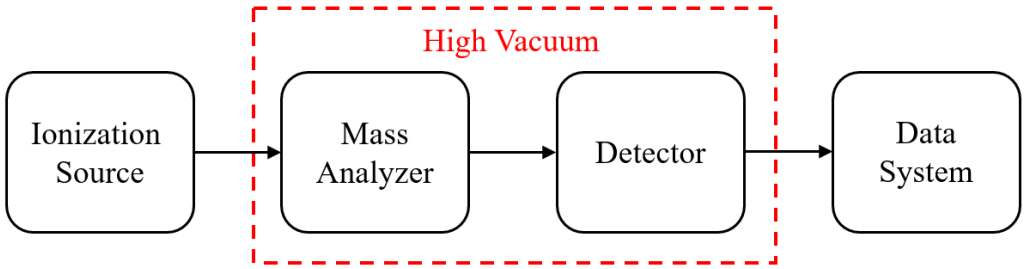

Figure 1.17. Principle components of a Mass Spectrometer (MS)

The sample is first introduced into the ion source and depending on the polarity used generates gas phase ions with an overall positive or negative charge. After ionization under high vacuum the gaseous phase ions are influenced by electric and/or magnetic fields imparted by a mass analyzer, which effectively sorts them based on their *m/z*. Once sorted, the ions reach the detector and generate an electrical signal, which is converted and computed into a mass spectrum.

Ionization can be achieved using numerous techniques including electron ionization (EI) and atmospheric pressure chemical ionization (APCI), which are classified as "hard" ionization techniques because they induce a large degree of fragmentation.[112] In contrast, "soft" ionization techniques result in a lower or negligent degree of parent ion fragmentation. Examples of "soft" ionization techniques include matrix-assisted laser desorption ionization (MALDI) and ESI.[112]

1.4.1 Electrospray Ionization (ESI)

ESI is one of the most common ionization techniques used in MS-applications and its ability to generate multiply charged ions makes it particularly useful for the analysis of large, non-

volatile biomolecules like proteins and nucleic acids.[113] Briefly, it involves the generation of charged droplets by passing a sample solution through a highly charged stainless-steel capillary (± 2-6kV). The generation of a high electric field results in the distortion of the solution at the capillary tip, known as a Taylor cone (Figure 1.18). When operating in positive ion mode, the electric field will force positive ions towards the tip of the Taylor cone at which point an aerosol of positively charged droplets are emitted. Through desolvation, commonly accompanied with elevated source temperatures and drying gases, solvent evaporates from the droplets decreasing their size effectively increasing the charge density near their surface (Figure 1.18). The surface charge density will increase until reaching a critical point at which positive ions are ejected from the droplet into the gaseous phase and subsequently transported into the first vacuum stage of the MS.

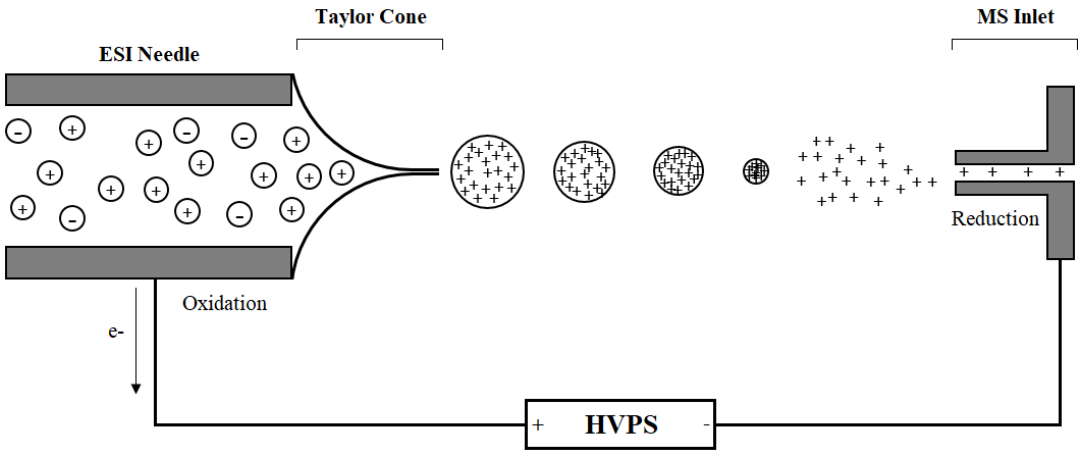

Figure 1.18. Schematic representation of electrospray ionization (ESI) operating in positive ion mode.

1.4.2 Quadrupole Mass Analyzer

Quadrupole mass analyzers are composed of four cylindrical or hyperbolic rods in parallel as depicted in Figure 1.19.[114] The rods are configured in pairs, whereby each pair have an applied positive (y-z plane) or negative (x-z plane) potential that cycles throughout the duration of the experiment. The generation of an oscillating electric field through the application of

radiofrequency (RF) and direct current (DC) potentials influences trajectories of ions according to their *m/z* as they pass through the centre of the rods (z-axis). Detection is dependent on the stability of ion-trajectory within the x-y plane, where ions with stable trajectories will pass through making it to the detector and ions with unstable trajectories will collide with the rods (neutralized) and not be detected. Manipulation of these voltages can enable the selection of ions with specific *m/z*. With the application of only RF potentials, quadrupoles act as an ion-guide allowing a large *m/z* range to pass through. However, upon superimposition of a DC potential, transmission of a narrower *m/z* range can be achieved. For example in positive ion mode, upon application of a positive DC potential to the rods in the x-z plane, trajectories of heavier ions are not sufficiently influenced by the RF potential and therefore are focused to the centre of the rods. Whereas lighter ions (below a certain *m/z*) will have unstable trajectories in this plane and consequently only heavier ions will be transmitted and detected. Conversely, a negative DC potential applied to the rods in the y-z plane destabilizes the trajectory of heavier ions (above a certain *m/z*) whereas lighter ions are influenced greatly by the RF potential, which effectively stabilizes their trajectories in this plane allowing transmission and subsequent detection.

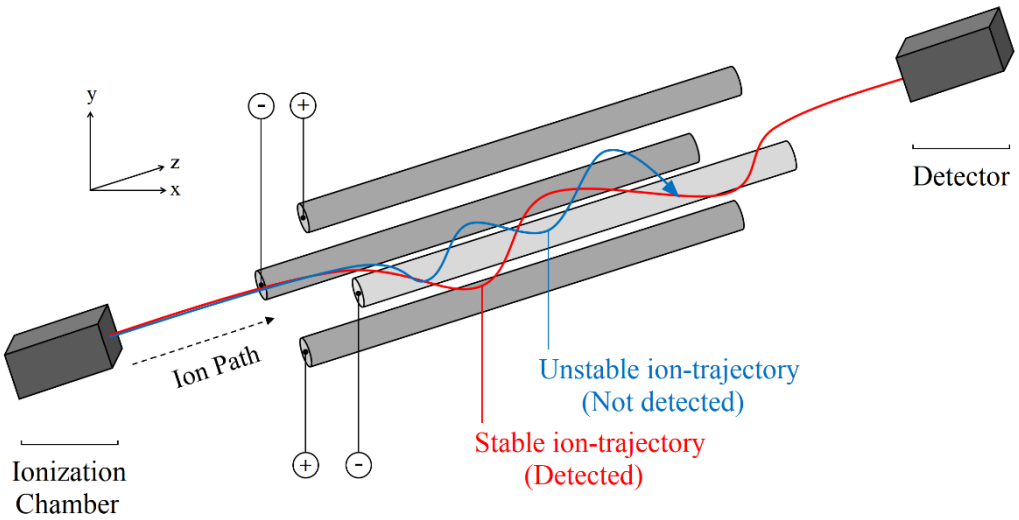

Figure 1.19. Schematic representation of a quadrupole mass analyzer.

1.4.3 Time-of-Flight (TOF)

A time-of-flight (TOF) mass analyzer accelerates packets of ions through a drift region of a flight tube (Figure 1.20).[115] Ions first enter a series of stacked plates, known as the pulser, whereby an electric potential is applied to the back plate accelerating the ions through a flight tube towards a detector. The time at which ions reach the detector is dependent on their velocities, which is directly proportional to their respective *m/z,* with smaller ions reaching the detector first followed by larger ions. The initial kinetic energies, location and orientation of ions within the pulser region can influence their arrival times to the detector. For example, two ions with the same *m/z* but differing starting positions in the pulser region will cause them to arrive at the detector at different times ultimately reducing resolution. Therefore, many modern TOF-MS instruments are equipped with a series of ring electrodes at the end of the flight tube known as a reflectron.[115] This device improves resolution by increasing the ion drift distance and by correcting for differences in kinetic energies to ensure arrival times of ions with identical *m/z* are the same.

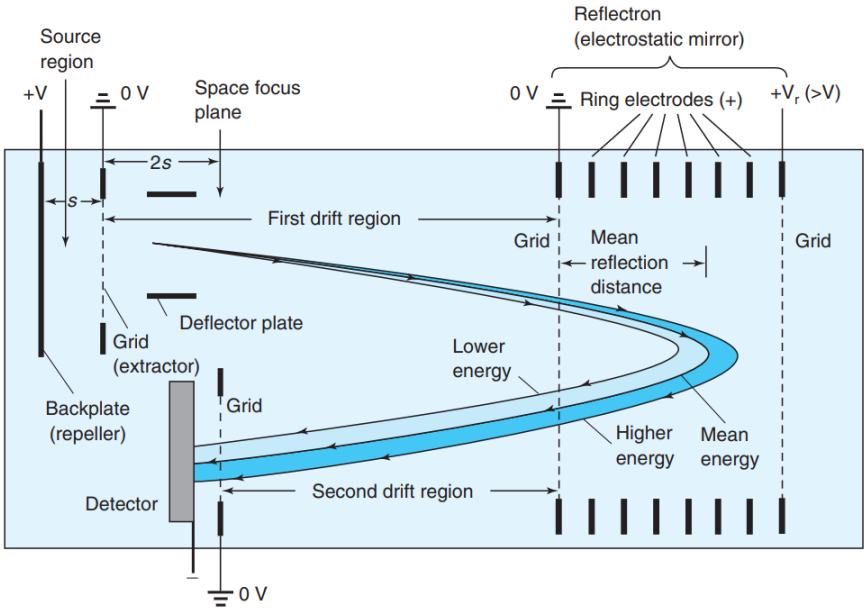

Figure 1.20. Schematic representation of a TOF mass analyzer. Adapted from Harris, D.C. 8th Ed.[116]

1.4.3 Ion Detector

Ion detection in mass spectrometry is achieved by converting ion current into quantifiable electrical signals. Due to low ion currents, amplification is generally required to achieve observable signals and this most commonly accomplished using a microchannel plate (MCP) detector.[117] An MCP detector is composed of a plate containing many semi-conductor coated cylindrical channels, each operating as individual electron multipliers (Figure 1.21). Upon ion contact with one of these channels, signal intensity is amplified by the generation of an electron cascade.

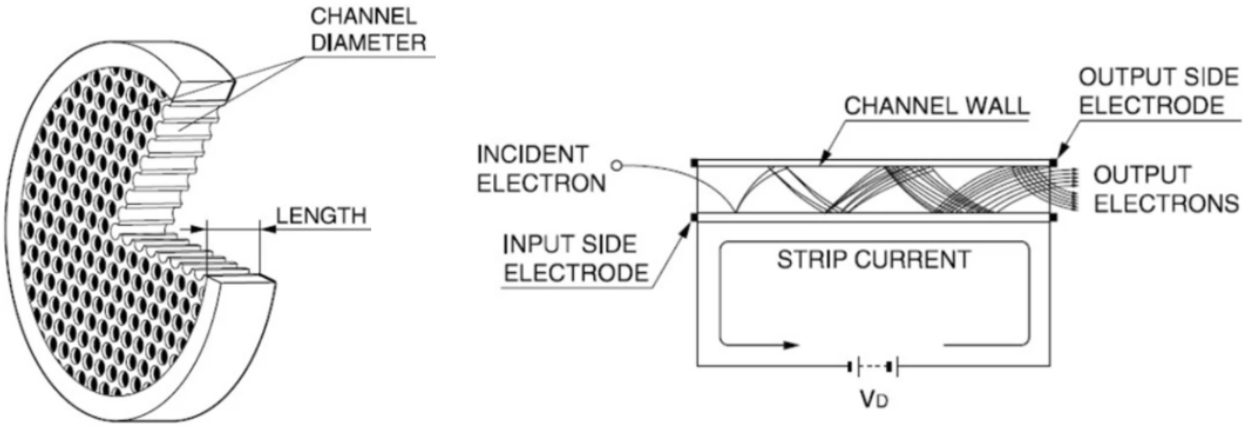

Figure 1.21. Schematic representation of a microchannel plate detector (MCP). Adapted from Chassela *et al.*[118]

1.4.4 Hybrid Quadrupole Time-of-Flight Mass Spectrometer

The instrument used for the majority of this study was the AB Sciex TripleTOF® 6600+ hybrid quadrupole time-of-flight mass spectrometer (QTOF-MS). The combination of quadrupole and TOF mass analyzers offers significant improvements in instrument acquisition speeds, resolution, sensitivity, and dynamic range. The general schematic of the AB Sciex TripleTOF® 6600+ is depicted in Figure 1.22. After ionization, gas phase ions enter the first stage of the MS vacuum and the initial ion beam is focused by the QJet® ion guide.[119] This initial focusing step

provides increased sensitivities through improved ion transmission rates. The ions then enter Q0 whereby the ion beam is further focused before entering into the first mass filtering quadrupole, Q1. In Q1, ions are filtered according their *m/z* and transmitted into the Q2 collision cell. In Q2, transmitted ions are fragmented via collisions with inert gas (N_2) molecules that are pumped in at a specific energies (10-100 eV), a process known as collision induced dissociation (CID). Fragmented ions (i.e. product ions) are then transmitted into the pulser region of the TOF mass analyzer before being accelerated through flight tube. Ion kinetic energies are corrected by the reflectron, directed towards an MCP detector and subsequently computed into a mass spectrum.

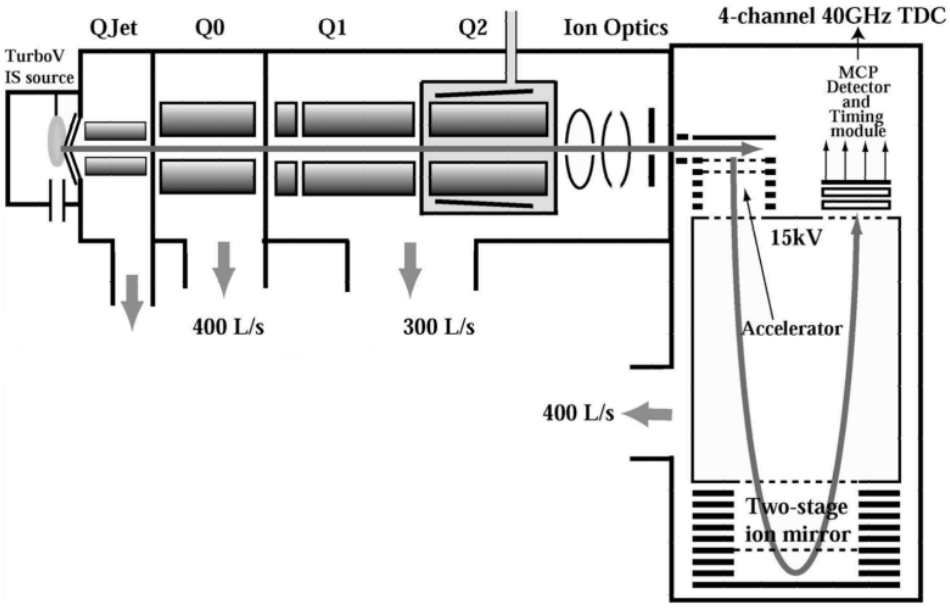

Figure 1.22. Schematic representation of a hybrid QTOF-MS. Figure adapted from Andrews *et al.*[120]

1.4.5 MS-Based N-Glycomics

Analysis and characterization of protein N-glycosylation remains challenging due to the extensive complexity of N-glycans on both the macro- and micro-heterogeneity levels. MS continues to be a powerful tool in many omics- related fields. Its ability to achieve high accuracy

with respect to mass confirmation and structural characterization makes it particularly useful in the complicated field of N-glycomics. Two strategies are typically employed for the characterization of protein glycosylation using MS, top-down and bottom-up approaches. Top-down MS refers to the direct analysis of glycoproteins at the intact level with no prior sample processing, thereby minimizing loss of important PTM related information.[121] Before the development of ESI and instrumentation with high resolving power, this approach was limited to the intact analysis of relatively small glycoproteins with simple glycosylation profiles. However, with recent advancements in high resolution MS instrumentation, top-down analysis of large complex biomolecules including mAbs is now possible.[122] Despite offering valuable information, top-down analysis of highly complex glycoproteins bearing many glycosylation sites (i.e. viral glycoproteins) remains extremely challenging primarily due to the diversity of generated glycoforms. Consequently, bottom-up MS-based strategies for the analysis of protein glycosylation remains the "gold-standard" approach. Bottom-up approaches first involve the enzymatic treatment of the glycoprotein sample with trypsin or PNGase F for the analysis of glycopeptides or released N-glycans, respectively. Trypsin catalyzes the cleavage of peptide bonds at the c-terminus side of lysine and arginine residues yielding peptides with an average molecular weight of 1kDa.[123] When subjected to MS/MS, peptides predominantly produce a series of characteristic y- and b-ion fragments (z-, c-, x-, and a-ions also possible), enabling the determination of peptide sequence (Figure 1.23a).[124] Many automated softwares platforms are available for the sequencing for peptides based off generated MS/MS spectra, and in combination with large comprehensive databases, accurate protein identification is possible. However, PTMs like N-glycosylation further complicate analysis. Upon CID fragmentation, similar to peptides, N-glycans produce their own series of characteristic y- and b-ion fragments (Figure 1.23b).

Consequently, when glycopeptides are subjected to MS/MS experiments, the generated spectra are composed of a combination of these two fragmentation pathways. Although glycopeptide analysis via MS offers crucial information about the level of site occupancy as well as the structures bound to specific glycosylation sites, structural interpretation is hindered due to MS/MS spectral complexity and the lack of automated software. Most softwares programs currently available can predict N-glycan monosaccharide composition based on monoisotopic mass but lacks the ability to elucidate structures, hence why most analysis is performed manually. Therefore, in order to simplify N-glycan structural determination they are enzymatically released using PNGase F prior to MS analysis (Figure 1.10).

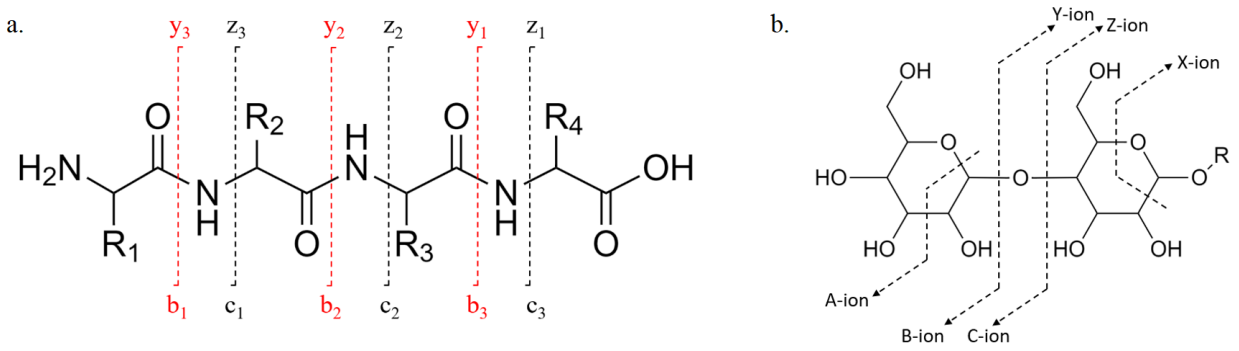

Figure 1.23. Common CID fragmentation pattern of (a) peptide and (b) oligosaccharides

For released N-glycans, the two most common ionization techniques used in MS-based analyses are MALDI and ESI. Commonly coupled with TOF mass analyzers, ionization of enzymatically released native N-glycans via MALDI generates primarily singly charged ions ($[M+H]^+$, $[M+Na]^+$, $[M+K]^+$). However, poor ionization efficiencies of native N-glycans negatively impacts sensitivity therefore, similar to LC-applications pre-derivatization prior to MALDI-TOF is typically performed.[125-126] Additionally, due to the structural diversity of N-glycans, front-end separation prior to MS analysis is preferred; however, coupling MALDI with

front-end separation techniques including LC and CE remains difficult.[127] Therefore, ESI has some advantages over MALDI as it can be easily coupled to common separation techniques. Similarly, ESI-MS analysis of native enzymatically released N-glycans yields predominantly $[M+H]^+$, $[M+Na]^+$, and $[M+K]^+$ ions. However, ESI-MS also suffers from poor ionization efficiencies of native N-glycans therefore prior derivatization is also performed .[128] Techniques such as permethylation whereby hydroxyl, amine and carboxyl hydrogens are methylated to increase hydrophobicity improve N-glycan sensitivities. Several MS-tags that target released glycosylamines are also available however, derivatization of the reducing end of N-glycans via reductive amination strategies as discussed in Section 1.2.7 are the most popular for MS-based N-glycomics.[58]

Fragmentation of enzymatically released N-glycans while operating in positive- or negative-ion mode yields different structural information. For example, in positive-ion mode upon CID fragmentation, N-glycans preferentially fragment at their glycosidic linkages producing predominantly y-and b-series ions, which enables N-glycan sequencing. Whereas operation in negative-ion mode, along with y- and b-ions CID fragmentation yields cross-ring fragment ions, enabling the determination of positional and linkage isomers.[129] Regardless, due to the increase in sensitivity and simplified MS/MS spectra, positive-ion mode is most commonly employed in MS-based N-glycomics, and was used accordingly in the following study. Due to their structural diversity, LC is the "gold-standard" technique used for N-glycan separation prior to MS analysis but recent advancements in the coupling of CE to MS has showed promise in the field of N-glycomic analysis.

1.5 Capillary Electrophoresis – Mass Spectrometry

CE with on-line MS detection was first demonstrated by Smith and coworkers in 1987.[130] Since then CE-MS has been a steadily emerging analytical technique used in many scientific fields including the pharmaceutical industry, metabolomics research, and forensic toxicology.[131-133] In the vast majority of CE-MS applications ESI sources are used and the coupling of CE to ESI-MS can be achieved through various interfacing options that can be broken down into two main categories: sheath-flow and sheathless interfaces. In sheath-flow interfaces, electrospray is facilitated with the help of a volatile sheath liquid, whereas in sheathless interfaces the BGE acts as both the separation medium and electrospray solvent. Sheath-flow interfaces are generally more robust in comparison to their sheathless counterparts; however, the sheath-liquid flow-rates required for electrospray results in analyte dilution and reduced ionization efficiencies. In sheathless interfaces, the facilitation and stability of ESI is highly dependent on BGE volatility as no sheath-liquid is used. Although this narrows the range of compatible BGE compositions, the low flow-rates typically generated in sheathless interfaces (5-50 nL/min) results in large sensitivity gains and diminished analyte dilution. Additionally, advancements in interfacing technologies has resulted in the commercialization of sheathless CE-MS systems. One of the first commercially available systems was Sciex's (formerly Beckman Coulter) CESI-8000+, which was used for this study.

1.5.1 Sheathless Capillary Electrophoresis – Mass Spectrometry

The sheathless CE-MS interface used in this study was first developed by Moini in 2007 before being licensed and commercialized by Sciex (Beckman Coulter) in 2009 and 2014, respectively.[134] Successful operation of this system requires specialized capillary cartridges and the primary components are depicted in Figure 1.24. The cartridges contain two capillaries

independent from one another, commonly referred to as the separation capillary and the conductive capillary. The separation capillary has a total length of 91 cm with a 30 µm inner diameter and contains a 2-3 cm hydrofluoric acid (HF) etched porous section surrounded by a conductive liquid (i.e. BGE) within a stainless steel ESI needle. The sample is injected and separated in this capillary and doubles as an emitter/sprayer tip. The porous section at the end of the separation capillary contains pores large enough to allow the exchange of ions between the inside of the capillary and outside surrounding conductive liquid, but small enough that there is no analyte loss. After sample injection and application of a high voltage across the separation capillary, this exchange of ions enables the completion of the electrical circuit. The conductive capillaries main function is to provide the stainless steel ESI needle with sufficient BGE to ensure this electrical circuit is maintained. Electrospray is then achieved by the application of voltage to the stainless steel ESI needle.

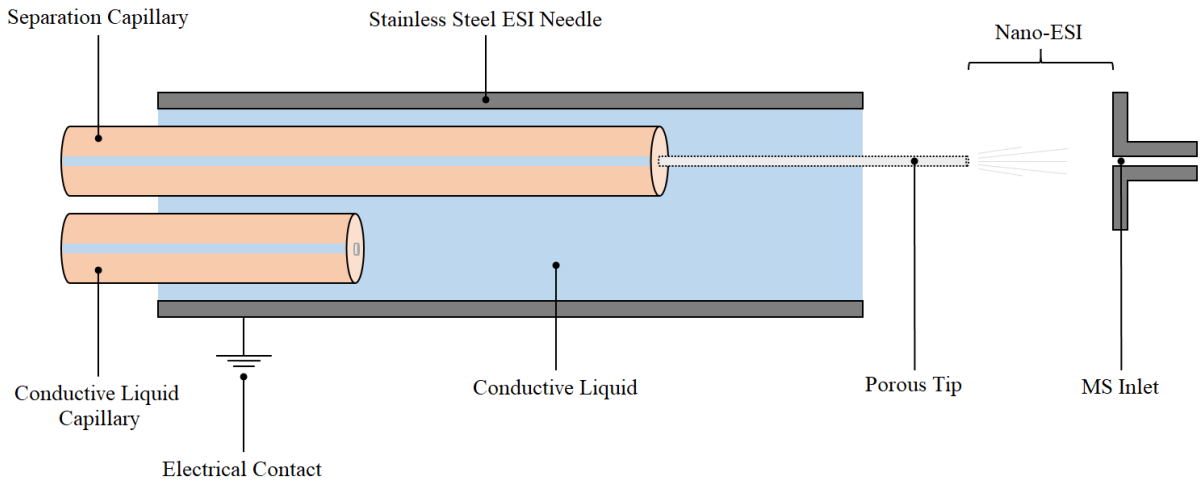

Figure 1.24. Schematic representation of the sheathless CE-MS interface developed by Moini [134] and commercialized by Sciex (CESI-8000 Plus).

1.6 Purpose of Study

Vaccine glycosylation has clear implications on immunogenicity and therefore should be considered a CQA during the manufacturing and regulation of seasonal influenza vaccines. Current potency evaluation methods (i.e. SRID) relying on antigen binding are not sensitive enough to capture differences in glycosylation of vaccine antigens; consequently, there is a requirement for alternative strategies. Physiochemical methods including RP-HPLC offer significant advantages over the SRID assay but alone lacks the ability to distinguish between conformationally active forms of HA. To address this, Lorbetskie *et al.* (2019) developed a combined quantitative RP-HPLC assay with an initial conformationally selective receptor-binding step for the assessment of HA content in influenza vaccines (Section 1.2.6). Interestingly, differences in receptor binding were observed between numerous manufacturers and lots from which two manufacturers of egg-derived H1N1 (A/California/07/2009) influenza vaccine monovalent bulks displayed near complete opposite outcomes (Figure 1.25). Manufacturer I contained HA material capable of binding to the synthetic sialic acid receptor (Figure 1.25a), whereas no binding of HA material was observed with manufacturer II's vaccine bulk (Figure 1.25b). The samples were evaluated with the traditional SRID assay but no differences in antigen-antibody agglutination from which potency is evaluated were observed suggesting that SRID could not discriminate between "structurally well folded" HA. It was suggested that the differences in receptor binding affinities could be attributed to a difference in glycosylation characteristics of the egg-derived HA material within the vaccine monovalent bulks. In order to test this hypothesis, enzymatically released N-glycans derived from each manufacturer's vaccine monovalent bulk were APTS-labeled and analyzed via CGE-LIF (Figure 1.25c). Interestingly, differences in the relative abundances of specific N-glycan species were observed for each manufacturer (∗). In particular, manufacturer II's APTS-labeled N-glycan

profile displayed increased relative abundances with respect to certain species when compared to manufacturer I. These results suggest that differences in glycosylation could be attributed to manufacturer IIs inability to bind to the synthetic sialic acid receptor. Therefore, due to the lack of standardized methods, the aim of this study is to develop and highlight the utility of orthogonal CE-based methods for the assessment of viral vaccine N-glycosylation.

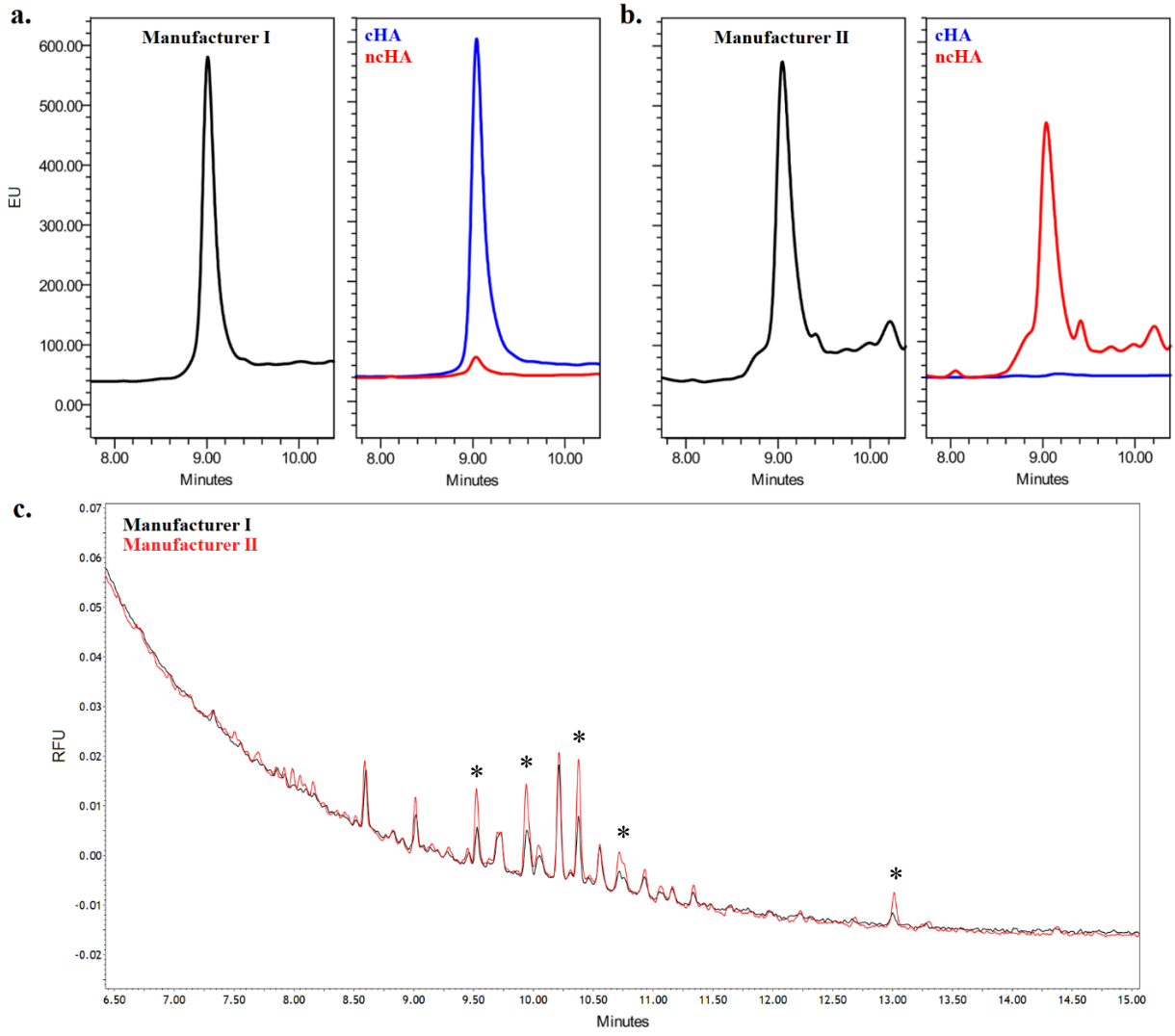

Figure 1.25. RP-HPLC chromatograms of an H1N1 (A/California/07/2009) monovalent vaccine bulk after selective capture with synthetic sialic receptor (α2,6-linked NeuAc) from manufacturer I (a) and manufacturer II (b).[52] Black traces represent maximal HA signal in a control sample. Blue and red traces represent cHA and ncHA, respectively. CGE-LIF enzymatically released APTS-labeled N-glycan profile of manufacturer I & II H1N1 (A/California/07/2009) monovalent vaccine bulks (c). * *highlights N-glycan species displaying differing relative abundance between manufacturers.*

Chapter 2: Materials & Methodology

2.1 General Materials

All chemicals used were of analytical grade and obtained from various sources. Optima™ LC-MS grade H_2O, acetonitrile, methanol isopropanol, and glacial acetic acid were purchased from Fisher Scientific (Waltham, MA, USA). Hydrochloric acid (1M), sodium hydroxide (1M), ammonium acetate (7.5M), ammonium hydroxide (25%, LC-MS grade), NP-40, iodoacetamide, dithiothreitol, sodium dodecyl sulfate, ε-aminocaproic acid, sodium cyanoborohydride (1M in THF), 2-methylpyridine complex, and Girard's Reagent T were purchased from Sigma-Aldrich (St. Louis, MO, USA). Girard's Reagent P and acetohydrazide were purchase from TCI chemicals (Tokyo, Japan). PNGase F (glycerol and glycerol-free) was purchased from New England BioLabs (Ipswich, MA, USA). The Fast Glycan Labeling and Analysis Kit containing 8-Aminopyrene-1,3,6-trisulfonic acid and carboxylated magnetic beads was purchased from AB Sciex (Brea, CA, USA).

2.2 N-Glycan Release, APTS Labeling and Purification for CZE-LIF Analysis

2.2.1 Sample Buffer Exchange

A 10kDa (MWCO) Amicon Ultra Centrifugal Filter unit (0.5 mL) was pre-wet and equilibrated with a 500 µL volume of LC-MS grade H_2O and spun using a benchtop centrifuge at 10,000g for 5 minutes. This pre-wetting step is used to activate the filter membrane and remove any potential contaminants left behind from the manufacturing process. The filter unit was equilibrated with an additional 400 µL volume of LC-MS grade H_2O and spun at 10,000g for 5 minutes. After equilibration, the remaining H_2O retained in the filter unit was removed (~ 100 µL) and the filter unit was transferred to a new collection tube. 10 µg of the glycoprotein sample was

added to the equilibrated filter unit and filled to the 500 µL mark with LC-MS grade H_2O. The glycoprotein sample was buffer exchanged by spinning at 10,000g for 5 minutes. The flow through in the collection tube was discarded and 400 µL of LC-MS grade H_2O was added to the 100 µL retentate before performing a second spin at 10,000g for 5 minutes. The previous step was repeated once more for a total of three buffer exchange steps. The buffer exchanged glycoprotein sample was then transferred to a 0.5 mL lo-bind Eppendorf tube and lyophilized using a Labcono centrifugal evaporator (~2 hours).

2.2.2 Denaturation, Reduction & Alkylation

In a 0.2 mL bubble top Eppendorf vial the denaturation/reduction/alkylation solution was prepared by adding 5 µL of 0.5% (v/v) Nonidet P-40 (NP-40), 1 µL of 5% (w/v) sodium dodecyl sulfate (SDS), 1 µL of 250mM iodoacetamide (IAA), and 1 µL of 50mM dithiothreitol (DTT). The solution was mixed by vortexing briefly. The lyophilized glycoprotein sample was re-suspended in 10 µL of LC-MS grade H_2O and vortexed until solubilized. The re-suspended glycoprotein sample was then transferred to a 0.2 mL bubble top Eppendorf vial followed by the addition of 5 µL of the denaturation/reduction/alkylation solution prepared above. The glycoprotein sample was incubated at 60°C for 8 minutes using a heat block. After incubation, the sample tube was vortexed and centrifuged briefly to remove any condensation from the vial cap.

2.2.3 Enzymatic Release of N-Glycans

In a separate 0.2 mL bubble top Eppendorf vial the digestion solution was prepared by adding 12 µL of 0.5% (v/v) NP-40 and 1 µL of PNGase F (NEB, 500 units, glycerol or glycerol free). The pipette was purged when adding the enzyme to the solution to maximize transfer. 12 µL of the digestion solution was then added to the glycoprotein sample and incubated at 60°C for 20

minutes using a heat block. After incubation, the sample tube was vortexed and centrifuged briefly to remove any condensation from the vial cap.

2.2.4 Released N-Glycan Capture via Carboxylated Magnetic Beads

Caboxylated magnetic beads (1 mg/mL) from the Sciex Fast Glycan Labeling and Analysis Kit were re-suspended by vortexing on maximum speed for 5-10 seconds. In a separate 0.2 mL bubble top Eppendorf vial, 200 µL of the re-suspended carboxylated magnetic beads were added. The tube was then placed on the magnetic stand for 2 minutes until the magnetic beads were pulled to the side. The supernatant (storage solution) was removed by pipetting from the bottom of the vial and discarded carefully not to remove any of the bead suspension. The tube was removed from the magnetic stand and the beads were re-suspended in 5 µL of LC-MS grade H_2O and vortexed briefly. 210 µL of acetonitrile (ACN) [97.7% final ACN concentration] was then added quickly and vortexed on maximum speed for 5-10 seconds. 200 µL of the ACN-bead suspension was then added to the PNGase F digested glycoprotein sample and incubated at room temperature for 2 minutes for glycan capture. After incubation, the sample tube was placed on the magnetic stand and once the beads were pulled to the side the supernatant (containing the de-glycosylated glycoprotein sample) was carefully removed and discarded.

2.2.5 APTS Labeling of N-Glycans Reducing End

In a separate 0.2 mL bubble top Eppendorf vial the labeling solution was prepared by adding 9 µL of 40mM APTS in 20% acetic acid (HAc), 3 µL of 0.5% (v/v) NP-40, 1 µL of internal standard (maltotriose) and 1 µL of 1M picoline borane in ACN. 11 µL of the prepared labeling solution was then added to the N-glycan-bead vial from the previous step, vortexed to mix followed by incubation at 60^{o}C for 1 hour using a heat block. After incubation, the sample tube was vortexed and centrifuged briefly to remove any condensation from the vial cap.

2.2.6 APTS-Labeled N-Glycan Purification and Elution

After APTS labeling, 10 µL of 0.5% (v/v) NP-40 was added to the sample tube a vortexed. 160 µL of ACN was added and the sample tube was vortexed for 5-10 seconds, followed by a 2 minute incubation at room temperature. The sample tube was then briefly centrifuged to remove any residual sample in the cap before being placed on the magnetic stand. Once the beads were pulled to the side, the supernatant was removed and discarded. For the wash step, the sample tube was removed from the magnetic stand, 20 µL of LC-MS grade H_2O was added, and briefly vortexed to re-solubilize the magnetic beads. 160 µL of ACN was added to the sample tube, vortexed for 5-10 seconds and allowed to incubate at room temperature for 2 minutes. The sample tube was place on the magnetic stand and once the beads were pulled to the side, the supernatant was removed and discarded. The wash step was repeated once more. Finally, the APTS labeled N-glycans were eluted by first removing the sample tube from the magnetic stand and adding 100 µL of LC-MS grade H_2O. The sample tube was vortexed for 5-10 seconds and placed on the magnetic stand. Once the beads were pulled to the side of the vial, the supernatant (containing APTS labeled N-glycans) was transferred to a PCR fitted CE sample vial for CE-LIF analysis.

2.3 Filter-Aided N-Glycan Dual Hydrazide Labeling for Sheathless CESI-MS Analysis

2.3.1 Sample Buffer Exchange

A 10kDa molecular weight cut off (MWCO) Amicon Ultra Centrifugal Filter unit (0.5 mL) was pre-wet and equilibrated with a 500 µL volume of LC-MS grade H_2O and spun using a benchtop centrifuge at 10,000g for 5 minutes. This pre-wetting step is used to activate the filter membrane and remove any potential contaminants left behind from the manufacturing process. The filter unit was equilibrated with an additional 400 µL volume of LC-MS grade H_2O and spun

at 10,000g for 5 minutes. After equilibration, the remaining H_2O retained in the filter unit was removed (~ 100 µL) and the filter unit was transferred to a new collection tube. 10 µg of the glycoprotein sample was added to the equilibrated filter unit and filled to the 500 µL mark with LC-MS grade H_2O. The glycoprotein sample was buffer exchanged by spinning at 10,000g for 5 minutes. The flow through in the collection tube was discarded and 400 µL of LC-MS grade H_2O was added to the 100 µL retentate before performing a second spin at 10,000g for 5 minutes. The previous step was repeated once more for a total of three buffer exchange steps.

2.3.2 Reduction & Alkylation

To the 100 µL buffer exchanged glycoprotein sample, 100 µL of 5mM DTT was added and incubated at room temperature for 1 hour. After reduction, 10 µL of 250mM IAA [12mM final] was added and incubated at room temperature for 30 minutes in the dark. After alkylation, the glycoprotein sample was buffer exchanged 3x with LC-MS grade H_2O to remove residual DTT and IAA. Each buffer exchange step was centrifuged at 10,000g for 5 minutes each.

2.3.3 Sialic Acid Derivatization

To neutralize and stabilize the sialic acid residues, 100 µL of 1M acetohydrazide (AH), 20 µL of 1N hydrochloric acid (HCl), and 20 µL of 2M 1-ethyl-3-(3-dimethylaminopropyl) carbodiimide (EDC) was added to the glycoprotein sample in the filter unit and incubated at room temperature for 4 hours. After derivatization, the sample was buffer exchanged 3x with LC-MS grade H_2O to remove residual/un-reacted AH. Each buffer exchange step was centrifuged at 10,000g for 5 minutes. These buffer exchange steps are crucial, as failure to remove residual AH will result in the neutral derivatization of the released glycans reducing end with AH.

2.3.4 Enzymatic N-Glycan Release & Collection

The N-glycans were released by adding 1 µL of PNGase F (NEB, 500 units, glycerol free). The pipette was purged to maximize the enzyme transfer into the protein solution. The Amicon Filter tube was parafilmed and incubated overnight (~17-18 hours) at 37ºC. After N-glycan release, the filter unit was transferred to a new collection tube. 200 µL of LC-MS grade H_2O was added and spun at 10,000g for 10 minutes to collect the released glycans.

2.3.5 Hydrazide Cationic Labeling of N-Glycans Reducing End

The collected N-glycans were transferred to a 0.5 mL Eppendorf tube and dried down using a Labcono centrifugal evaporator (~1.5 hours). To the dried N-glycans, 5 µL of 50mM Girard's reagent T (GT) in 90% ethanol (EtOH) and 10% HAc was added and incubated at 60ºC for 1 hour using a heat block. The GT-labeled N-glycans were then dried down using a centrifugal evaporator (~ 0.5 hours).

2.3.6 Sample Preparation for Sheathless CESI-MS Analysis

The dried AH-GT-labeled N-glycans were reconstituted in 40 µL 50 mM ammonium acetate, pH 4.0, vortexed to mix for 10-20 seconds, and briefly centrifuged with a benchtop micro centrifuge for 1-2 seconds. The 40 µL sample was then split into 10 µL aliquots in 0.2 mL Eppendorf tubes and stored at -20ºC for future use. 9 µL of one of the aliquot was transferred to a CESI nano-vial followed by the addition of 1 µL of ACN. Sample was then loaded into the CESI sample tray for CESI-MS analysis.

2.4 Sample Preparation for RP-HPLC Analysis

HA samples were transferred to a 1.5 mL Eppendorf tube followed by the addition of 5 µL 400 mM DTT ($[DTT]_{final}$ = 20 mM) and 5 µL 1.0% (w/v) Tween-80 ($[Tween\text{-}80]_{final}$ = 0.05%),

and heated in boiling water for 3 minutes. After reduction, samples were briefly centrifuged and transferred to a polypropylene HPLC vial for analysis.

2.5 Instrumentation & Methods

2.5.1 Capillary Zone Electrophoresis – Laser Induced Fluorescence Detection

All CZE-LIF analysis was performed using a Beckman Coulter (AB Sciex – Brea, CA) PA800 Plus Pharmaceutical Analysis System equipped with a solid state laser induced fluorescence detector (λ_{ex} = 488 nm / λ_{em} = 520 nm).

All separations were carried out using a background electrolyte (BGE) consisting of 7.5mM Ammonium Acetate pH 4.5, 10% Isopropanol in a 50cm effective length (60cm total length), 50µm I.D. polyvinyl alcohol (PVA) coated capillary. At the beginning of each experiment, capillaries were first conditioned by rinsing with LC-MS grade H_2O for 3 minutes at 75 psi followed by BGE for 5 minutes at 75 psi. Before each injection the capillary is rinsed with LC-MS grade H_2O for 3 minutes at 75 psi followed by BGE for 2 minutes at 75 psi. Samples were injected hydrodynamically by applying 0.5 psi forward pressure for 10 seconds (Equivalent to approximately 9 nL). Separations were performed for 20 minutes at a voltage of 30kV in reversed polarity mode (cathode at injection site), and a separation temperature of 20^{o}C. 32Karat (Sciex, version 10.1) was used for data acquisition and processing.

2.5.2 Sheathless Capillary Electrophoresis – Electrospray Ionization – Mass Spectrometry

All sheathless CESI-MS experiments were performed on a Beckman Coulter (AB Sciex – Brea. CA) CESI-8000 Plus capillary electrophoresis system coupled to a TripleTOF 6600+ hybrid quadrupole time-of-flight mass spectrometer (AB Sciex – Brea, CA).

All separations were carried out using a BGE consisting of 10% HAc (pH 2.2) on a bare fused silica surface OptiMS capillary cartridge (91 cm x 30 μm I.D.) (AB Sciex – Brea, CA). At the beginning of each experiment, capillaries were first conditioned following the manufacturers protocol. With the porous sprayer tip submerged in 5 mL of methanol (MeOH), the separation capillary was rinsed with MeOH for 10 minutes at 100 psi followed by a conductive line rinse with MeOH for 3 minutes at 100 psi. The porous sprayer tip was submerged in 5 mL of LC-MS grade H_2O for the remainder of the conditioning. The separation line and conductive line was rinsed with LC-MS grade H_2O for 10 minutes and 3 minutes, respectively, at 100 psi. The separation line was then rinsed successively with 0.1M NaOH, 0.1M HCl, LC-MS grade H_2O, and BGE for 10 minutes each at 100 psi. Conditioning was completed by performing a final BGE rinse of the conductive capillary for 3 minutes at 100 psi.

Prior to each injection the separation line was rinsed at 100 psi with LC-MS grade H_2O for 2 minutes, 0.1M NaOH for 2.5 minutes, LC-MS grade H_2O for 2 minutes, 0.1M HCl for 2.5 minutes, LC-MS grade H_2O for 4 minutes and BGE for 4 minutes, followed by a conductive line rinse of BGE at 75 psi for 3 minutes. Samples were injected hydrodynamically by applying 5 psi forward pressure for 60 seconds (Equivalent to approximately 51 nL) followed by an injection of a BGE post plug for 25 seconds at 0.5 psi. Separations were performed for a total of 60 minutes at 20 kV (normal polarity – anode at injection side) with a 1 minute ramp. The separation temperature and sample storage temperature was set to 25ºC and 10ºC, respectively. To prevent capillary damage and enhance lifetime the separation voltage was ramped down to 1 kV at the end of each experiment. 32Karat (Sciex, version 10.1) was used for data acquisition (separation current only).

MS data was acquired using an ion spray voltage of 1.9 kV, curtain gas of 5 psi and an interface heater temperature of 50ºC. The MS was operated with a resolving power (RP) of 30,000

(FWHM) for TOF-MS scans. The switch criteria for IDA were as follows, TOF-MS survey scans were acquired for 0.25 seconds with 10-20 candidate ions per cycle with a charge state between +2 and +3, that exceeded a minimum ion intensity threshold of 250 counts per second. A rolling collision energy with a collision energy spread of ± 10 eV was applied to all precursor ions for CID. Candidate ions were between 500-1450 Da and former target ions were excluded for 20 seconds after 2 occurrences. Analyst (Sciex, version 1.8.1) and Peak View (Sciex, version 2.2.0.11391) were used for data acquisition and processing, respectively.

2.5.3 Reversed-Phase High-Performance Liquid Chromatography

All RP-HPLC experiments were performed on a Waters Alliance 2695 chromatograph coupled to a Waters 2475 Multichannel Fluorescence Detector (λ_{ex} = 280 nm / λ_{em} = 335 nm). The system was equipped with a column heater and an auto-sampler with a sample cooling device. Data acquisition and processing was performed with Empower Chromatography Data Software (Waters, version 3).

Separations were carried out on a MICRA® HPLC NPS-ODSI, 33 mm × 4.6 mm, 1.5 µm particle or a MICRA® HPLC NPS-ODSI, 100 mm × 4.6 mm, 3 µm particle non-porous silica based column (Eprogen, Darien, IL, USA) for HA analysis and collection, respectively. Chromatographic separations were carried out at 55 °C with an AB gradient elution of 19 min at a flow rate of 1.0 mL/min as shown in Table 2.1. Eluent A was 0.04% (v/v) aqueous trifluoroacetic acid (TFA) and eluent B was 0.03% (v/v) TFA in 25% ACN and 75% IPA.

Table 2.1. RP-HPLC AB gradient method applied for HA separations and collections

Time (min)	Flow Rate (mL/min)	% A	% B
0.0	1.0	95	5
0.5	1.0	80	20
7.5	1.0	80	20
13.5	1.0	71	29
15.0	1.0	5	95
16.0	1.0	5	95
17.0	1.0	95	5
19.0	1.0	95	5

Chapter 3: CZE-LIF Method Development for the Analysis of HA N-Glycosylation in Influenza Vaccine Formulations

3.1 N-Glycan Profiling of Influenza HA via Traditional CGE-LIF Methods

Within the last decade, the use of CE for N-glycan analysis has steadily increased in popularity and is now becoming one of the gold standards in the field. As was briefly mentioned in section 1.2., there are some challenges associated with the analysis of N-glycans that need to be carefully considered. Glycans lack a chromophore or fluorophore and consequently cannot be detected by traditional optical methods like UV absorption. Additionally, the majority of N-glycans generally are not charged unless they contain acidic residues like sialic acid, glucuronic acid, or iduronic acid.[107] Therefore, from a CE perspective, since an analyte needs to be charged for sufficient migration in an electric field (Equation [1]), separation of enzymatically released N-glycans in their "native" uncharged state is not possible by CE. To overcome these two drawbacks, labeling of the N-glycans reducing end with a fluorescent tag is employed after enzymatic cleavage. The most common and well established fluorescent derivative for the glycan analysis by CE is 8-aminopyrene-1,3,6-trisulfonate (APTS), however there are several others that can be used.[102] APTS not only provides a fluorophore that enables their detection by LIF (λ_{ex} = 488nm, λ_{em} = 520nm) but also imparts three fixed negative charges, which facilitates migration within an electric field. APTS labels N-glycans through reductive amination (Figure 3.1). Under acid catalyzed conditions, the primary amine moiety of APTS reacts with the aldehyde group on the reducing end of the sugar, forming an intermediate Schiff base. The resulting imine is further reduced yielding a stable secondary amine APTS-labeled N-glycan.

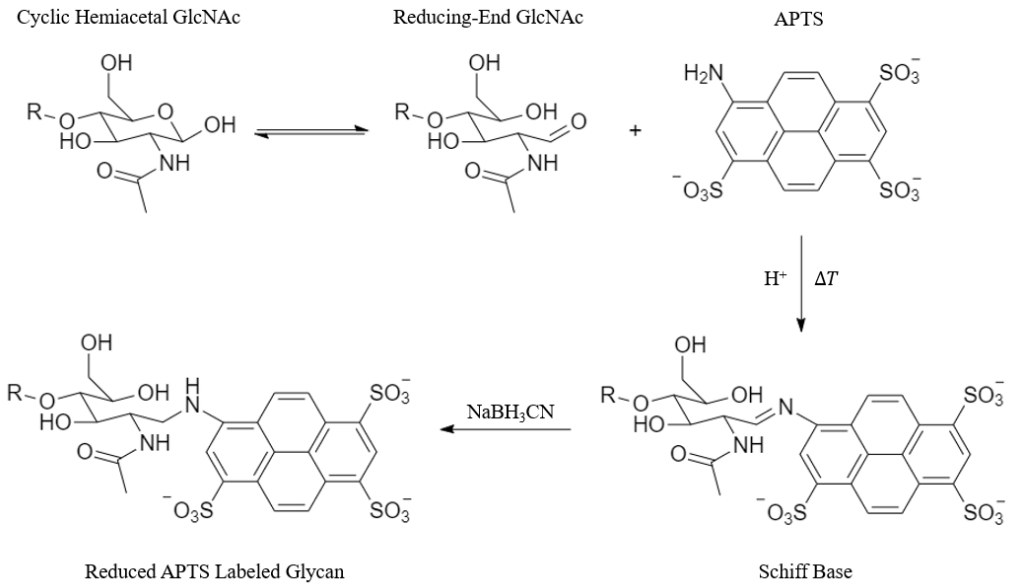

Figure 3.1. Reductive amination reaction mechanism for the reducing-end labeling of N-glycans via 8-aminopyrene-1,3,6-trisulfonate (APTS).

Traditionally, glycan separations by CE are performed with BGE's containing viscosity altering additives including linear polymers. The addition of these polymers results in BGE's with a gel-like consistency which ultimately affects the overall resolution of the separations. In addition to the use of gel-based BGE's, separations are commonly performed within capillaries that have been coated with a neutral polymer (i.e. linear polyacrylamide or PVA), effectively neutralizing the inner silanol groups, reducing or completely eliminating EOF. Therefore, with a lack of EOF contribution, the migration of the analyte is solely dependent on its electrophoretic mobility (μ_{ep}) or charge-to-size ratio.

Reichl and coworkers are responsible for the majority of the published methods on the analysis of influenza glycosylation by CE-based methodologies and employ these two principles (i.e. gel BGE & neutral capillary).[135-139] Although well established, these methods have some limitations. Firstly, CE methods that employ gel-based BGEs typically require strict capillary regeneration procedures to acquire reproducible results between experiments. In addition, gels

have a tendency to polymerize therefore requiring frequent cleaning and maintenance of instrumentation. However, the major disadvantage of gel-based methodologies is the restriction to electrokinetic injection as hydrodynamic injection can disrupt the gel matrix potentially resulting in issues with separation performance including the loss of resolution and poor run-to-run reproducibility.[140] Furthermore, because electrokinetic injection involves the application of a voltage across the capillary, injection biases are unavoidable and small highly charged molecules in the sample will be preferentially injected. In addition to injection bias, sample depletion will also occur as the concentration of the analyte reduces through subsequent injections.

Figure 3.2 highlights the background contribution of un-reacted APTS through injection bias following traditional gel-based methodologies. In this example, 100 µg of HA (H1N1, A/California/07/2009) from an influenza monovalent bulk vaccine sample was deglycosylated with PNGase F and APTS-labeled following standard vendor protocols from New England Biolab's and Beckman Coulter (Sciex), respectively. In general, glycan labeling reactions involving APTS require the reagent in large excess (typically 1000x) in order to drive the reaction to completion. With this method in particular, after APTS labeling, no additional clean up steps are performed to remove the residual un-reacted reagent. Instead, a series of dilutions are performed before CGE-LIF analysis. In some cases, dilution is sufficient to obtain good glycan signal intensities, however this is only the case if large amounts of starting material are digested (mg quantities).[141] The H1 HA enzymatically released N-glycan profile from a 100 µg PNGase F digest can be seen in the zoomed in portion of Figure 3.2 and the section denoted with an asterisk displays the significant contribution of unreacted APTS. This dilution strategy is not ideal in this situation because the starting amounts were low (100 µg). This however represents a significant amount of starting material for HA given that the typical concentration in a vaccine formulation is

typically only 15 µg/strain. Therefore, based on these initial results following traditional gel-based methods, it is evident that clean up or additional purification steps to remove excess APTS are required.

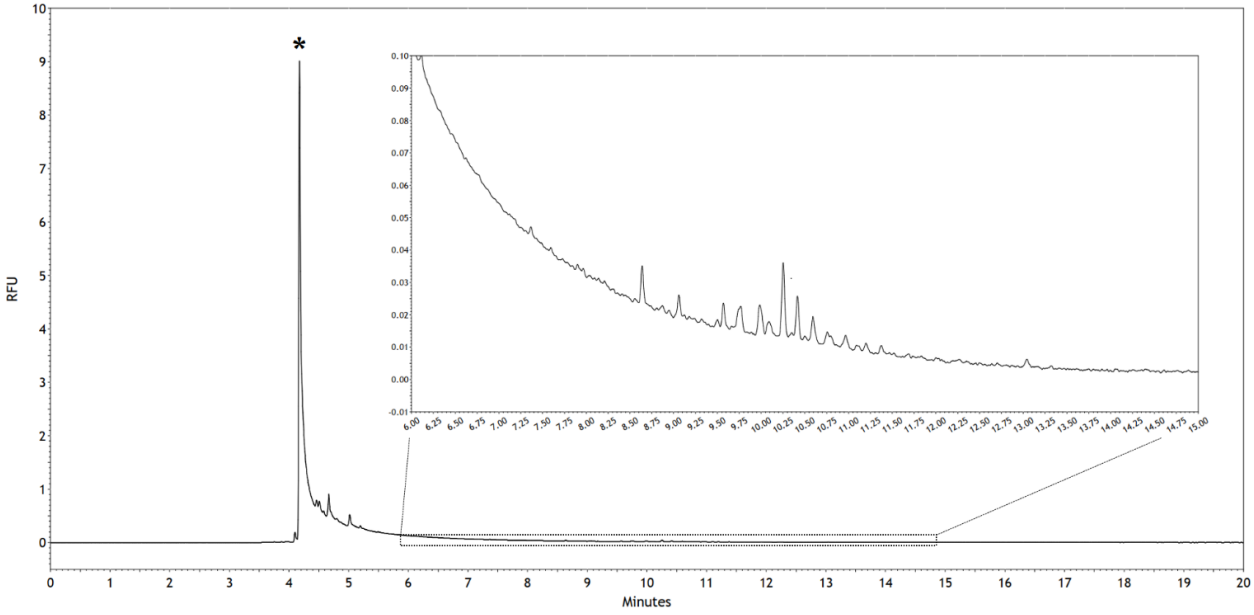

Figure 3.2. CGE-LIF electropherogram displaying the enzymatically released APTS-labeled N-glycan profile derived from a 100 µg PNGase F digest of an H1N1 (A/California/7/2009) vaccine monovalent bulk.* *highlights contribution of un-reacted APTS due to electrokinetic injection bias*

3.2 Optimization of Carboxylated Magnetic Bead-Based Purification of APTS Labeled N-Glycans

Various techniques can be used and have shown to be effective for the removal of salts, proteins, nucleic acids, and excess fluorescent dyes like APTS. HILIC extraction cartridges, gel filtration resins including Sephadex G10 and G25 or DPA-6S normal phase resins have all been successfully implemented for the removal of APTS from labeling reactions.[141-143] There are also several commercial kit options available, however most contain proprietary reagents and can be costly. Resin based purification methods, while effective, commonly require significant user manipulation due to the strict resin pre-equilibration and washing steps, as well as time-consuming

centrifugation steps as most are available in packed column formats. Furthermore, pre-concentration before analysis is typically required due to the large elution volumes after clean up.

Magnetic bead based technologies are another sample purification technique that are commonly used in the field of genomics and proteomics for nucleic acid and affinity purifications, respectively.[144] Recently, magnetic bead-based methods that utilize solid phase reversible interaction (SPRI) mechanisms are becoming increasingly popular for glycan purifications. In 2014, Váradi *et al.* developed a rapid sample preparation technique using magnetic beads for the analysis of mAb glycosylation that has since been commercialized by AB Sciex (Fast Glycan Labeling and Analysis Kit).[145] This method uses carboxyl derivatized magnetic beads in the presence an organic solvent (e.g. acetonitrile) which act as a crowding agent causing the glycans to interact with the surface of the beads (Figure 3.3). There are two possible explanations for the bead-glycan interactions. The first is that in an environment where the concentration of ACN is >80%, hydrophilic interactions dominate and bind the glycans to the binds. The second is that after enzymatic digestion with PNGase F at operating pH (7-8), the resulting glycosylamine is positively charged and is electrostatically attracted to the negatively charged carboxylic acids on the surface of the beads. Although both are possible, the former is likely responsible for the majority of the interactions as the resulting glycosylamines that are formed following PNGase F digestion will hydrolyze into their reducing sugar counterparts and thereby lose the positive charges.

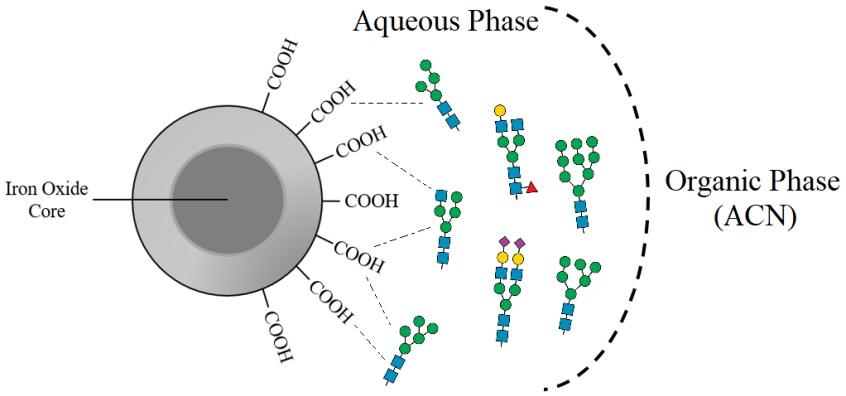

Figure 3.3. Representation of carboxyl derivatized magnetic beads used for the solid phase reversible interaction (SPRI) purification of enzymatically released and labeled N-glycans.

The commercialized Fast Glycan protocol was developed and optimized using model glycoproteins, such as mAbs, because they have relatively simple glycosylation characteristics. Therapeutic mAbs have only two conserved glycosylation sites on the fragment crystallisable (Fc) region and they are both readily accessible to enzymes like PNGase F. In addition to the limited sites, the glycosylation profiles are simple. Due to steric hindrance imparted in the Fc region, key enzymes and glycotransferases have restricted access during processing resulting in glycans without tri- and tetra-antennary structures.[146] In order to test the viability of the magnetic bead-based sample preparation approach for CGE-LIF N-glycan analysis, enzymatically released N-glycans from a commercial therapeutic mAb (Trastuzumab) were APTS-labeled and purified following the vendors protocol. Figure 3.4 shows glycan profile of Trastuzumab obtained using this method. Separations were performed on 20/30 cm x 50µm I.D. bare-fused silica using the proprietary high-resolution separation gel (HR-NCHO) as the electrolyte. Samples were injected electrokinetically in reverse polarity at 2 kV (cathode at injection site) for 2 seconds and separated in reverse polarity at 30 kV for 6 minutes. Detection was achieved by LIF with an excitation (λ_{ex}) and emission (λ_{em}) wavelength at 488 nm and 520 nm, respectively. Glycan identification was performed using the Sciex automated software package that is included in the kit. Using bracketing

standards with varying degrees of polymerization (DP), the software uses the relative migration times of a given peak to calculate its glucose unit (GU) value. Once calculated, using the provided database, it automatically assigns possible glycan structures based on these migration characteristics. As seen in Figure 3.4, the overall simplicity of the mAb glycosylation profile is highlighted. Five main peaks were observed and the proposed glycan structures are displayed with their corresponding calculated GU values. The N-glycan species and relative abundances observed are in accordance with current literature on Trastuzumab N-glycosylation.[147]

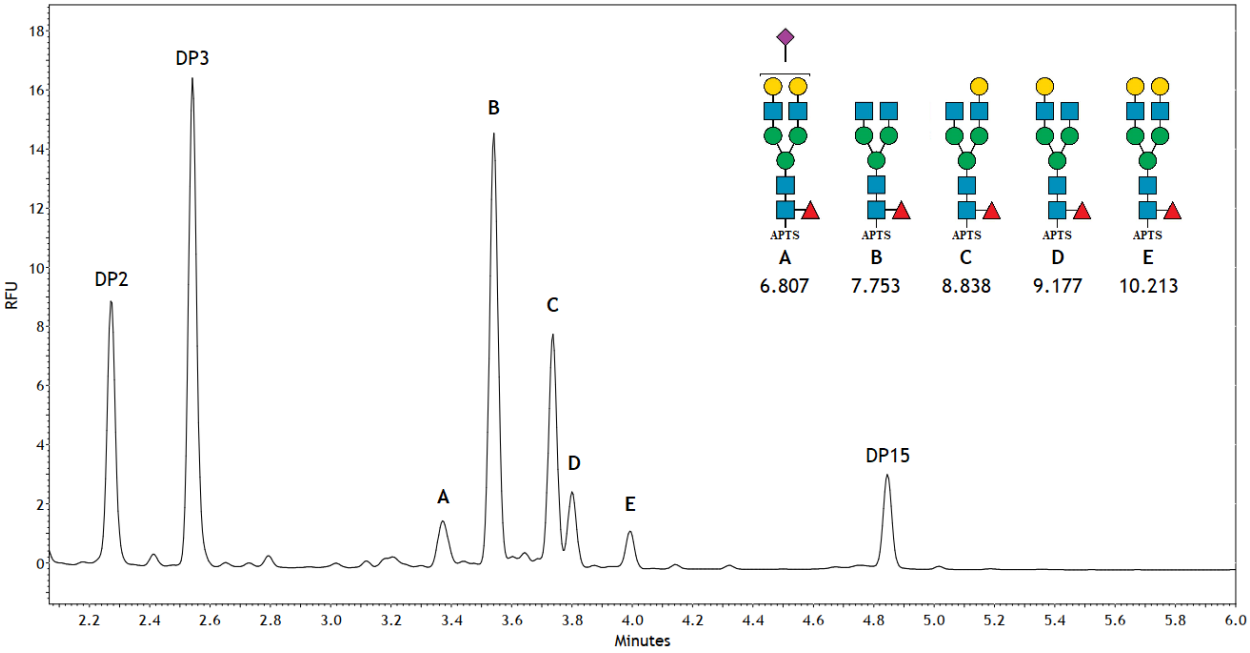

Figure 3.4. CGE-LIF electropherogram displaying the APTS labeled N-glycan profile derived from a 25 µg PNGase F digest of Trastuzumab. Proposed glycan structures with corresponding GU value, (A) A1F (B) G0F (C) G1F (D) G1F' (E) G2F. DP2, DP3, and DP15 represent bracketing standard peaks of oligosaccharides with varying degrees of polymerization (DP).

First attempts at adapting this current methodology for use on more complicated samples like viral glycoproteins (e.g. HA) yielded poor glycan recoveries resulting in low LIF signal intensities (data not shown). It was observed during these preliminary experiments that the solubility of the magnetic beads drastically decreased during the glycan capture step after the enzymatic digestion with PNGase F. In addition to aggregation, the magnetic beads were

irreversibly interacting with the reaction vessel (Eppendorf tube). It was hypothesized that excipients in the sample including Triton X-100 may potentially be competing for interaction with the beads resulting in solubility issues. Therefore, to remove residual Triton X-100, an initial buffer exchange step with LC-MS grade H_2O using an Amicon centrifugal filter (10kDa, MWCO) was implemented. Removal of the excess detergent improved the overall solubility of the magnetic beads resulting in improved glycan recoveries. Figure 3.5 displays the enzymatically released APTS-labeled N-glycan profile of a 25 µg egg-derived H1N1 (A/California/07/2009) HA PNGase F digest. Although recovery was low in these initial experiments, compared to the glycosylation profile obtained from a typical mAb digest (Figure 3.4), there is a significant increase in the amount of peaks present in the released N-glycan profile of HA.

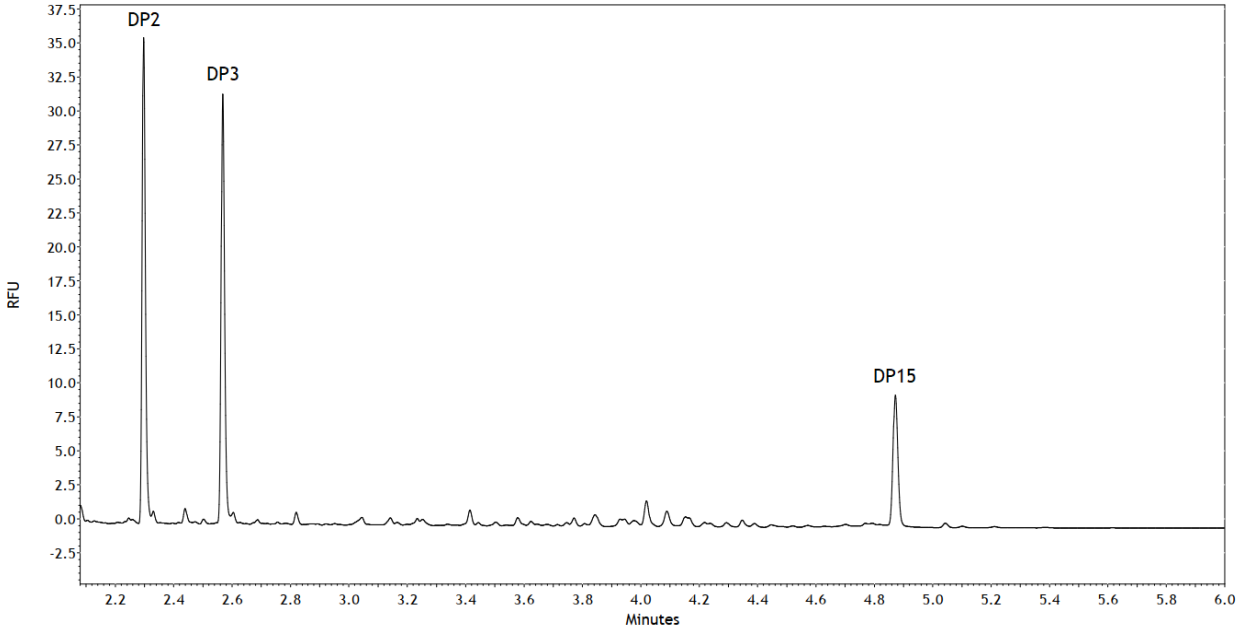

Figure 3.5. CGE-LIF electropherogram displaying the APTS labeled N-glycan profile from a 25 µg PNGase F digest of a H1N1 (A/California/07/2009) egg-derived vaccine monovalent bulk. DP2, DP3, and DP15 represent bracketing standard peaks of oligosaccharides with varying degrees of polymerization (DP).

Although the removal of residual detergent enabled the detection of N-glycans derived from an influenza vaccine monovalent bulk, N-glycan recovery and overall signal intensity

remained low. It was observed that the magnetic bead solubility remained un-optimized, even with the removal of detergent. In the original protocol provided by the vendor, the glycoprotein sample is mixed with the magnetic beads before proceeding with the denaturation/reduction and PNGase F digestion steps. During these steps the magnetic beads are exposed to multiple incubations at elevated temperatures. It was hypothesized that fluctuations between incubation (60^{o}C) and room temperatures affected the overall bead solubility throughout the sample preparation. Since the main function of the magnetic beads is to capture the glycans and clean up the reaction, adding them in at a later step in the protocol would prevent them from being exposed to these initial incubation steps. Therefore after N-glycan release with PNGase F, a magnetic bead-ACN suspension ([ACN] = 97.7%) was added to capture the released N-glycans. By doing this, APTS labeling and clean-up are the only steps remaining in the protocol, therefore exposing the beads to one round of incubation. A comparison of H1N1 HA glycan profiles obtained using (i) the original protocol versus (ii) the modified protocol is depicted in Figure 3.6. An approximate 7-fold increase in peak intensity was observed when using the modified protocol. Additionally, the glycan profile obtained with the modified protocol used 40% less starting material (15 µg) than that was obtained with the original protocol (25 µg). Therefore, our new method increased peak intensity by approximately 10-fold. Moreover, with increased recoveries, the overall complexity of HA glycosylation became immediately evident especially in comparison to that of a mAb.

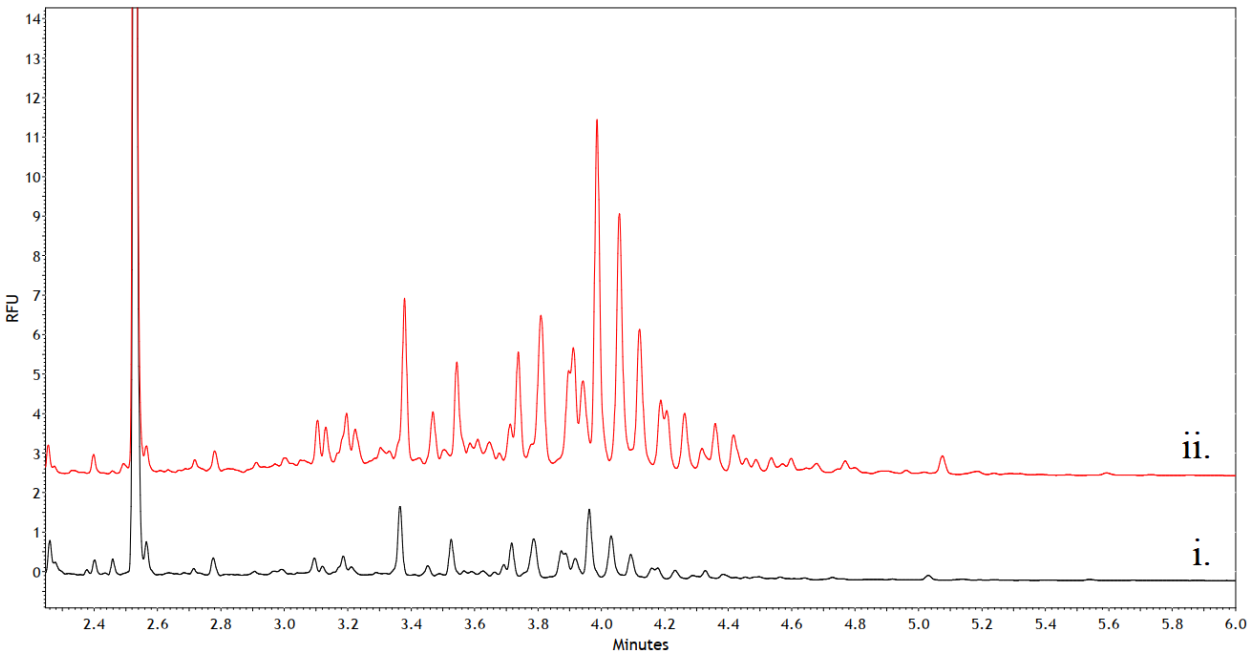

Figure 3.6. CGE-LIF electropherograms of APTS labeled N-glycan profiles obtained from a (i) 25 µg and (ii) 15 µg PNGase F digest of an H1N1 (A/California/07/2009) egg-derived vaccine monovalent bulk. Comparison between (i) original protocol and (ii) modified protocol.

Glycan identification using only CE separations remains challenging without purified standards or comprehensive GU value databases, especially when dealing with highly diverse N-glycan profiles. Therefore as it currently stands, this approach can be used to qualitatively assess enzymatically released N-glycan profiles but for accurate N-glycan identification, mass and structural confirmation using MS is required.

3.3 Assessment of Various MS Compatible BGE Compositions via CZE-LIF

CE separation can be coupled to MS using a variety of configurations which fall within two main categories, sheath-flow or sheathless. As outlined in section 1.5, sheathless CE-MS does not use a sheath liquid to aid in electrospray. Therefore, these types of configurations require volatile BGE's that can facilitate electrospray without the need of a sheath liquid. In general, CE BGE's are high ionic strength, low conductivity buffers commonly containing phosphate, borate,

or TRIS compositions.[148] As a result, most BGE compositions for optimal CE separations are not compatible with MS. The same is true for the BGE in the above-described method, in which a gel-based buffer system is used. Therefore, to couple CE to MS, a compatible BGE composition needs to be investigated.

A sheathless CE-MS configuration is used in this study; therefore, a volatile BGE composition is required to facilitate electrospray. Several groups have successfully demonstrated the use of CE-MS for glycan analysis; however, in most cases a sheath-flow interface is used. As a means of testing separation performance, the BGE compositions used in these studies were investigated further in stand-alone CZE with LIF detection. All experiments were performed on a 40 cm effective length (50 cm total length) PVA-coated capillary with a 50 μm I.D. Samples were injected hydrodynamically by applying 0.5 psi for 10 seconds, resulting in a 9 nL injection volume. Separations were performed by applying 30 kV in reverse polarity (cathode at injection site) for 20 minutes with a capillary cartridge temperature of 20°C.

Gennaro and coworkers (2009)[149] used a sheath-flow CE-MS configuration to investigate sample preparation artifacts from APTS-glycan derivatization reactions. In this method, an Ɛ-aminocaproic acid (ƐACA) with hydroxypropyl methylcellulose (HPMC) BGE composition was used (40 mM ƐACA, pH 4.5 [adjusted with concentrated HAc], 0.2% HPMC). A sheath liquid composed of 50% IPA and 0.2% ammonia was employed to facilitate electrospray. Analysis of enzymatically released APTS-labeled N-glycans was performed in both stand alone CGE using LIF detection and CE coupled to MS. Due to HPMC's incompatibility with MS, it was removed from the final CE-MS BGE composition. As highlighted previously, BGE volatility is crucial with sheathless configurations because there is no sheath-flow to help facilitate and maintain electrospray. This BGE composition was tested at various pH levels and separation performance

was evaluated. A pH value of 4.5, 4.3, 4.0 and 3.8 were tested, with final HAc concentrations of 25, 50, 100, and 150 mM, respectively. Enzymatically released N-glycans derived from 15 µg of an HA (H1N1, A/California/07/2009) influenza vaccine monovalent bulk were APTS labeled and purified using the optimized method described in Section 3.2. As seen in Figure 3.7, based on baseline separation and peak width, the overall separation performance with respect to peak shape and resolution was better with the BGE containing lowest final concentration of HAc (pH 4.5). Consequently, this BGE composition was tested further using the Sciex sheathless CESI-MS interface with a neutral coated OptiMS cartridge, however, electrospray was not able to initiate (data not shown). Therefore, the BGE composition containing the highest amount of HAc (highest overall volatility) was tested as well, and similarly, stable electrospray was not established (data not shown).

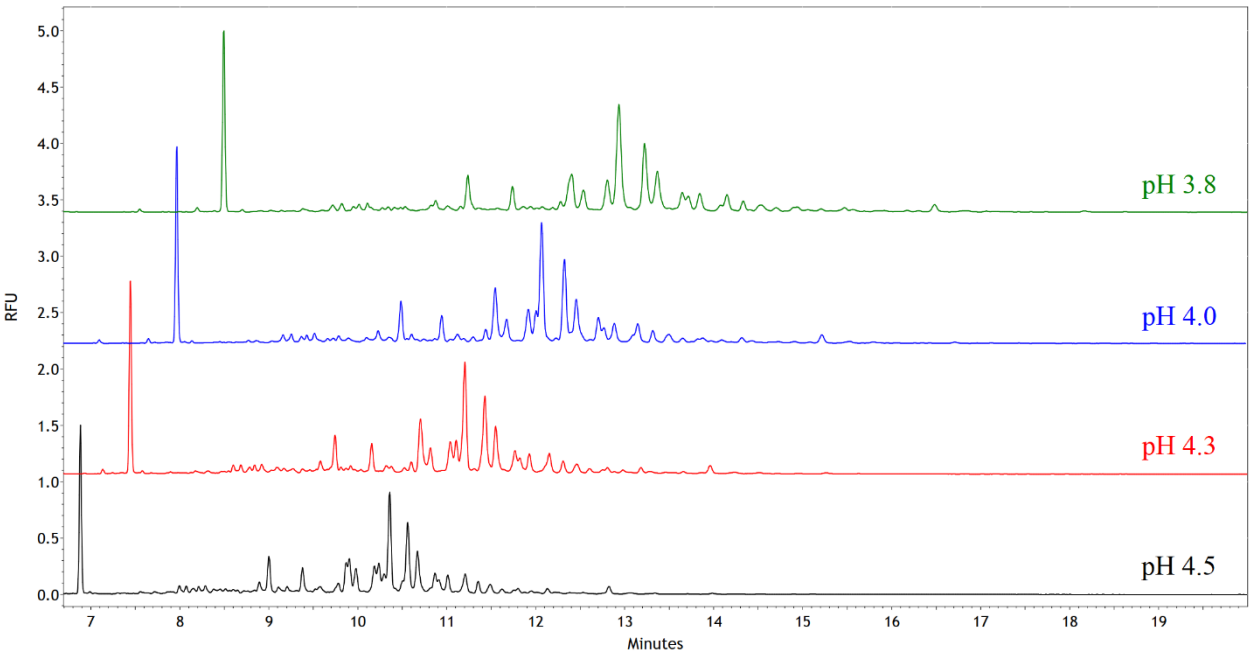

Figure 3.7. CZE-LIF electropherograms of enzymatically released APTS-labeled N-glycan profiles obtained from a 15 µg PNGase F digest of a H1N1 (A/California/07/2009) egg-derived vaccine monovalent bulk. BGE consisted of 40mM ƐACA adjusted to pH 4.5, 4.3, 4.0, and 3.8 concentrated HAc. Samples were injected at 0.5 psi for 10 seconds (~8.9 nL) and separations were performed at 30 kV in reverse polarity (cathode at injection site) for 20 minutes in a 40/50 cm x 50 µm I.D. PVA coated capillary.

Haselberg et al. (2015) [150] used similar final concentrations of HAc (25 mM) on the sheathless interface and was able to obtain stable electrospray. It is possible that the ƐACA component in the previous BGE is not compatible with sheathless CESI-MS applications. Using the same experimental parameters described above, a BGE containing 25 mM HAc at various pH values (adjusted with 0.1 M ammonium hydroxide, AmOH) were tested, and the results are displayed in Figure 3.8. Overall, the peak shape and resolution was enhanced with the addition of AmOH. However, other than minor shifts in migration time, no improvement of separation performance in terms of peak shape and resolution was observed between the BGEs at pH 3.1, 3.2 and 3.3.

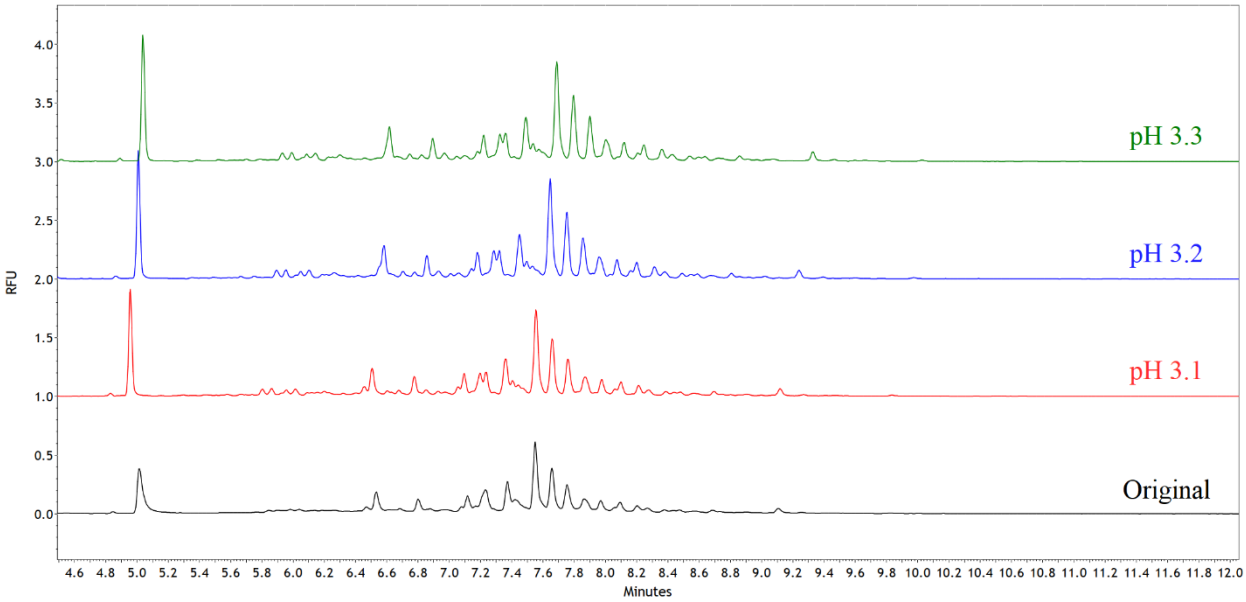

Figure 3.8. CZE-LIF electropherogram of enzymatically released APTS-labeled N-glycan profiles obtained from a 15 µg PNGase F digest of a H1N1 (A/California/07/2009) egg-derived vaccine monovalent bulk. BGE consisted of 25mM HAc adjusted to pH 3.1, 3.2, and 3.3 with 0.1M AmOH. Samples were injected at 0.5 psi for 10 seconds (~8.9 nL) and separations were performed at 30 kV in reverse polarity (cathode at injection site) for 20 minutes in a 40/50 cm x 50 µm I.D. PVA coated capillary.

With the two previously mentioned methods offering promising results, peak resolution still required further improvement. Recently, Jacobson and coworkers (2017) [151] used sheathless

CESI-MS for the analysis and structural identification of APTS-labeled N-glycans derived from serum. The BGE employed was composed of 7.5mM ammonium acetate (pH 4.5) with 10% IPA. This BGE composition was tested using the same method parameters as the previous two methods and separation performance of HA (H1N1, A/California/07/09) derived APTS-labeled N-glycans was evaluated (Figure 3.9). The IPA content affected the overall viscosity of the BGE, which resulted in extended migration times. However, when comparing to the previous BGE compositions, separation performance was exceptional. In particular, the selectivity and peak resolution with respect to minor species was enhanced in comparison to the other methods described (Figure 3.7 & 3.8). This BGE composition has not been previously reported for use of N-glycan profiling by CZE with LIF detection.

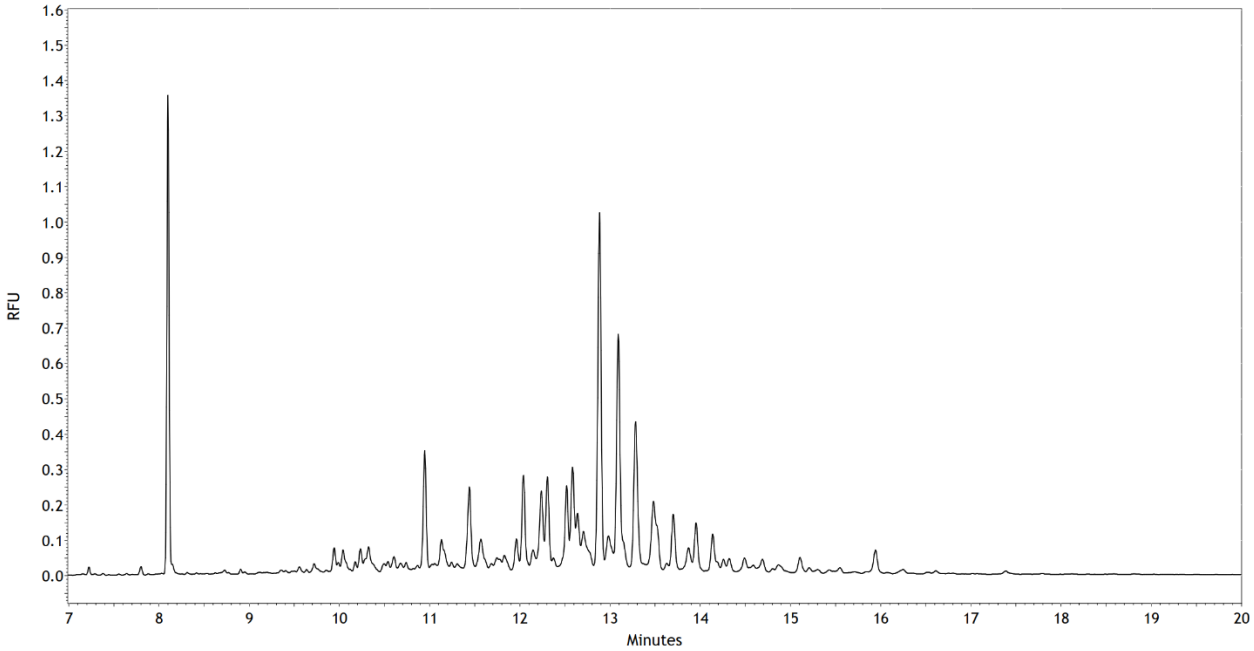

Figure 3.9. CZE-LIF electropherogram displaying the enzymatically released APTS-labeled N-glycan profile obtained from a 15 µg PNGase F digest of a H1N1 (A/California/07/2009) egg-derived vaccine monovalent bulk. BGE consisted of 7.5mM AmAc pH 4.5 (adjusted with 10% HAc) + 10% IPA. Samples were injected at 0.5 psi for 10 seconds (~8.9 nL) and separations were performed at 30 kV in reverse polarity (cathode at injection site) for 20 minutes in a 40/50 cm x 50 µm I.D. PVA coated capillary.

Unlike traditional N-glycan profiling methods, which use gel-based separation buffers, this method offers some unique advantages. For example gel-based separations are restricted to electrokinetic injection, and suffer from injection biases; however this solvent-based method enables hydrodynamic injections to be used. This not only eliminates injection biases but also improves the quantitative capacity of the method because sample depletion is reduced and injection volumes can now be more accurately estimated using the Poiseuille equation (Equation [4]). Where ΔP is the pressure differential across the capillary, r is the inner radius of the capillary, t is the time or injection period, η is the electrolyte viscosity, and L_t is the total length of the capillary.

$$V_c = \frac{\Delta P \pi r^4 t}{8 \eta L_t} \quad [4]$$

Additionally, this CZE-LIF method also minimizes instrument contamination as gel-based buffers have a tendency to polymerize and get deposited on the vial caps which introduce cross contamination into samples or reagents. Gel-based buffers can also accumulate on the electrode and ejector assemblies, which can result in current disruptions and capillary clogging. Therefore, these advantages over traditional gel-based methodologies make it a much more versatile method, and a great method candidate for N-glycan profiling in high-throughput settings, including what would be required for influenza vaccine production. Furthermore, the use of this method is not limited to only profiling influenza N-glycosylation but can also be applied to enzymatically released N-glycans derived from other viral glycoproteins. The SARS-CoV-2 trimeric spike protein is highly glycosylated and contains 66 potential glycosylation sites (22 sites per monomer).[152-153] An APTS-labeled N-glycan profile obtained from a 10 µg PNGase F digest of SARS-CoV-2 spike protein expressed using the freestyle 293 expression system can be seen in Figure 3.10. Unlike with IFVs, coronaviruses including the SARS-CoV-2 virus do not contain

sialidases on their surface, therefore the resulting N-glycans expressed on the spike protein retain sialic acid residues increasing the level of structural diversity. The additional negative charges increase the electrophoretic mobility (charge-to-size ratio) of sialic acid bearing N-glycans, which would explain the increase in relative abundances of early migrating peaks (9.5 - 11.5 minutes). Additionally, the following spike protein samples were produced using recombinant DNA technology, which could further explain the increase in N-glycan microheterogeneity.

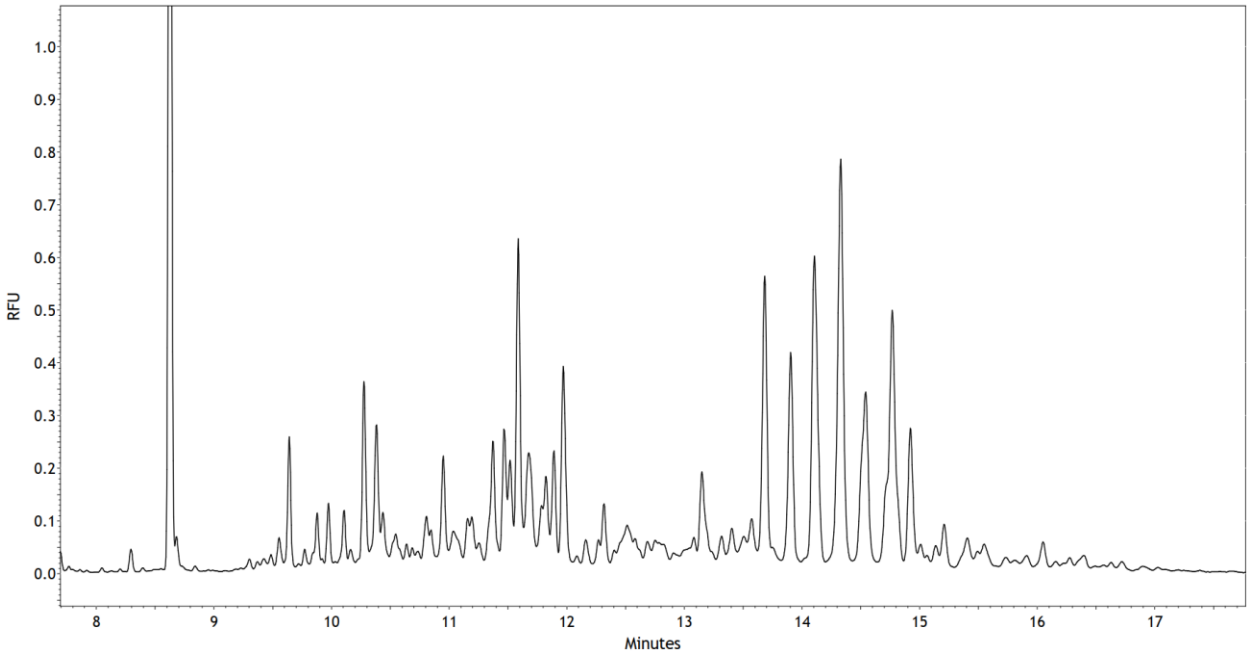

Figure 3.10. CZE-LIF electropherogram displaying the enzymatically released APTS-labeled N-glycan profile obtained from a 10 µg PNGase F digest of SARS-CoV-2 Spike protein expressed using the freestyle 293 expression system. BGE consisted of 7.5mM AmAc pH 4.5 (adjusted with 10% HAc) + 10% IPA. Samples were injected at 0.5 psi for 10 seconds (~8.9 nL) and separations were performed at 30 kV in reverse polarity (cathode at injection site) for 20 minutes in a 40/50 cm x 50 µm I.D. PVA coated capillary.

The developed method has also been used for the evaluation of enzymatically released N-glycan profiles derived from other complex biological samples. Recently published, the CZE-LIF method was used for the qualitative assessment of enzymatically released N-glycans derived from extracellular vesicles (EVs) produced by human bone marrow-derived mesenchymal stromal cells

(hBM-MSCs).[154] EVs were produced using a hollow-fiber cell bioreactor system and the APTS-labeled N-glycan profiles from four hBM-MSC donors were qualitatively assessed at various days of production (day 1, 13, and 25) (Figure 3.11). The utility of the following method has clearly been demonstrated for qualitative assessment of enzymatically released APTS-labeled N-glycan profiles of various complex biological samples. However, accurate structural determination remains challenging, therefore requiring MS coupling.

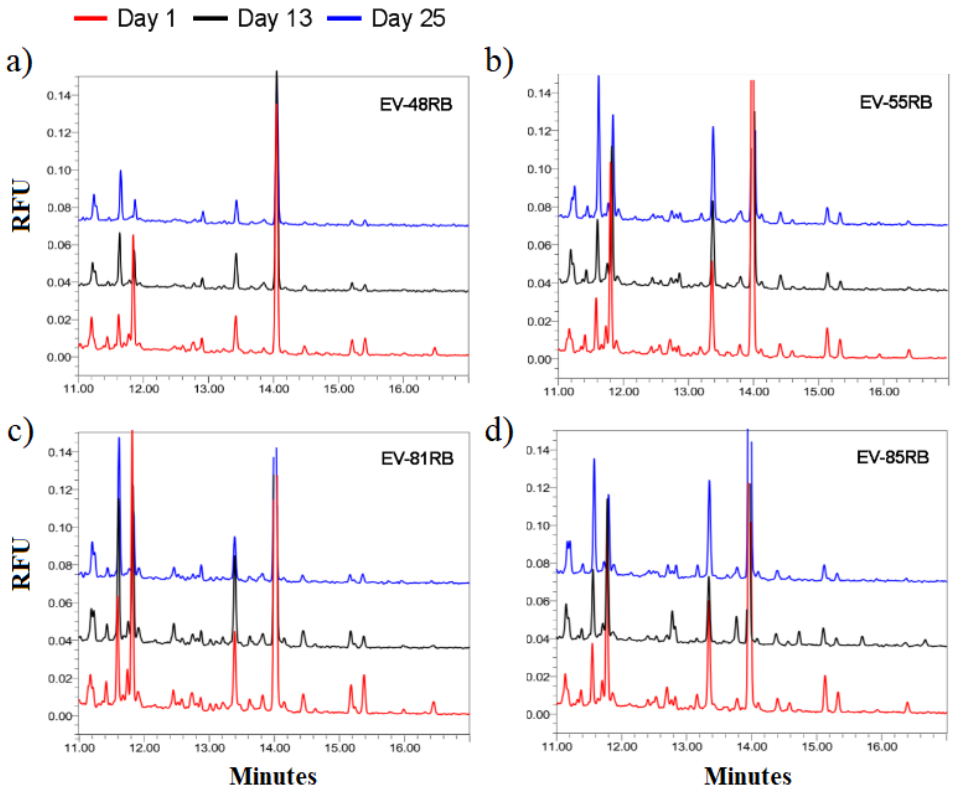

Figure 3.11. Qualitative assessment of APTS labeled N-glycans derived from EVs produced by four hBM-MSC donors (a-d). EVs were produced using a hollow-fiber cell bioreactor system and N-glycan profile assessment was performed at day 1, 13, and 25 of production. Adapted from Gobin *et al.* (2021).[154]

Chapter 4: CESI-MS Method Development for the Analysis of HA N-Glycosylation in Influenza Vaccine Formulations

Following the development of a method for rapid N-glycan fingerprinting of influenza HA, efforts were made to create methods for the structural characterization using sheathless CESI-MS. Jacobson and coworkers (2017) [151] demonstrated the utility of this BGE (7.5mM ammonium acetate, pH 4.5 +10% IPA) on the sheathless CESI-MS platform for glycan characterization and structural elucidation. Initial attempts at transferring the method to the sheathless CESI-MS platform were unsuccessful as quality concerns regarding the specialized capillary cartridges (OptiMS cartridges) required for interfacing the two technologies (as seen in Section 1.5.1) were paramount. Problems ranged from conductivity issues, electrospray establishment and stability problems, as well as frequent capillary clogging. When a functioning capillary was found, the method was applied to a standard APTS-labeled neutral N-glycan mixture. Although stable electrospray was established and conductivity issues seemed to be resolved, no N-glycans were detected (data not shown). After many attempts, the group who published the original method[151] was contacted and it was determined that the neutral coated OptiMS capillaries were not suitable for the analysis of glycans. As privately communicated by their research group, both native and fluorescently labeled N-glycans irreversibly interact the proprietary neutral coating, hence why they primarily used bare-fused silica OptiMS capillaries. This however would be problematic because of the separation mechanisms at play. As displayed in Figure 4.1a, the desired separation mechanism would be similar to the CZE-LIF method outlined in Chapter III. In a neutral-coated capillary, there is no contribution to apparent mobility from EOF and therefore the only driving force with respect to overall migration is the electrophoretic mobility of the analyte. Operating in reverse polarity mode, negatively charged APTS-labeled N-glycans will migrate towards the

positively charged electrode (anode). However, in a system where EOF is now a factor (i.e. bare-fused silica capillaries), reversed polarity separations will result in a counter EOF with respect to negatively charged APTS-labeled N-glycans (Figure 4.1b). This poses a problem, especially in sheathless CESI-MS applications because with EOF being the bulk movement of flow, a counter EOF will result in no electrospray. The Jacobson research group supplemented their CE voltage separation with a high pressure applied to the capillary, which was necessary to facilitate electrospray. However, under these conditions CE loses its most intrinsic property – native separations.

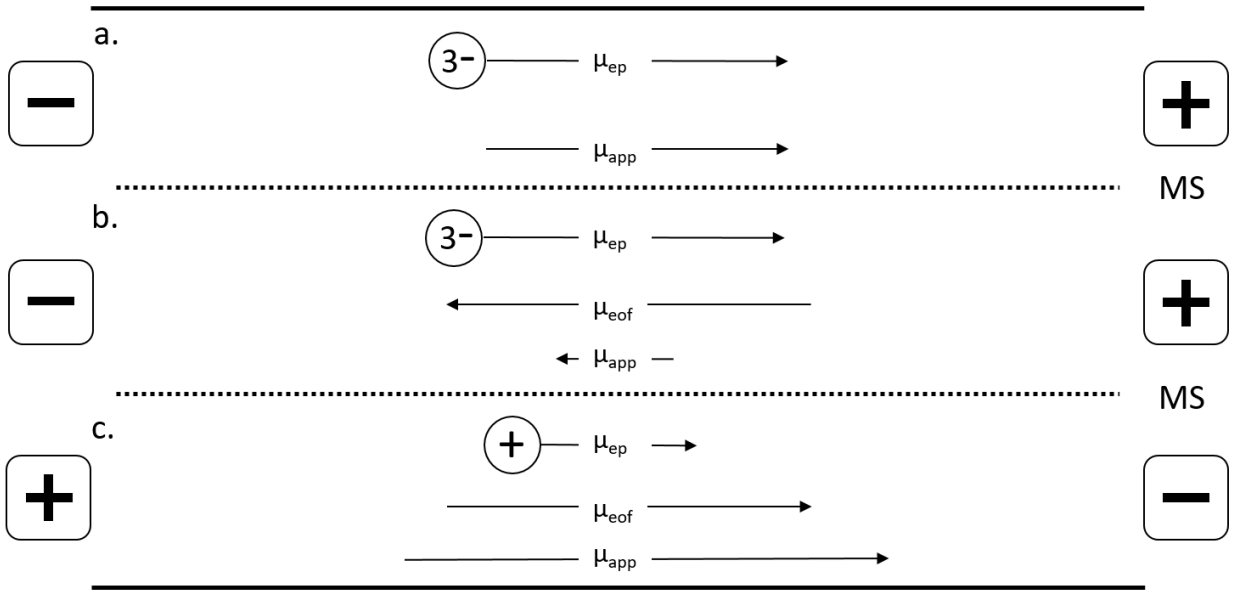

Figure 4.1. CE separation mechanisms displaying direction and migration velocity of μ_{ep}, μ_{eof}, and resultant μ_{app}. (a) Reverse polarity separation mechanism of APTS labeled N-glycans in a neutral (PVA) coated capillary. (b) Reverse polarity separation mechanism of APTS labeled N-glycans in a bare-fused silica capillary. (c) Normal polarity separation mechanism of GT labeled N-glycans in a bare-fused silica capillary.

In addition to separation mechanism limitations, the large excess of labeling reagent required for derivatization can pose problems with MS analysis including ion suppression and source contamination.[155] Furthermore, negative ion mode is also generally less sensitive in

comparison to positive ion mode and MS/MS of N-glycans in negative ion mode yield more complicated spectra making structural interpretation difficult.[156] Therefore, alternative N-glycan derivatization strategies were explored. Manfred Wuhrer's research group from Leiden University developed a sheathless CESI-MS method for the analysis of enzymatically released N-glycans derived from complex biological samples.[157] In this method, released N-glycans were labeled with Girard's Reagent P (GP), a positively charged hydrazide tag (Figure 4.2). This allowed analyses to be performed in positive ion mode, which yielded better sensitivities and simplified MS/MS spectral interpretation due to the generation of predominantly y- and b-series fragment ions. Additionally, separation was performed in normal polarity mode, which improved the overall separation mechanism. Operating in normal polarity (Figure 4.1c), the electrophoretic mobility of the analyte (positively labeled N-glycan) as well as the EOF, have the same migration direction (towards the cathode, MS). This enabled both the detection of the analyte and the resultant EOF provided high enough flow rates to facilitate electrospray without the need of supplemental pressure.

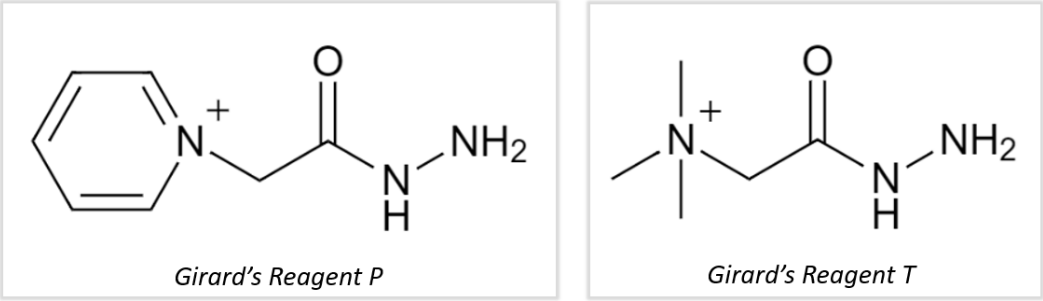

Figure 4.2. Structures of Girard's Reagent P (GP) and T (GT) hydrazide tags.

Currently, there are only two commercially available positively charged hydrazide derivatives (Figure 4.2). The Wuhrer research group used GP in their study and justified their choice based on the sensitivity gains over Girard's Reagent T (GT), as well as potentially being

able to detect GP-derivatized N-glycans with standard optical detection methods like UV absorbance.[157] The overall reaction mechanism is similar to reductive amination with APTS however; no intermediate Schiff base is formed. Additionally, unlike APTS labeling, there is no requirement for large reagent excess, therefore post derivatization clean-up steps are not required and samples can be immediately subjected to MS analysis.[158] Due to the stability of the resultant hydrazone formation, further reduction is not necessary (Figure 4.3). Furthermore, it has been shown recently that N-glycan hydrazone formation chemistry is superior to traditional reductive amination strategies with regards to labeling reaction yields.[158]

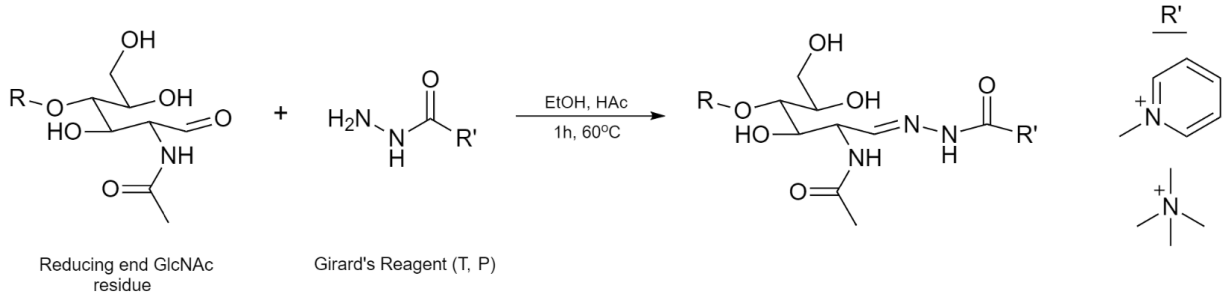

Figure 4.3. Reaction mechanism for the cationic labeling of N-glycans reducing end via Girard's reagent hydrazide tags.

The utility of GP and GT hydrazide tags for sheathless CESI-MS analysis was evaluated by labeling a neutral N-glycan mixture (4.5 μM) and comparing performance. Both samples were labeled using the same solvent conditions (90% EtOH, 10% HAc) and molar ratio of labeling reagent (50 mM).[157] What became immediately evident was the differences in solubility between the two labeling reagents. GP has a much lower solubility in polar organic solvents than GT, which could potentially cause issues downstream with labeling consistencies. For CESI-MS analysis, both the GT- and GP-labeled neutral N-glycan mixtures were injected at 5psi for 60s (50 nL, 225 fmol) and separation was performed at 20 kV (normal polarity) for 45 minutes with a 10% HAc BGE using a bare-fused silica OptiMS capillary. In terms of sensitivity gains, N-glycans labeled

with GP on average showed a 30% increase in sensitivity (peak intensity) over GT-labeled N-glycans (Figure 4.4). Additionally, faster migration times were observed for GP-labeled N-glycans in comparison to GT-labeled N-glycans (29 min vs. 33.5 min), and yielded peaks with higher separation efficiencies. However, due to the decreased solubility of GP, GT was used as the primary labeling reagent for the remainder of the study. Furthermore, sheathless CESI-MS analysis of enzymatically released GT-labeled N-glycans derived from influenza HA has never been explored or published previously, further enhancing the novelty of this application.

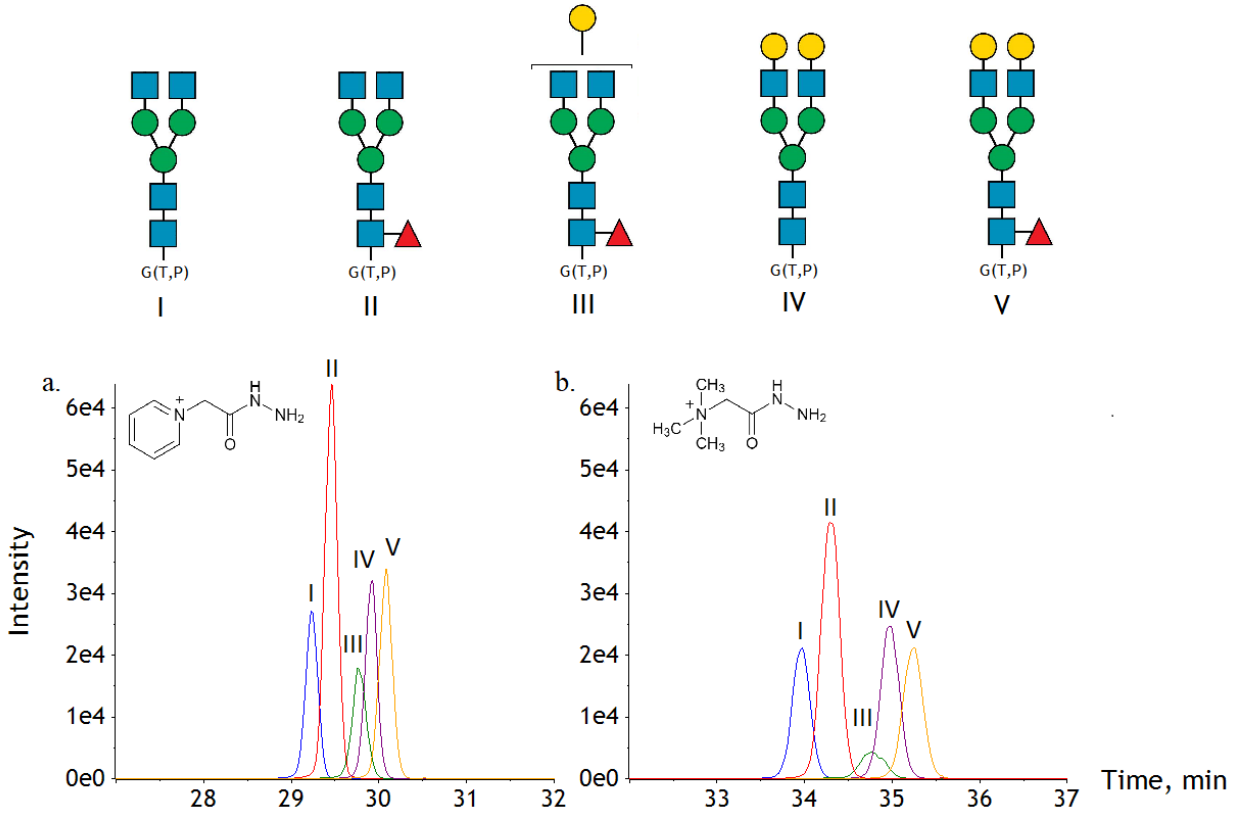

Figure 4.4. CESI-MS XIC's of a neutral N-glycan mixture labeled with (a) GP and (b) GT. The neutral N-glycan mixture consisted of (I) G0, (II) G0F, (III) G1F, (IV) G2 and (V) G2F N-glycans.

4.2 Filter-Aided Sample Preparation for Sheathless CESI-MS Analysis of GT-Labeled N-Glycans

Sample preparation approaches for N-glycan release and labeling commonly involve the use of various detergents that are not MS compatible. Traditionally, detergents including SDS and

NP-40 are used to assist with glycoprotein denaturation and subsequent PNGase F digestion, however, these detergents are difficult to remove and therefore typically avoided in sample preparations intended for MS-based analyses.[159]

Filter-aided sample preparation (FASP) approaches are widely used in the field of MS based glycoproteomics as they help minimize sample preparation artifacts and increases throughput capabilities. [160-162] Van Cott and coworkers (2010) developed a quantitative FASP approach for the analysis of enzymatically released N-glycans via MALDI-TOF.[161] Using their method as a starting point, a modified version was developed and adopted as a viable sample preparation approach for sheathless CESI-MS applications. Figure 4.5 outlines the complete sample preparation protocol from (a) initial glycoprotein buffer exchange, (b) reduction, alkylation and PNGase F digestion, (c) glycan isolation and hydrazide labeling, and (d) sample reconstitution for sheathless CESI-MS analysis.

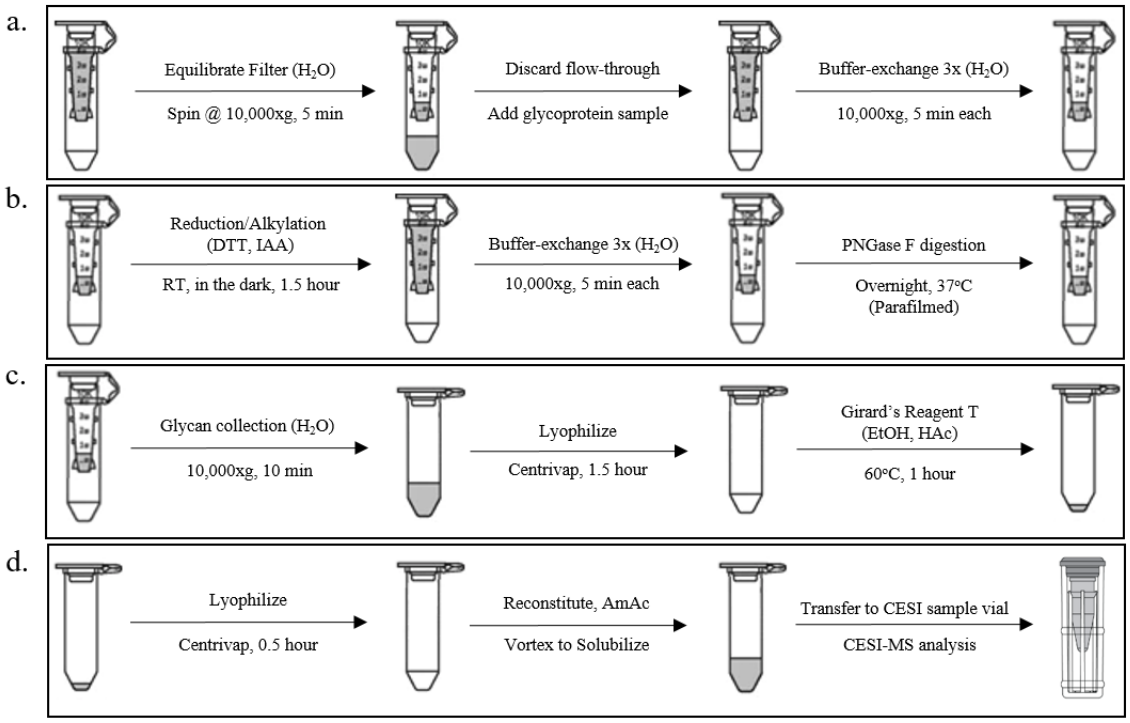

Figure 4.5. Filter aided sample preparation (FASP) for sheathless CESI-MS analysis of enzymatically released GT-labeled N-glycans.

4.3 Information Dependent Acquisition Switch Criteria Optimization

An un-targeted MS-based approach was used in this study via information dependent acquisition (IDA). With this type of analysis, various data dependent criteria are specified prior to sample analysis. The main criteria include *m/z* range, ion intensity threshold, and ion charge state. During analysis, if an ion is detected in the survey scan (TOF-MS^+) that falls within the pre-set criteria, additional experiments are triggered. In this case, a product ion scan (dependent scan) is performed and a subsequent MS/MS spectrum is generated.

Following the sample preparation protocol outlined in Section 2.3, enzymatically released GT-labeled N-glycans derived from an influenza HA (H3N2, A/Kansas/14/2017, 10 µg) vaccine monovalent bulk were used for IDA optimization. The released GT-labeled N-glycan samples were injected hydrodynamically at 5 psi for 60 seconds, resulting in a total injection volume of 50 nL (~26 mm plug length) and separated at 20 kV (normal polarity) for 60 minutes. An example sheathless CESI-MS current trace (10%HAc) from one of these separations can be seen in Figure 4.6.

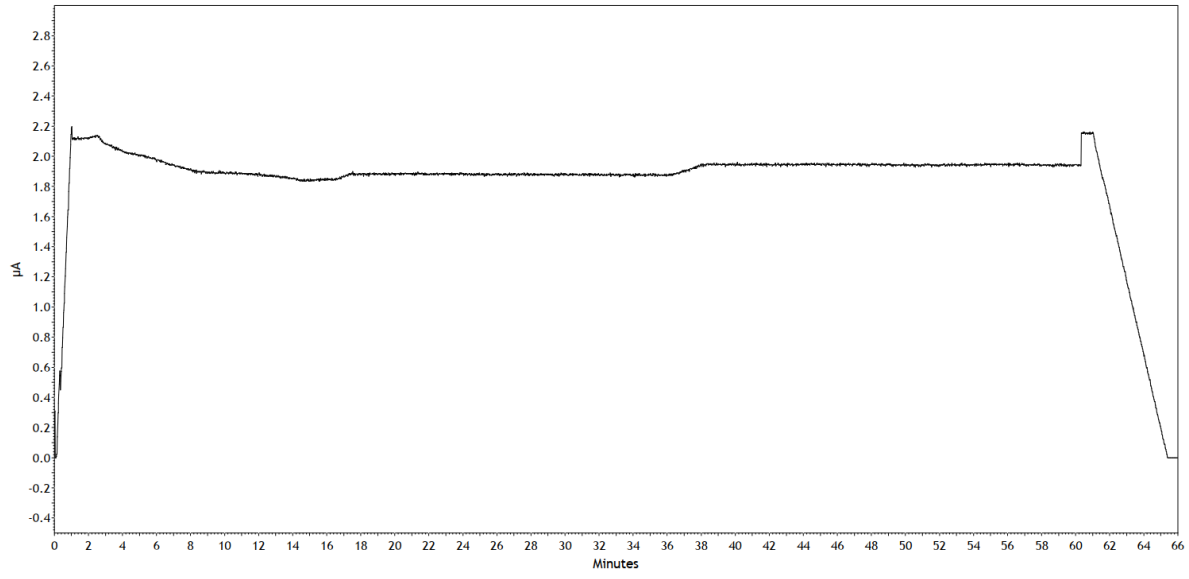

Figure 4.6. Representative current trace for a typical sheathless CESI-MS experiment using 10% HAc BGE.

To establish a baseline, initial experiments were performed with broad IDA switch criteria. For example, 20 candidate ions per cycle with *m/z* values over 100, intensities greater than 100 counts, and bearing charge states between +2 and +4 were selected for MS/MS experiments. Consequently, this resulted in poor quality product ion spectra; therefore, further refinement of the IDA criteria was necessary. Lowering the potential candidate ions per cycle to 10 and increasing the ion intensity threshold to 250 counts greatly enhanced product ion spectral quality. Additionally, the use of a rolling collision energy with an energy spread of 10 eV (±5 eV) provided further enhancement. This is because optimal collision energies were calculated in real-time based on the properties (*m/z* and charge) of each individual target ion, allowing for more complete fragmentation. Although MS/MS spectral quality was improving, it was observed that most observed ions with charge states above +2 yielded similar fragmentation patterns to abundant co-migrating species. Interestingly, based of monoisotopic mass it was determined that the majority of these highly charged ions were GT-labeled N-glycan multimers, and were primarily of high mannose type. An example of this can be seen in Figure 4.7. Along with the predominant $[M+H]^{2+}$ ion, $[2M+H]^{3+}$, $[3M+H]^{4+}$, and $[4M+H]^{5+}$ ions were also observed.

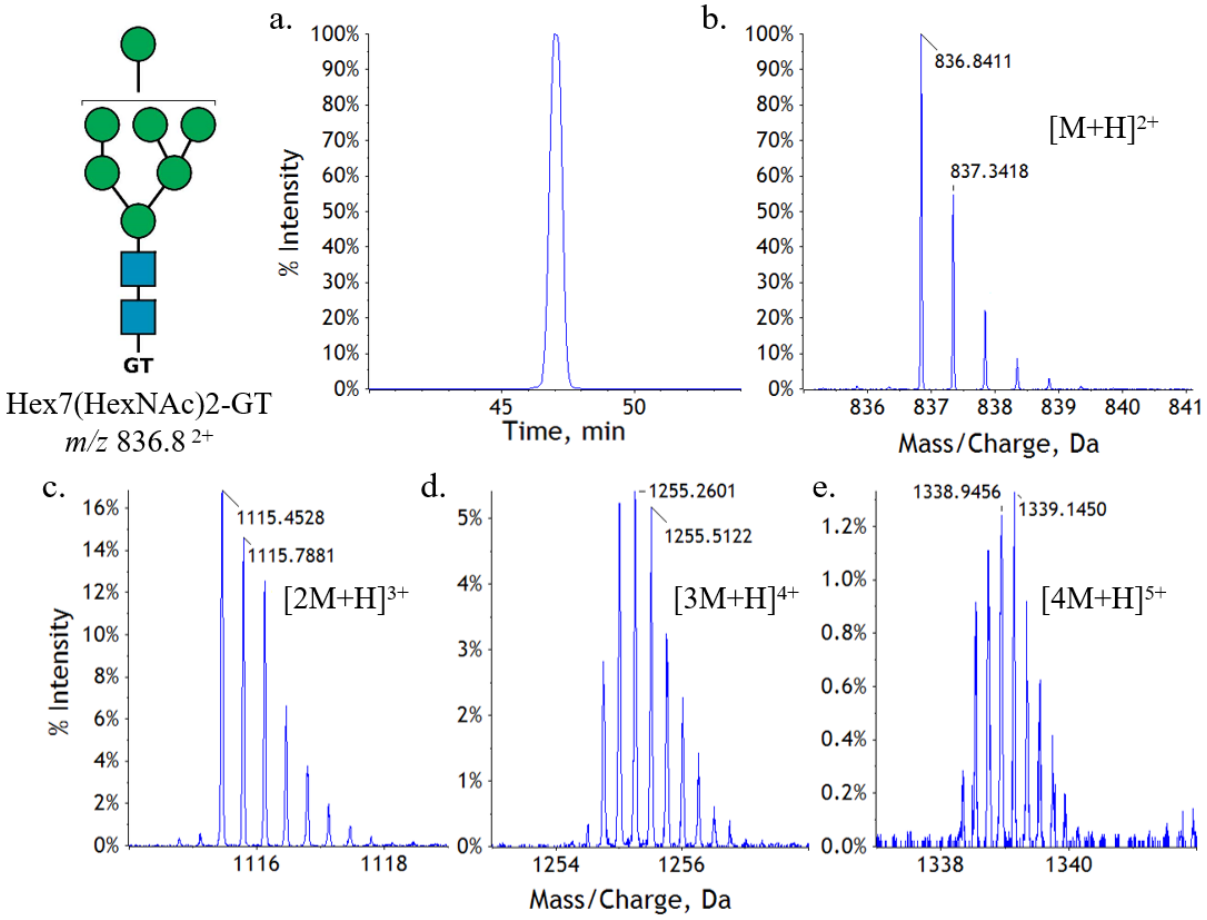

Figure 4.7. Observed multimer formation of *m/z* 836.8 $^{2+}$. (a) XIC of *m/z* 836.8 $^{2+}$. MS spectra of (b) $[M+H]^{2+}$ and multimers (c) $[2M+H]^{3+}$, (d) $[3M+H]^{4+}$, and (d) $[4M+H]^{5+}$

Similar to adduct formation, gas-phase formation of multimers is a common phenomenon in ESI.[163] Adjusting specific source parameters including curtain gas flow rates and temperatures can help reduce multimer formation.[164] However, these types of modifications would be detrimental to the spray stability in sheathless CESI-MS applications, primarily due to the sensitive nature of the porous tip (ESI emitter). Due to the ultra-low flow rates achieved in sheathless CESI-MS applications (10-20 nL/min), increasing source temperatures too high would result in rapid desolvation rates, leading to spray inconsistencies. Furthermore, if curtain gas flow rates are too high it can cause the porous tip (~35 µm outer diameter) to move, adding to the spray fluctuations. Optimizing declustering potentials can also help reduce ion clustering but no improvement was

observed when varying between 40-120V. The use of organic modifiers have also been investigated previously but their ability to reduce multimer formation remains inconclusive.[164] To further investigate this, ACN was chosen as an organic modifier and spiked into the sample at a final concentration of 10% to see if the degree of multimerization was affected during CESI-MS analysis. As seen in Figure 4.8, the addition of ACN (10%) to the sample decreased overall multimer formation by approximately 35% with respect to overall peak intensity. Higher concentrations of ACN were tested but offered no additional reduction in multimer formation and began negatively impacting the sensitivity of the main $[M+H]^{2+}$ species. In addition to its effect on multimer formation, ACN had some additional benefits that were observed and are explained in the subsequent section (4.4). Unfortunately, multimer formation is a common unavoidable occurrence in ESI-MS studies; therefore, with no success at completely eliminating multimeric ion formation, for the purpose of this study the IDA parameters were adjusted accordingly to only focus on target ions with a +2 charge state.

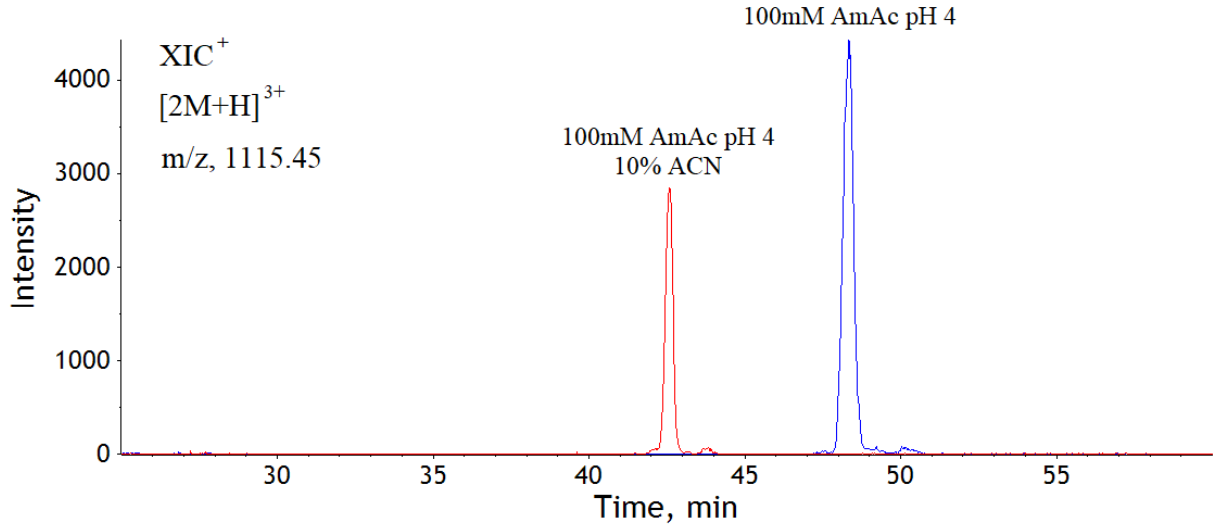

Figure 4.8. CESI-MS XIC's of *m/z* 1115.45 $^{3+}$ $[2M+H]^{3+}$ multimer with and without ACN sample spike in red and blue, respectively.

4.4 Acetonitrile Field-Amplified Sample Stacking

In addition to a reduction in observed multimeric ions, ACN addition provided some additional benefits with respect to GT-labeled N-glycan peak shape, sensitivity and product ion spectral quality. Sample stacking is a common technique used in CE applications, wherein the sample being analyzed is diluted with a lower ionic strength buffer in comparison to the BGE.[106] In doing this, the electrical resistance and resultant electric field across the injected sample plug is higher than the surrounding electrolyte. This causes the ions within the sample plug to move faster towards the electrolyte boundary (lower electric field) and concentrate or "stack" into zones, resulting in high efficiency separations with increased sensitivity.

ACN as an organic modifier to enhance sample stacking has been used in a variety of CE applications.[165-168] The improvements observed herein is likely explained by field-amplified sample stacking (FASS). By adding ACN to the sample matrix, the conductivity is further reduced thereby increasing the resultant electric field across the injected sample plug. As seen in Figure 4.9, ions corresponding to GT-labeled high mannose N-glycan species were extracted and the effect of ACN addition was evaluated. Not only did the overall peak shape improve, but the efficiency and sensitivity also increased (Figure 4.9, i). Additionally, the sharper peak profiles provided further enhancement to MS/MS spectral quality because IDA dependent scans were being triggered at higher ion intensities (Figure 4.9, ii & iii). This enhancement was particularly important for the analysis of low and trace abundance GT-labeled N-glycans as prior to the addition of ACN, MS/MS spectral quality was low due to decreased ion intensities.

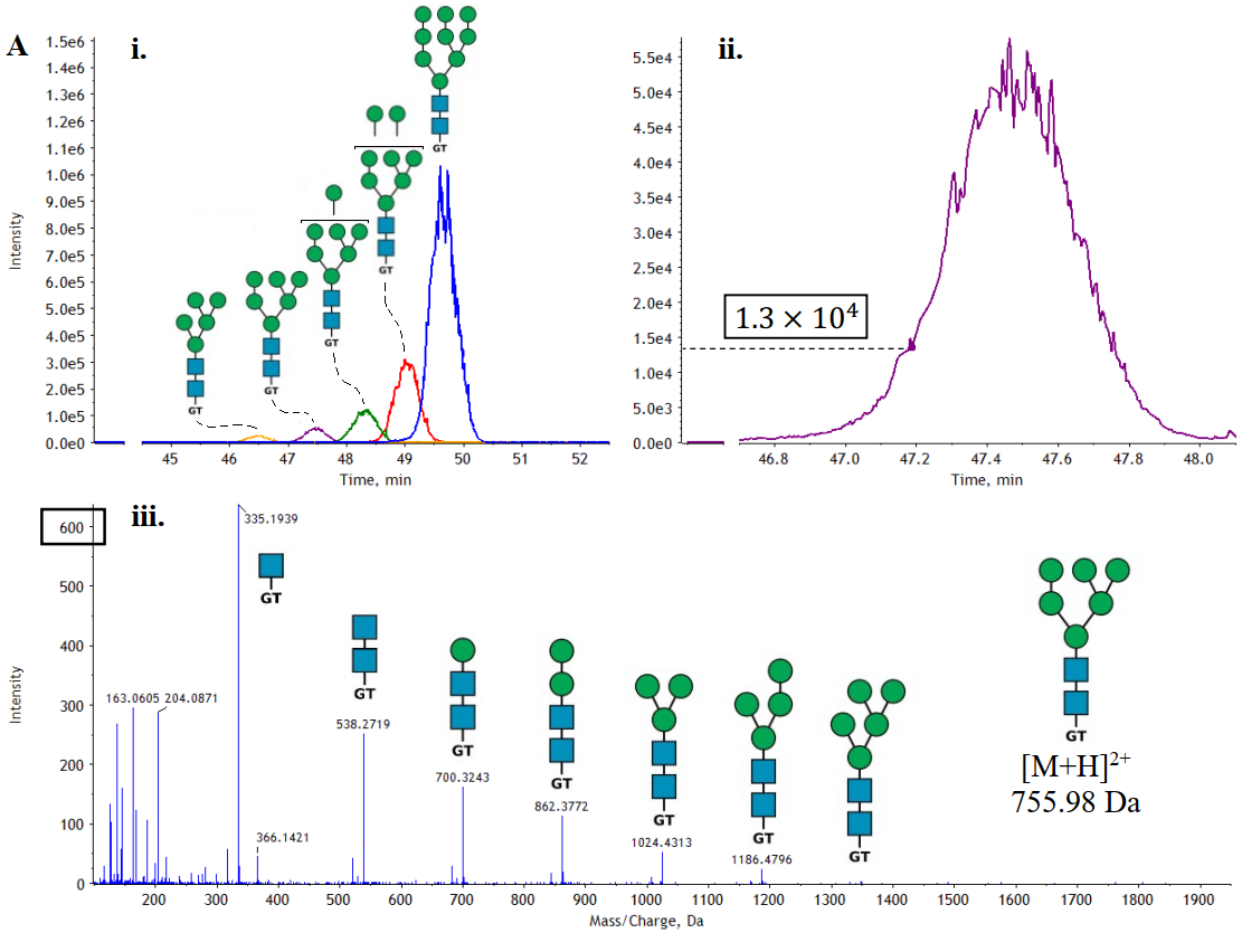

Figure 4.9. CESI-MS of a GT-labeled high-mannose N-glycan mixture varying sample buffer (A) 100mM AmAc pH 4.0 (B) 100mM AmAc pH 4.0 + 10% ACN(i) XICs of GT-labeled high-mannose N-glycan mixture (ii) XIC of *m/z* 755.98 $^{2+}$, (iii) MS/MS spectrum of precursor ion *m/z* 755.98 $^{2+}$.

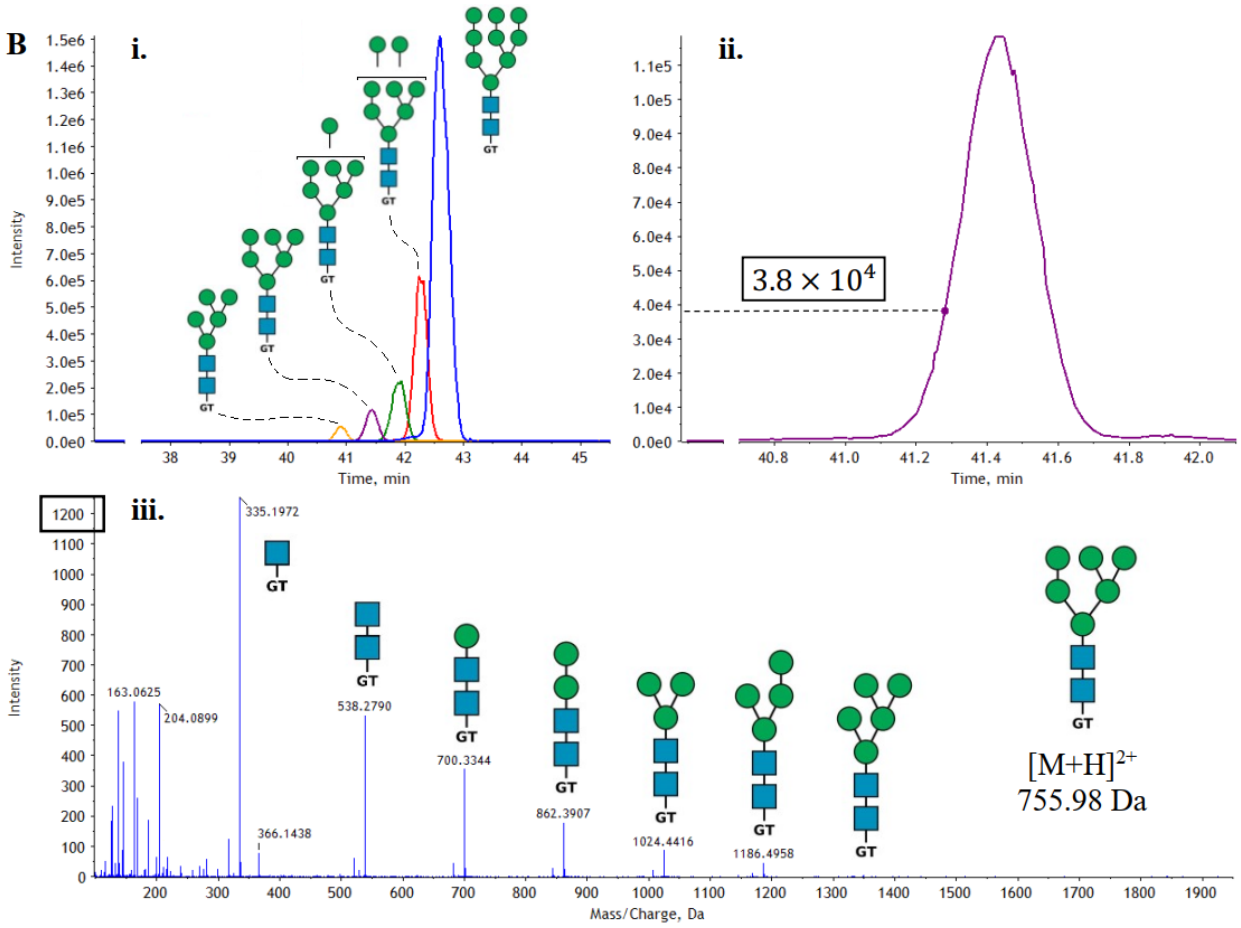

Figure 4.9 Continued. CESI-MS of a GT-labeled high-mannose N-glycan mixture varying sample buffer (A) 100mM AmAc pH 4.0 (B) 100mM AmAc pH 4.0 + 10% ACN(i) XICs of GT-labeled high-mannose N-glycan mixture (ii) XIC of *m/z* 755.98 $^{2+}$, (iii) MS/MS spectrum of precursor ion *m/z* 755.98 $^{2+}$.

4.5 Spectral Interpretation & GT-Labeled N-Glycan MS/MS Structural Elucidation

The analysis of enzymatically released enzymatically released GT-labeled N-glycans via sheathless CESI-MS yielded primarily doubly charged species with a split signal between protonated and ammoniated ion adducts, $[M+H]^{2+}$ and $[M+NH_4]^{2+}$, respectively, which impacted the sensitivity of the MS-based analyses (Figure 4.10). Unfortunately, adduct ion formation is a common and typically unavoidable occurrence in ESI-MS analyses as it can arise from several sources including impure solvents, contaminated glassware and certain mobile phase additives.[169]

In this case, the sample matrix containing 100 mM ammonium acetate explained the presence of the ammoniated species. Alkali metal salts adducts (Na^+ & K^+) are also commonly observed in ESI-based studies, and can further impact sensitivity, however, were not observed in this work. This can be explained by two reasons, (1) the filter-aided approach used in this study effectively desalted the sample prior to sheathless CESI-MS analysis, reducing sodium and potassium contribution and (2) the use of ammonium acetate in the sample matrix competed with alkali metal salts for adduct ion formation.

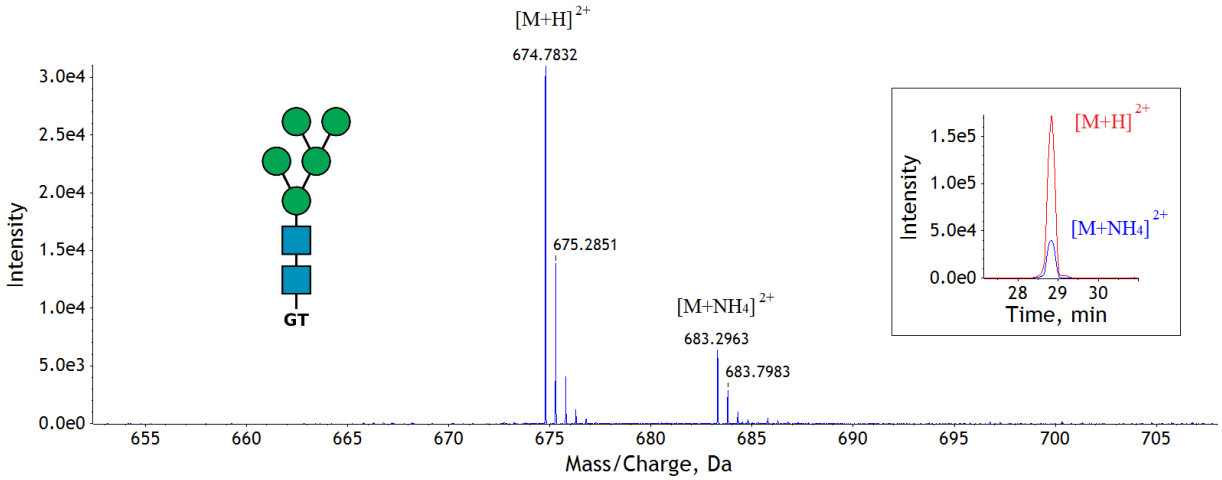

Figure 4.10. CESI-MS spectra of a GT-labeled high-mannose N-glycan (*m/z* 674.78 $^{2+}$) displaying split signal between protonated and ammoniated ion adducts, $[M+H]^{2+}$ and $[M+NH_4]^{2+}$, respectively. Representative XIC's for each ion-adduct are displayed in the figure inlay.

Upon fragmentation, GT-labeled N-glycans produce a series of characteristic ions that aid in structural interpretation. As outlined in section 1.4.5, when fragmented via CID in positive ion mode, N-glycans dissociate at their glycosidic linkages yielding primarily y- and b-series fragment ions; among others. The y-ion series consists of fragments wherein the positively charged GT label on the reducing end is retained. In Figure 4.11, the major y- and b-ions are shown. Sequential fragmentation from the terminal end of GT-labeled N-glycans resulted in the neutral loss of 162.05, 203.08, and 146.06, which corresponds to the monoisotopic mass of mannose/galactose,

N-acetylglucosamine (GlcNAc), and fucose monosaccharide residues, respectively (Figure 4.12). The y-ion detected at *m/z* 335.19 $^{1+}$ corresponds to the reducing end GlcNAc labeled with GT and with core-fucosylation yielded an ion at *m/z* 481.25 $^{1+}$. The presence of a bisecting GlcNAc was indicated by y-ions at *m/z* 1049.46 $^{1+}$ and 903.40 $^{1+}$, representing bisecting glycans with or without core fucosylation, respectively.

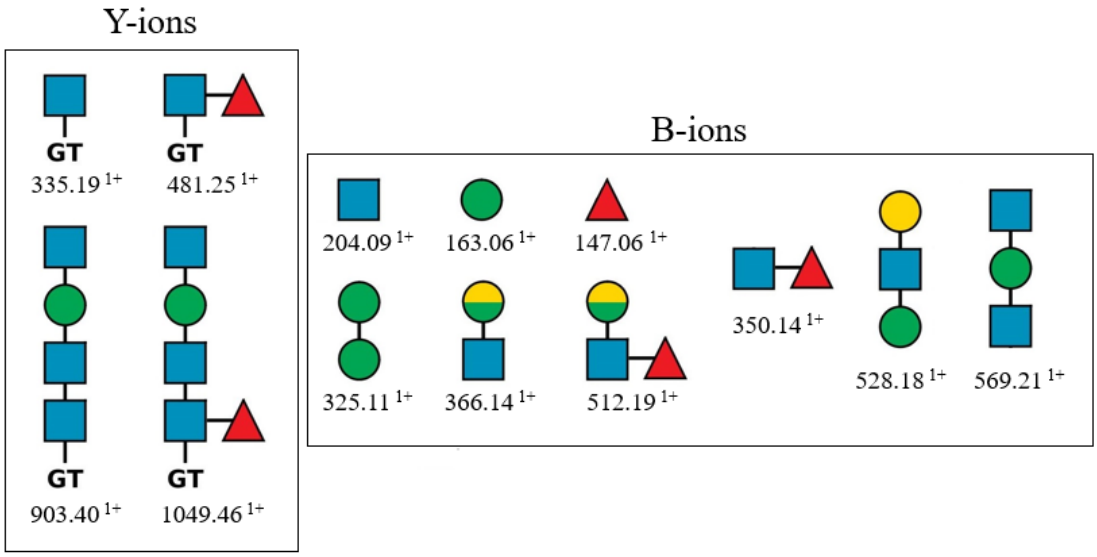

Figure 4.11. Proposed structures of GT-labeled N-glycan y-ions and b-series oxonium ions. N-acetylglucosamine, mannose, galactose, and fucose residues are represented as blue squares, green circles, yellow circles, and red triangles, respectively.

The b-ion series, also commonly referred to as oxonium ions, consisted of fragments in which the charge was retained on the terminal end of the glycan. B-ions at *m/z* 204.09 $^{1+}$, 163.06 $^{1+}$, and 147.06 $^{1+}$ correspond to GlcNAc, mannose/galactose and fucose oxonium ions, respectively. Additional diagnostic fragments including ions at *m/z* 350.14 $^{1+}$, 512.19 $^{1+}$, 528.18 $^{1+}$ aided in determining the presence of terminal galactosylation and fucosylation. Several other characteristic ions were also present in CID-based analyses of GT-labeled N-glycans including dehydrated species and additional cross-ring fragments (i.e. *m/z* 138.05 $^{1+}$) (Figure 4.13).

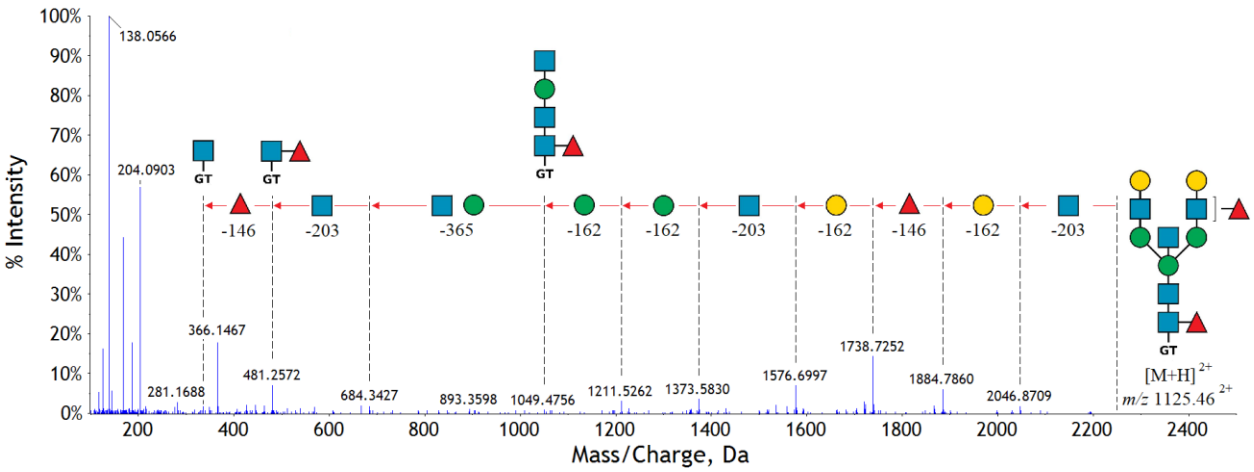

Figure 4.12. CESI-MS/MS spectra of precursor ion *m/z* 1125.46 $^{2+}$. Displaying neutral loss of mannose (162), galactose (162), N-acetylglucosamine (203), and fucose (146) monosaccharide residues. Core-fucosylation with GlcNAc bisection indicated by fragment ion at *m/z* 1049.47 $^{1+}$.

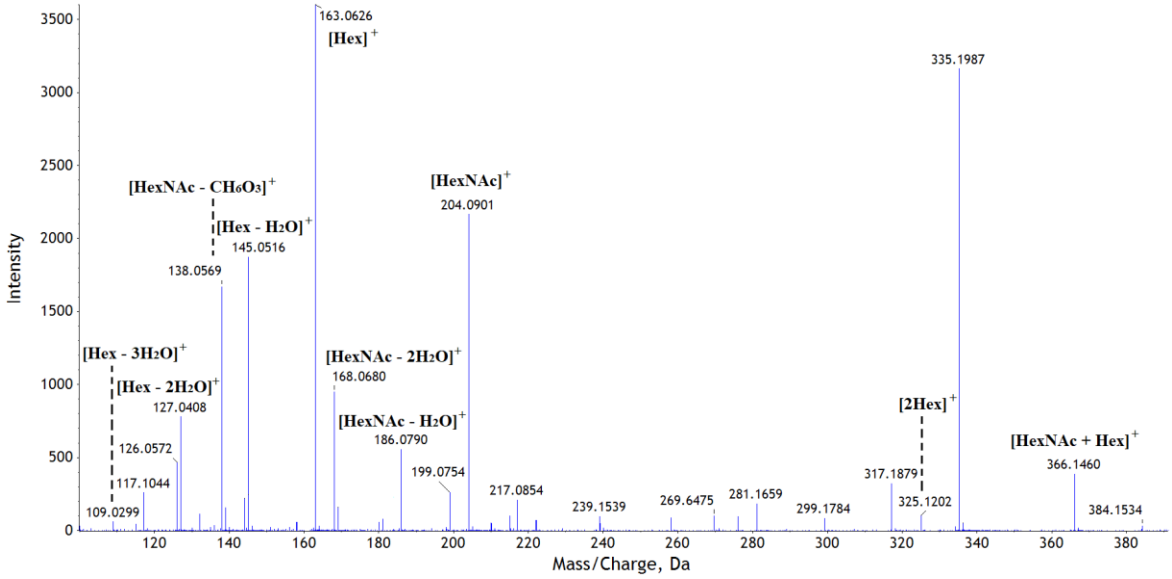

Figure 4.13. CESI-MS/MS spectra of precursor ion *m/z* 674.78 $^{2+}$ displaying common b-series oxonium ion fragments.

With an optimized sheathless CESI-MS method established for the analysis if enzymatically released GT-labeled N-glycans derived from influenza vaccine monovalent bulks, sampling size can be increased for further evaluation.

Chapter 5: Assessment of Influenza Vaccine Glycosylation from Different Manufacturers Using Orthogonal CZE-LIF and Sheathless CESI-MS Methods

5.1 Assessment of HA Content in Influenza Vaccine Monovalent Bulk Samples via RP-HPLC

With both methods established, N-glycosylation of HA content in influenza vaccine monovalent bulks from three different manufacturers was assessed (Table 5.1). For the remainder of the study, egg-derived H3N2 (A/Kansas/14/2017) HA vaccine monovalent bulks were analyzed. In addition to H3N2 viruses being seemingly more prone to egg-adaptations during vaccine production, these samples were also chosen due to their differences in receptor-binding affinities determined by our in-house receptor-binding/RP-HPLC assay.[52, 170] Each H3N2 monovalent bulk displayed receptor-binding affinities ranging from 40% to 94% (Table 5.1). Considering the effect of N-glycosylation on HA receptor binding, the binding affinity spread exhibited by these samples made them excellent candidates for assessment of enzymatically released N-glycans via CZE-LIF and CESI-MS.

Table 5.1. Egg-derived H3N2 (A/Kansas/14/2017) vaccine monovalent bulk information for three manufacturers.

Manufacturer	Strain	HA Concentration* (µg/mL)	Binding Affinity (%)
A	H3N2 A/Kansas/14/2017	205	71
B		223	94
C		286	40

**Manufacturer provided concentrations determined by SRID*

Prior to analysis, the amino acid sequence of the A/Kansas/14/2017 H3N2 strain was retrieved through the GISAID (Global Initiative on Sharing Avian Influenza Data) EpiFlu database with accession number EPI_ISL_346457. To get a better understanding of the degree of glycosylation of H3, potential N-glycosylation sites were predicted using the NetNGlyc 1.0 web server (Figure 5.1A). A total of 10 potential N-glycosylation sequons were identified and their

locations with respect to the HA1 and HA2 domains are depicted in Figure 5.1B. Amino acid positions 24, 38, 54, 61, 262, 301, and 499 are all located on the stalk region. Whereas positions 79, 149, and 181 are located on the globular head.

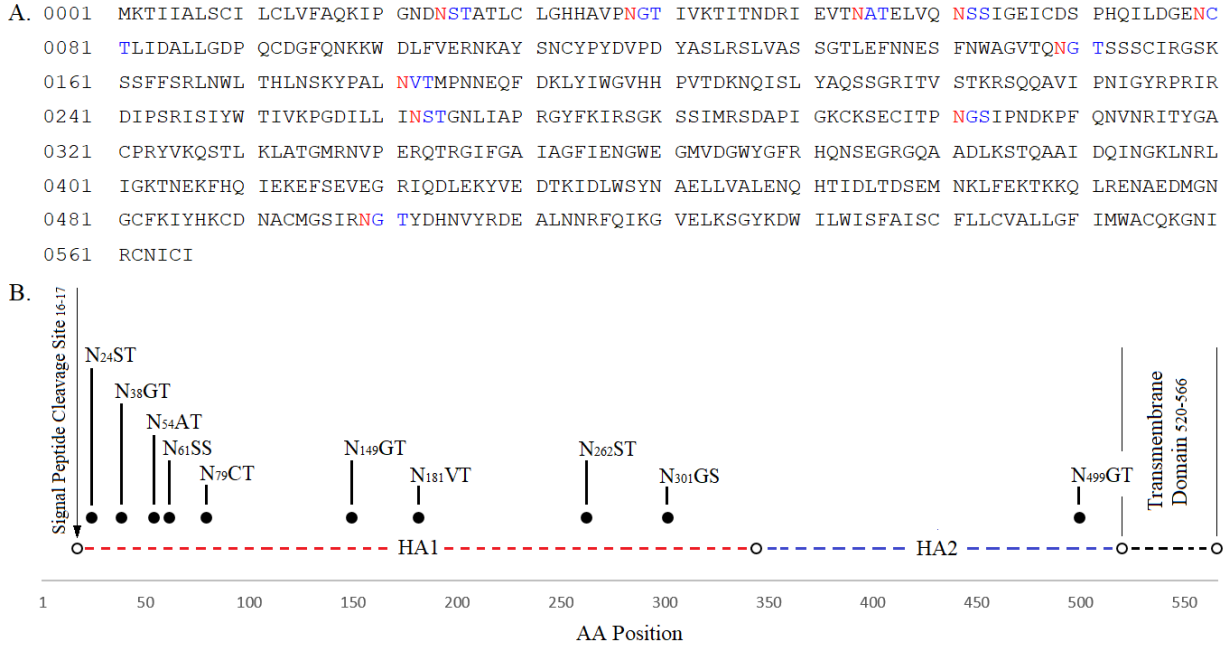

Figure 5.1. (A) Predicted A/Kansas/14/2017 HA (EPI_ISL_346457) N-glycosylation sites using NetNGlyc 1.0 web server (https://services.healthtech.dtu.dk/service.php?NetNGlyc-1.0). (B) Glycosylation site locations with respect to the HA1 and HA2 domains. Signal peptide cleavage site is located at amino acid (aa) position 16-17 and the transmembrane domain is located between aa position 520-566.

Before proceeding with N-glycan assessment, the HA content of all three H3N2 influenza vaccine monovalent bulks was evaluted using RP-HPLC. These preliminary experiments were performed to ensure that the SRID concentration values provided by the manufacturer were accurate and that no HA degradation was present. Each monovalent bulk was diluted to a final concentration of 50 µg/mL using the concentrations provided by the manufacturer and 20 µL was injected on column and analyzed via RP-HPLC following the method details outlined in Section 2.5.3. As seen in Figure 5.2, each monovalent bulk yielded similar HA1 peaks with respect to retention time and overall peak area, confirming that the provided SRID concentration values are

accurate and comparable between manufacturers. Furthermore, peak shape was consistent between each manufacturer indicating that no degradation of HA content was observed in any of the candidate samples.

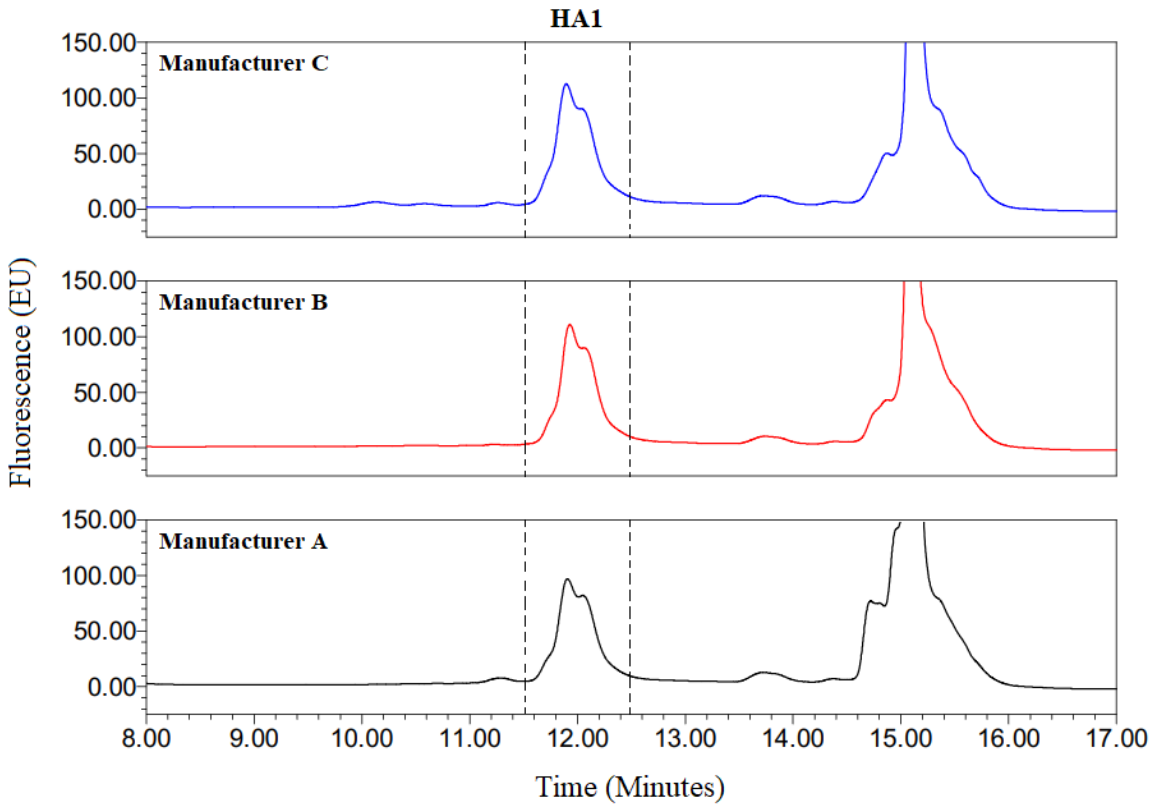

Figure 5.2. Representative native fluorescence RP-HPLC chromatograms from a 20 µL injection of manufacturer A, B, and C's H3N2 (A/Kansas/14/2017) vaccine monovalent bulk (50 µg/mL). Peak highlighted with dashed lines represents HA1.

5.2 APTS-Labeled N-Glycan Profiling of HA (H3N2) Vaccine Monovalent Bulks via CZE-LIF

Following the evaluation of the HA content of each manufacturers H3N2 vaccine monovalent bulk, enzymatically released N-glycans derived from 10 µg of HA from each sample were APTS-labeled and analyzed via CZE-LIF following the sample preparation protocol and analysis method outlined in section 2.2 and 2.5.1, respectively. The electropherograms in Figure

5.3 depict the APTS-labeled N-glycan profiles for each sample. For accurate comparison, each sample trace was normalized to the maltotriose internal standard peak at 8.5 minutes.

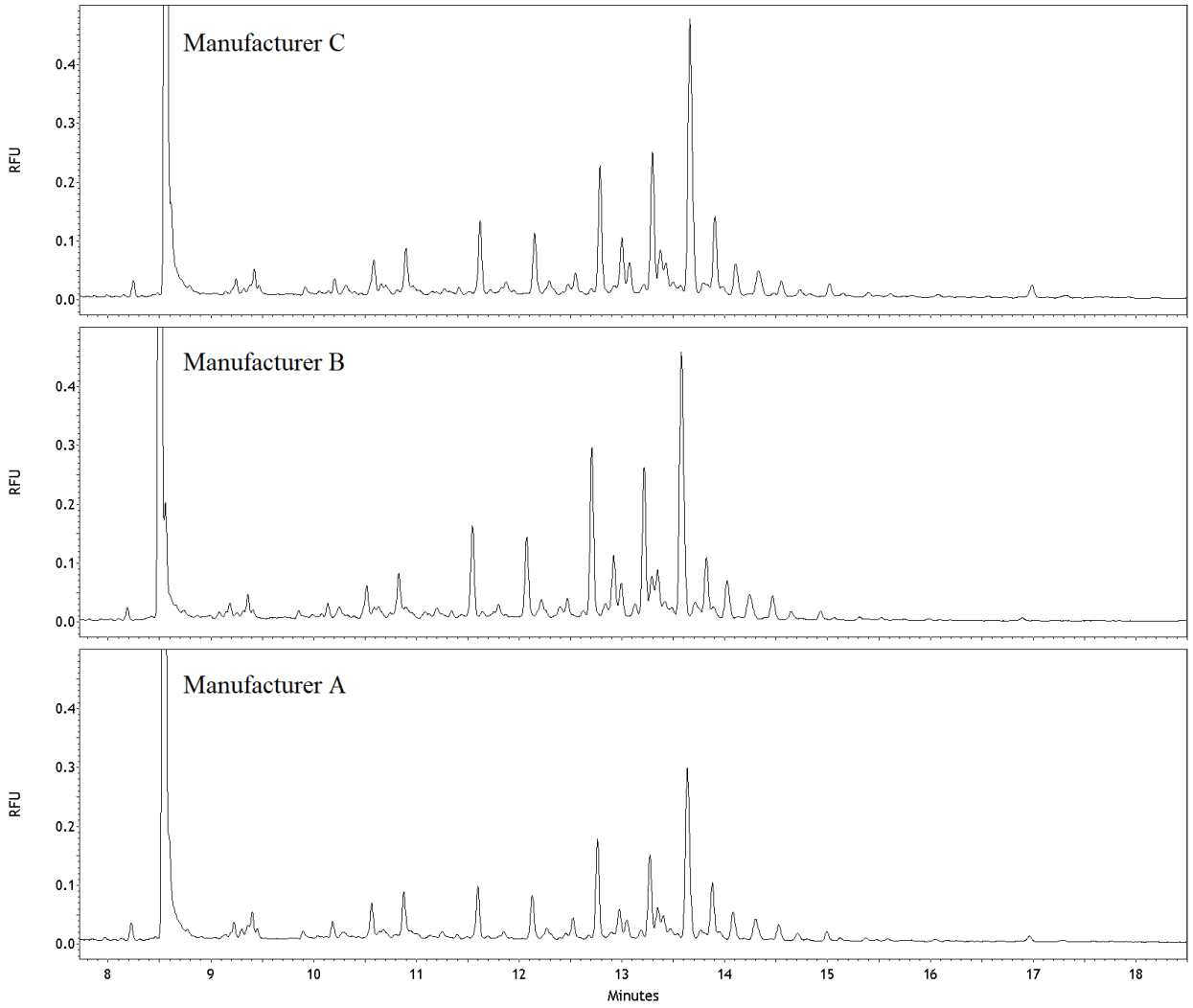

Figure 5.3. Representative CZE-LIF electropherograms of A/Kansas/14/2017 H3N2 HA APTS-labeled N-glycan profiles from vaccine monovalent bulk Manufacturer A, B, & C. Sample traces were normalized to the maltotriose internal standard peak at 8.5 minutes.

As expected, each sample displayed identical N-glycan profiles because all of which were egg-derived monovalent vaccine bulks. However, some differences were observed with respect to expression levels of certain N-glycans species among the manufacturers (Figure 5.4).

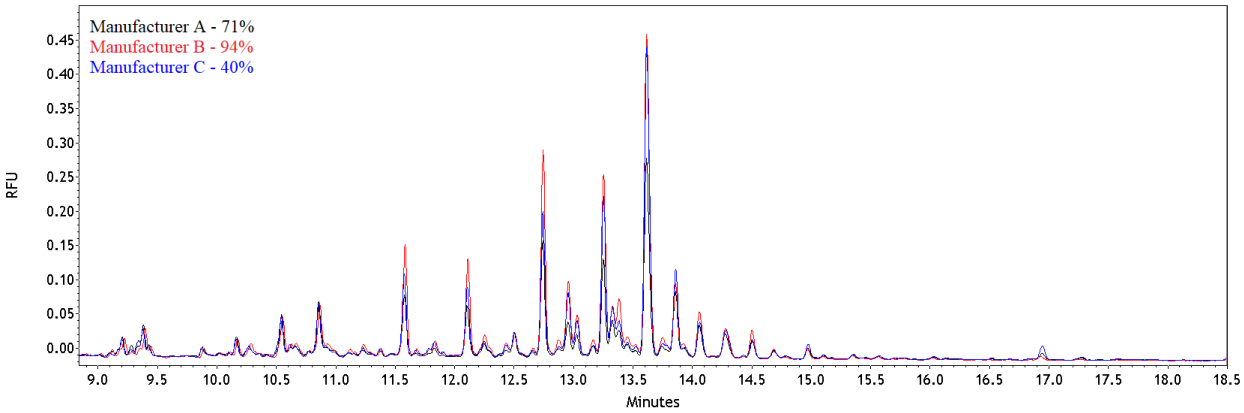

Figure 5.4. CZE-LIF Electropherogram overlay of manufacturer A, B, and C's H3N2 (A/Kansas/14/2017) vaccine monovalent bulk enzymatically released APTS-labeled N-glycan profiles. Traces were normalized to the maltotriose standard peak at 8.5 minutes (not shown).

Manufacturer B, which displayed a 94% receptor binding affinity yielded a higher abundance of lower molecular weight glycans (faster migration times) than manufacturers A and C. This observation is interesting because from a steric effect perspective, it is possible that HA expressing a higher abundance of lower molecular weight N-glycan species (potentially reduced steric hindrance around HA-RBS) could explain the higher binding affinity. Conversely, with respect to manufacturer C, which exhibited the lowest receptor binding affinity (40%) displayed some higher molecular weight glycan species with elevated abundances (13.8 min & 17 min). Whether these minor differences seen in the N-glycosylation profiles correlate with receptor binding affinities remains unclear and would require further investigation with an increased sample size. Regardless, mass confirmation and structural identification could potentially offer additional evidence to determine any significant differences that may explain the different receptor binding affinities that were observed.

5.3 N-Glycan Profiling & Structural Identification of HA Content in H3N2 Vaccine Monovalent Bulks via CESI-MS

Enzymatically released N-glycans derived from 10 µg of HA (manufacturer A) were GT-labeled and analyzed via CESI-MS following the sample preparation protocol and analysis method outlined in sections 2.3 and 2.5.2, respectively. A total of 25 unique N-glycan species were observed (Figure 5.5 A) and arranged in accordance to their relative abundances (Figure 5.5 B-E). Based on the CID fragmentation pattern of each N-glycan species, structural elucidation was possible. Confirmation of each N-glycan structure was performed manually (Figure 5.6).

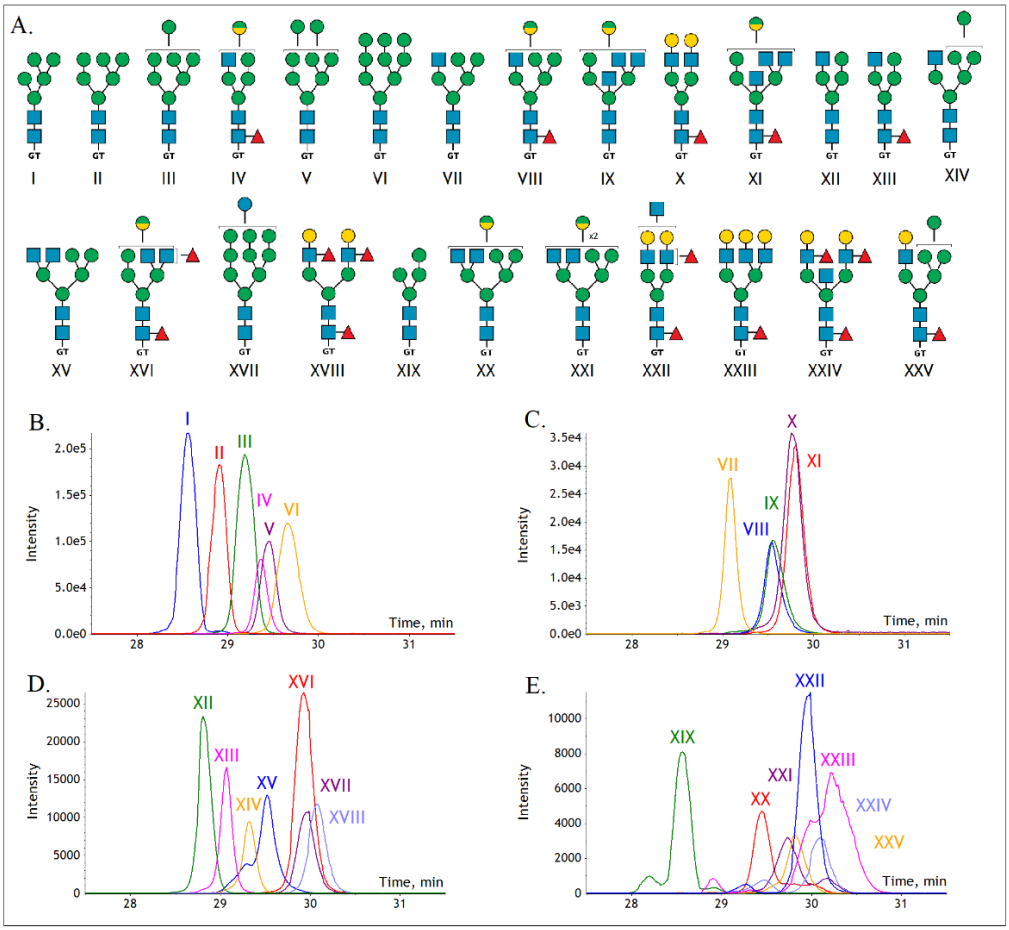

Figure 5.5. (A) 25 proposed structures for the most abundant N-glycans in manufacturer A's H3N2 (A/Kansas/04/2017) monovalent bulk determined via sheathless CESI-MS arranged from left to right in accordance to their relative abundances. XICs for all 25 N-glycan species are displayed in (B), (C), (D), and (E), representing species with high, intermediate, low and trace abundances, respectively.

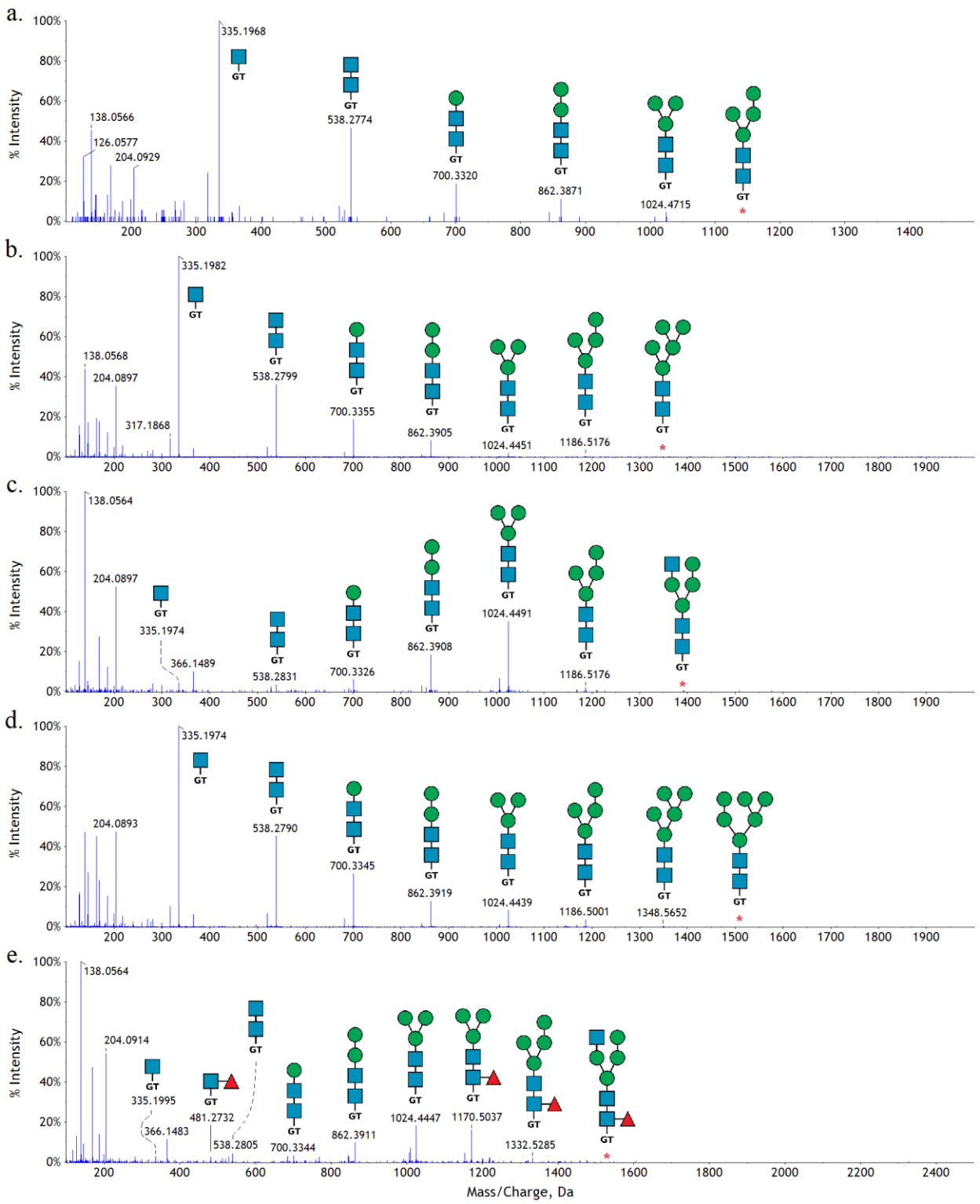

Figure 5.6. CESI-MS/MS product ion spectra of H3N2 (A/Kansas/14/2017) HA GT labeled N-glycans. Targeted precursor ions (*m/z*) (a) 593.75 $^{2+}$, (b) 674.77 $^{2+}$, (c) 695.29 $^{2+}$, (d) 755.80 $^{2+}$, and (e) 768.31 $^{2+}$.

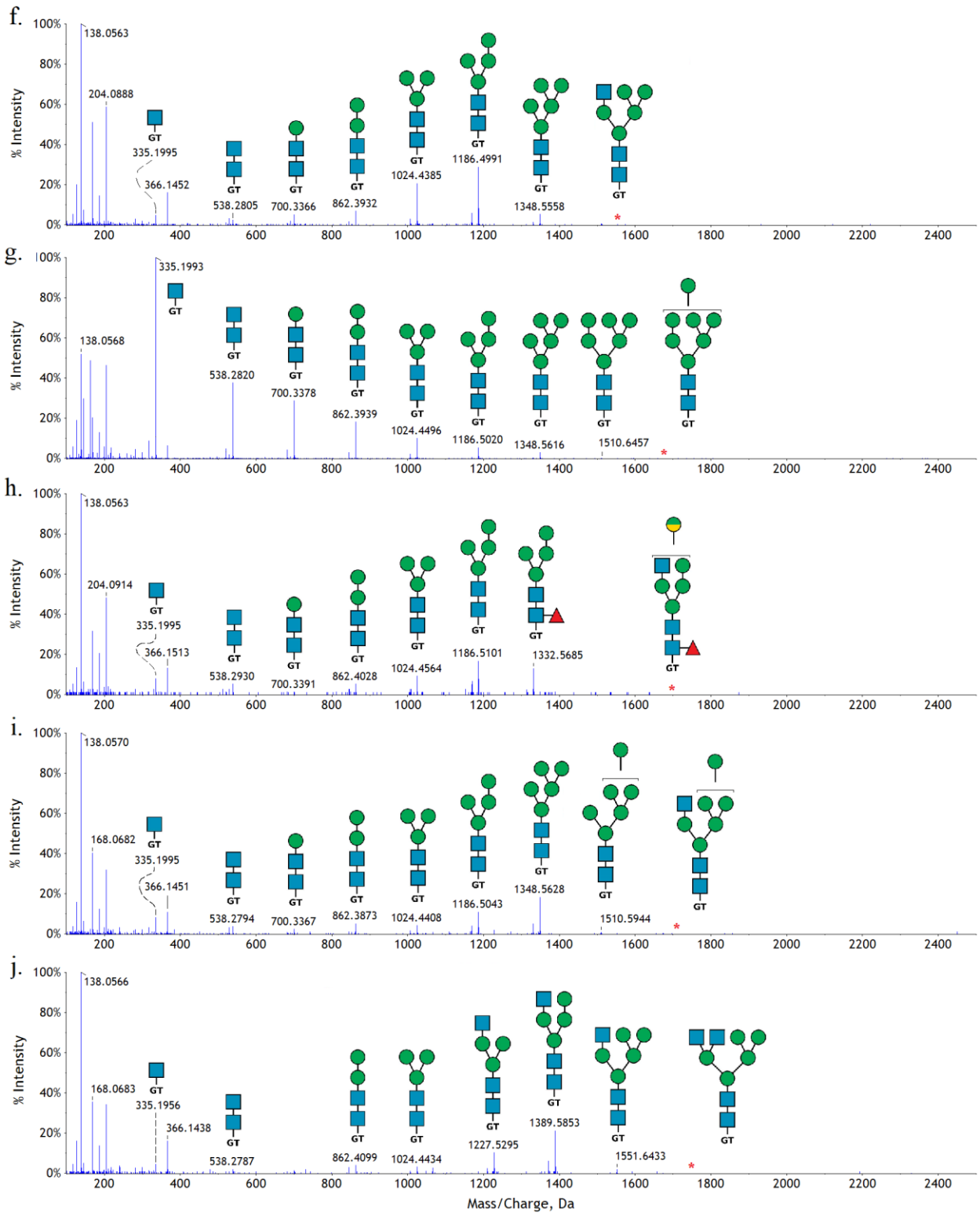

Figure 5.6 Continued. CESI-MS/MS product ion spectra of H3N2 (A/Kansas/14/2017) HA GT labeled N-glycans. Targeted precursor ions (*m/z*) (f) 776.31 $^{2+}$, (g) 836.83 $^{2+}$, (h) 849.34 $^{2+}$, (i) 857.34 $^{2+}$, and (j) 877.85 $^{2+}$.

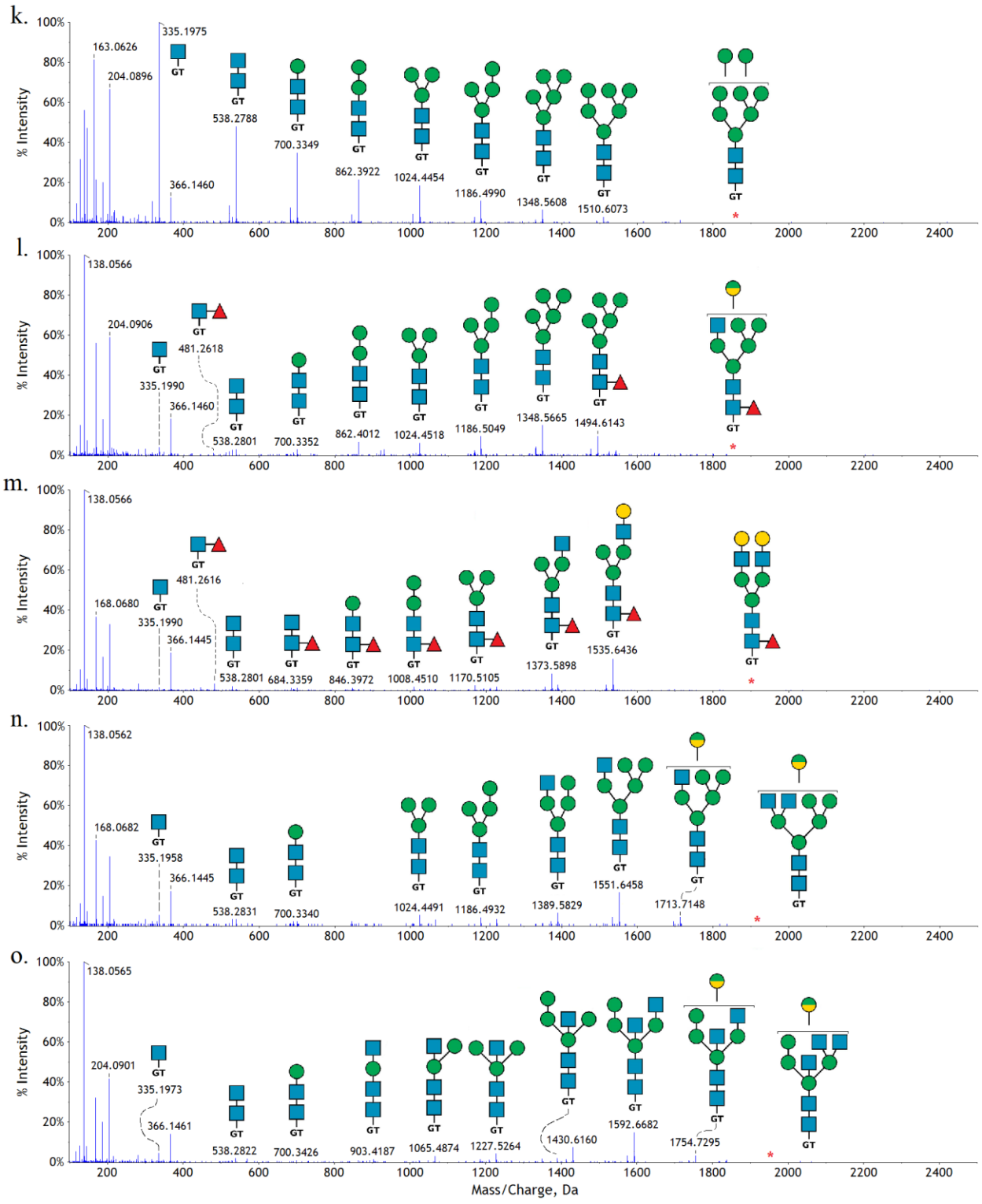

Figure 5.6 Continued. CESI-MS/MS product ion spectra of H3N2 (A/Kansas/14/2017) HA GT labeled N-glycans. Targeted precursor ions (*m/z*) (k) 917.85 $^{2+}$, (l) 930.37 $^{2+}$, (m) 950.88 $^{2+}$, (n) 958.88 $^{2+}$, and (o) 979.39 $^{2+}$.

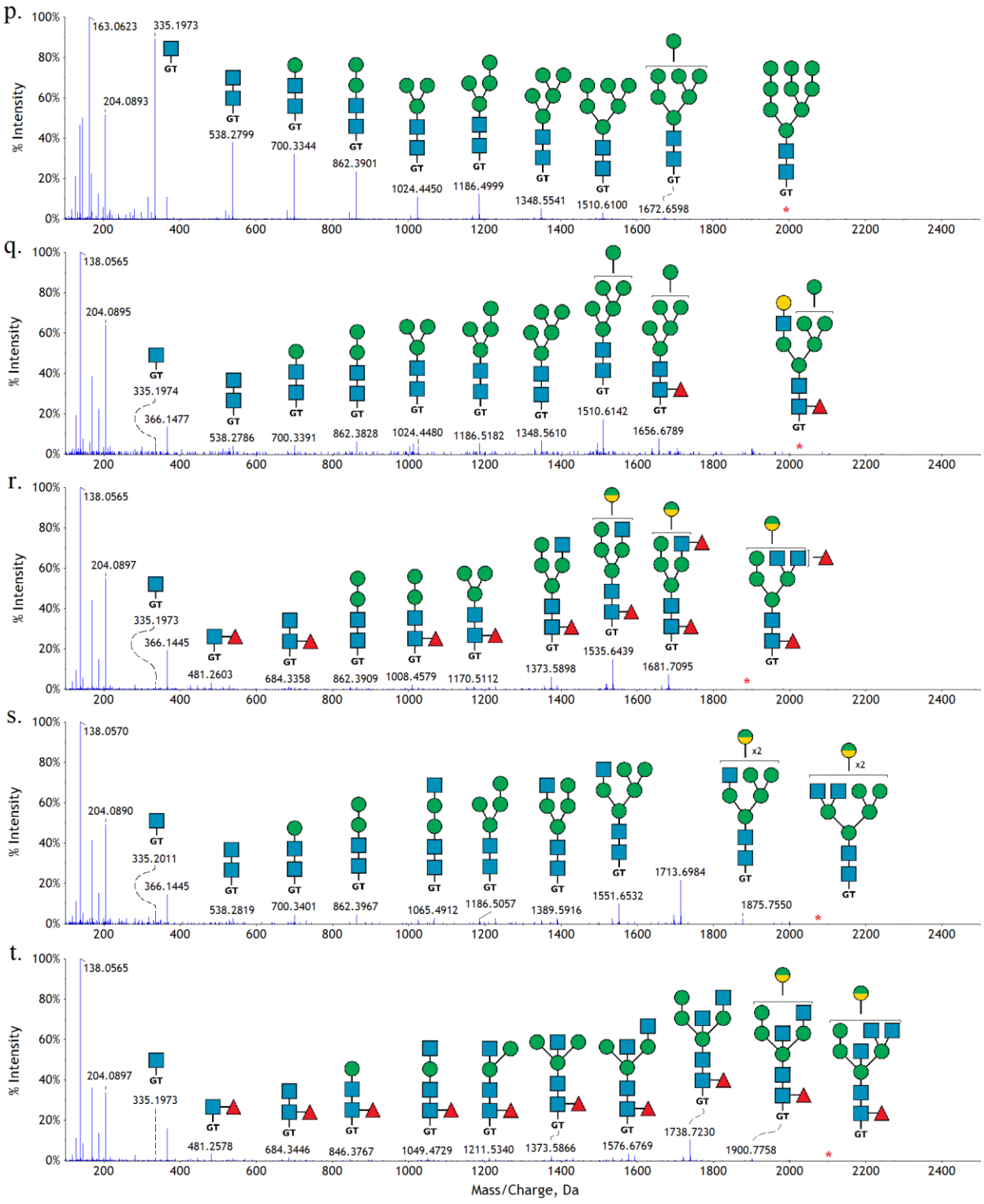

Figure 5.6 Continued. CESI-MS/MS product ion spectra of H3N2 (A/Kansas/14/2017) HA GT labeled N-glycans. Targeted precursor ions (*m/z*) (p) 998.88 $^{2+}$, (q) 1011.39 $^{2+}$, (r) 1023.91 $^{2+}$, (s) 1039.90 $^{2+}$, and (t) 1052.42 $^{2+}$.

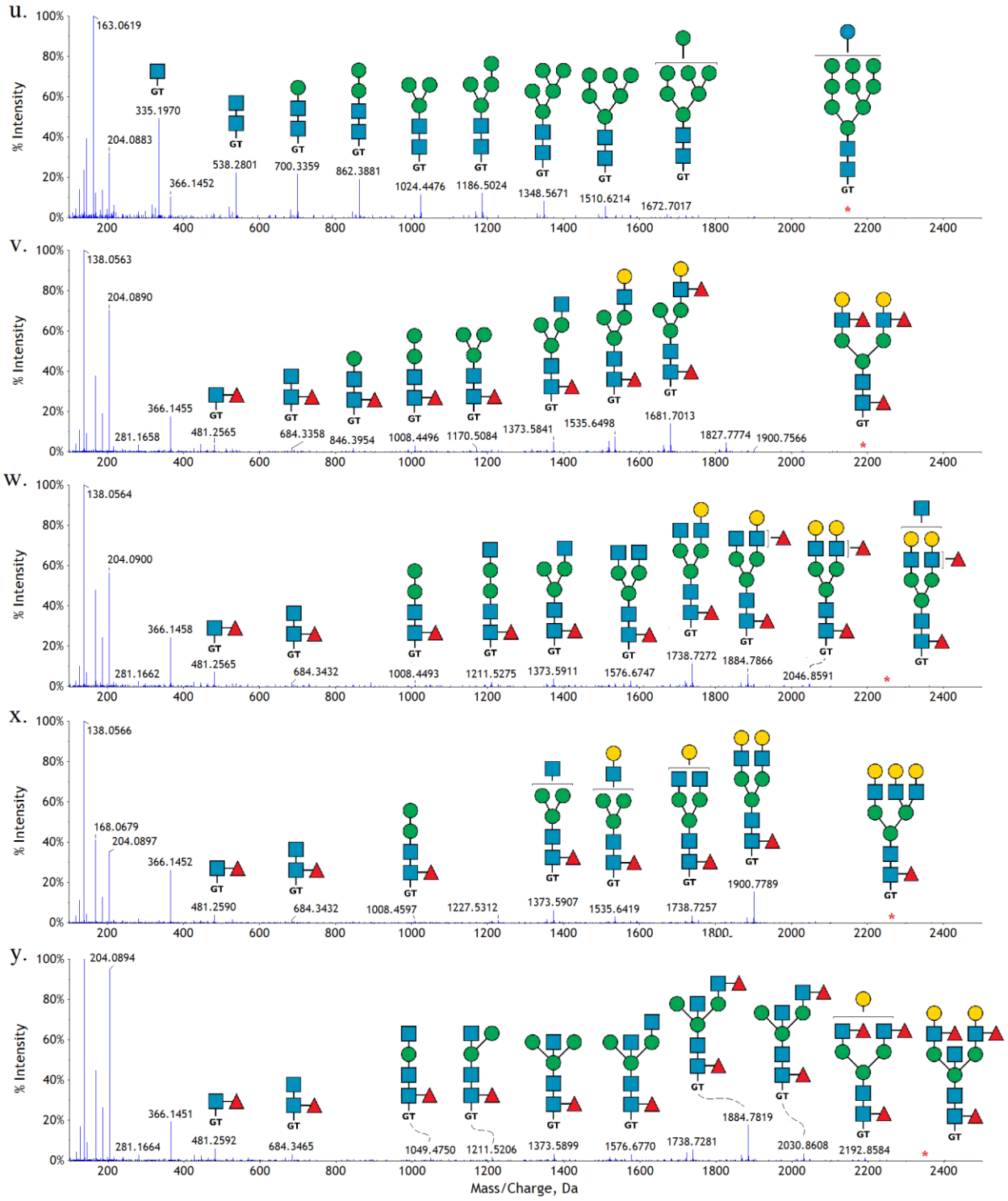

Figure 5.6 Continued. CESI-MS/MS product ion spectra of H3N2 (A/Kansas/14/2017) HA GT labeled N-glycans. Targeted precursor ions (*m/z*) (u) 1079.90 $^{2+}$, (v) 1096.94 $^{2+}$, (w) 1125.45 $^{2+}$, (x) 1133.45 $^{2+}$, and (y) 1198.48 $^{2+}$.

The relative abundances of each N-glycan subtype were calculated as a fraction of the total abundance (Figure 5.7). The results show that high mannose type glycans account for roughly 70% of the total N-glycans observed, where as hybrid and complex subtypes accounted for 23% and 7%, respectively. This is in agreement with current literature on egg-derived HA (H3N2, A/Kansas/14/2017) N-glycosylation.[55, 171]

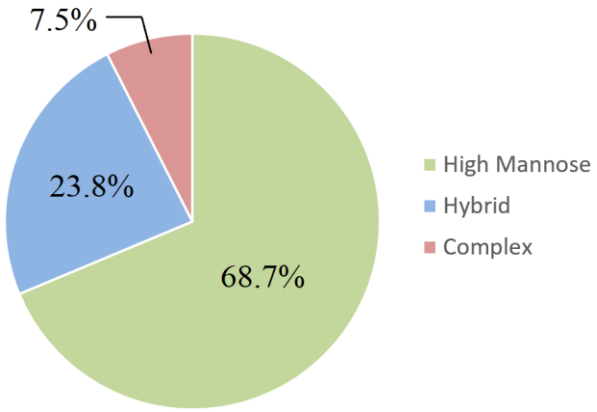

Figure 5.7. Relative abundances of H3N2 (A/Kansas/14/2017) HA N-glycan subtypes determined by CESI-MS

Although primarily from HA content, these results also include N-glycan contribution from other components within these monovalent bulk samples. These samples are sucrose-purified split virus vaccine bulks; consequently, upon enzymatic treatment with PNGase F there will be some N-glycan contribution from other viral glycoproteins (i.e. NA) as well as endogenous expression system specific proteins (i.e. egg-based proteins). With this in mind, further purification is required to isolate the HA component within these samples.

5.4 RP-HPLC HA1 Fraction Collection

In order remove unwanted N-glycan contribution, purification via RP-HPLC with fraction collection was employed. Typical RP-HPLC analyses performed with the method described in section 2.3.3 involve injections of dilute samples (50 µg/mL). Following this method would result in only 1 µg of HA injected on column which is not a sufficient amount of starting material for further processing and N-glycan analysis via CZE-LIF and CESI-MS. Therefore, the amount of HA injected on column needed to be increased to provide enough material for subsequent N-glycan analysis after collection. Unfortunately, with the standard column used for these types of separations (MICRA® HPLC NPS-ODSI, 33 mm × 4.6 mm, 1.5 µm particle), injection of highly concentrated samples resulted in high back pressures which if not addressed could lead to column damage. Therefore, in order to enable higher injection volumes of higher concentrations of material, a longer column with increased pore size (MICRA® HPLC NPS-ODSI, 100 mm × 4.6 mm, 3 µm) was employed. Although retention times were extended due to the length of the column, the overall HA1 profile was conserved when compared to the standard method (Figure 5.2). Each H3N2 monovalent bulk was diluted to a final concentration of 200 µg/mL and 50 µL was injected on-column (equivalent to 10 µg of HA). A total of two collections of the eluting HA1 peak were performed for each manufacturers monovalent bulk sample for downstream analysis of enzymatically released APTS- and GT-labeled N-glycans via CZE-LIF and CESI-MS, respectively (Figure 5.8).

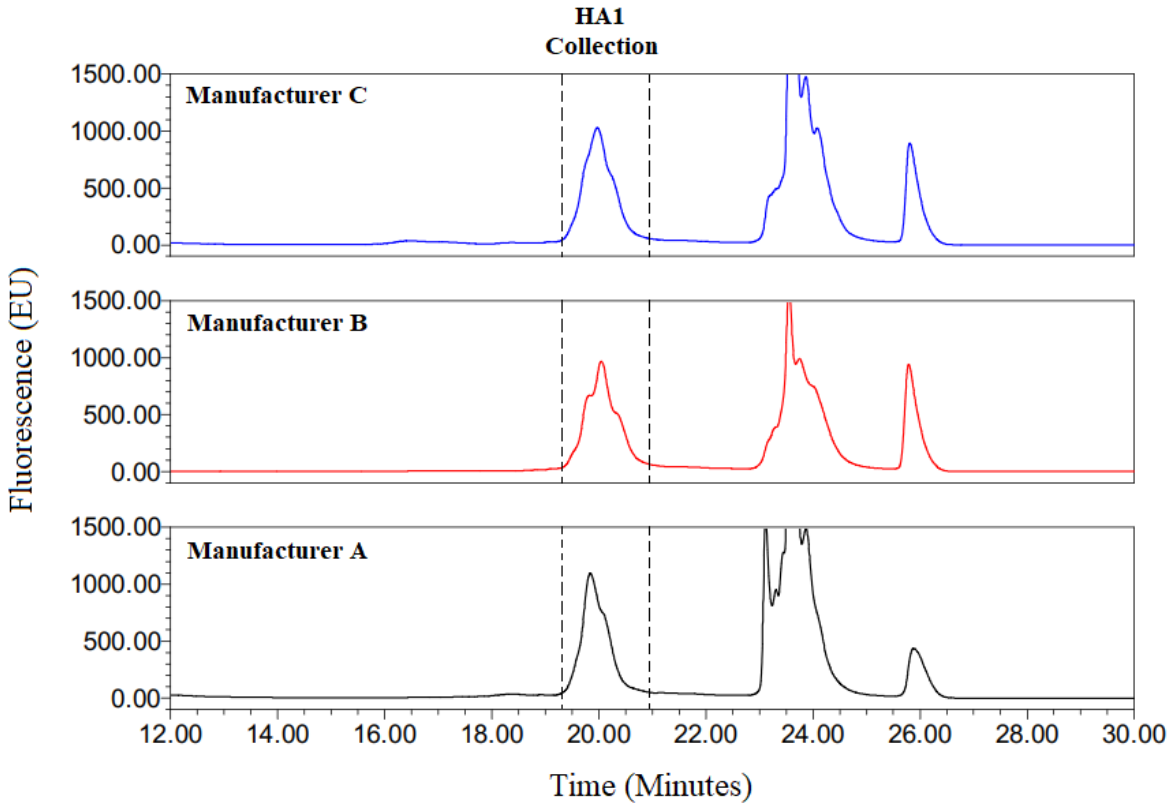

Figure 5.8. Representative native fluorescence RP-HPLC chromatograms from a 50 µL injection of manufacturer A, B, and C's H3N2 (A/Kansas/14/2017) vaccine monovalent bulk (200 µg/mL). Dashed lines highlight when collection of HA1 peaks were performed.

Due to the elution width of the HA1 peak (~2 min), the standard flow-rate of 1 mL/min resulted in a collection volume of approximately 2 mL. Therefore, concentration into a smaller volume was required prior to N-glycan processing. This was achieved by performing several concentration steps using a 10kDa (MWCO) Amicon centrifugal filter (10,000g, 5 min). The total volume of the filter unit was 500 µL thereby requiring 4-5 concentration steps. Once concentrated, each sample was subsequently buffer exchanged in LC-MS grade H_2O using the same filter unit. For CZE-LIF analysis, the concentrated and buffer exchanged sample (~50 µL) was lyophilized using a centrivap before performing the CZE-LIF sample preparation protocol outlined in section 2.2. For CESI-MS analysis, the sample was left in the filter unit after concentration and buffer exchanging and the sample preparation protocol outlined in section 2.3 was followed.

The CZE-LIF electropherograms of each samples enzymatically released HA1 APTS-labeled N-glycan profile are displayed in Figure 5.9. Similar N-glycan profiles were observed as seen in the unpurified vaccine monovalent bulk in section 5.2, however, the overall peak intensities from the HA1 collection sample were lower on average.

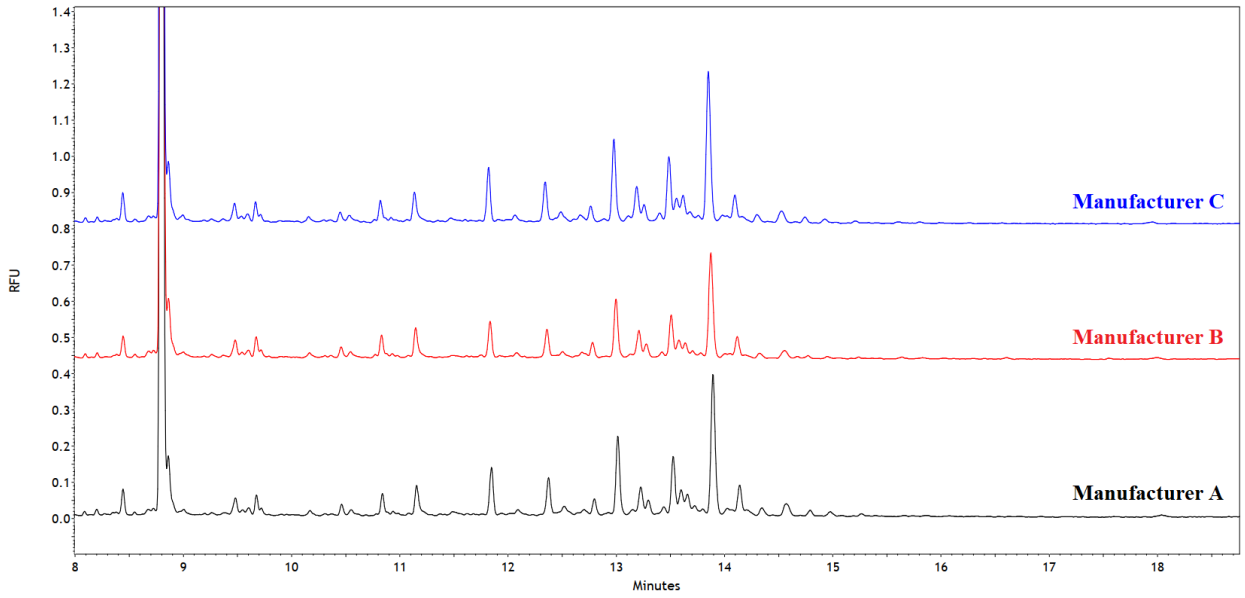

Figure 5.9. CZE-LIF electropherograms of APTS-labeled N-glycans derived from 10 µg HA1 RP-HPLC collections of manufacturer A, B, and C's H3N2 A/Kansas/14/2017 monovalent bulk. Traces were normalized to the maltotriose internal standard peak at 8.8 minutes.

For sheathless CESI-MS analysis, the collected HA1 samples were analyzed with their whole vaccine bulk counterparts for GT-labeled N-glycan profile comparison (Figure 5.10). The relative abundances of each N-glycan species was calculated as a fraction of the total abundance and arranged from left to right in order of increasing molecular weight. As seen in Figure 5.10, the same N-glycan species were observed in both the HA1 RP-HPLC purified collection and the whole vaccine monovalent bulk. Additionally, the relative abundances of the majority of observed N-glycan species were predominantly conserved when comparing the two samples. However, there are some notable differences that can be seen. For example, in the HA1 purified collections there

is an observable increase in relative abundances of the larger high mannose species bearing 7-9 mannose residues. Whereas in the manufacturer control samples (enzymatically released N-glycans derived from the whole vaccine monovalent bulk) there is an increase in relative abundance observed across the larger molecular weight hybrid and complex N-glycan species specifically those bearing both core and terminal fucosylation.

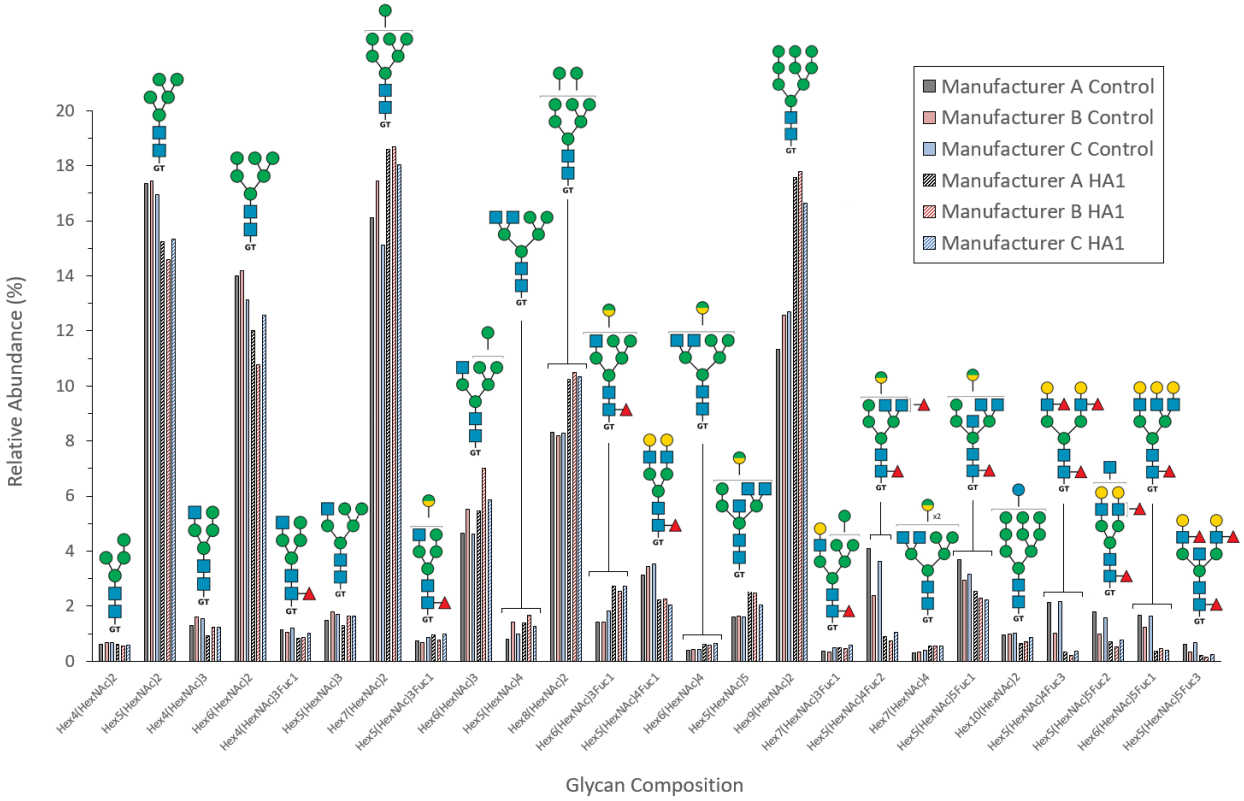

Figure 5.10. Relative abundances of 25 H3N2 A/Kansas/14/2017 glycoforms determined by CESI-MS. Comparison between whole vaccine monovalent bulk (solid) and RP-HPLC HA1 collections (mesh).

5.5 Evaluation of CESI-MS Method Repeatability

To increase confidence in these results, the repeatability of the sheathless CESI-MS method was evaluated. To accomplish this, HA1 collection via RP-HPLC of manufacturer A's H3N2 monovalent bulk was performed in triplicate. For each replicate, 50 µL of a 200 µg/mL sample, corresponding to 10 µg of HA, was injected and the eluting HA1 peak was collected (~ 2 mL/collection). Similarly to Section 5.4, each collection was concentrated and buffer exchanged into LC-MS grade H_2O using separate 10 kDa (MWCO) Amicon centrifugal filters prior to filter-aided N-glycan release and GT-labeling following the protocol outlined in Section 2.3.

After enzymatic release and GT-labeling, each collection was analyzed in triplicate via sheathless CESI-MS following the method described in Section 2.4.2. For each replicate, samples were injected hydrodynamically by applying 5 psi for 60 seconds, corresponding to a 50 nL injection volume, and separated in normal polarity mode (anode at injection site) at 20 kV for 60 minutes. The relative abundances of each N-glycan species for every replicate was calculated as a fraction of the total abundance and averaged. The corresponding standard deviations were calculated and displayed in Figure 5.11. The %RSD values ranged from < 1% to > 25% (Table 5.2). Larger %RSD values were observed for the higher molecular weight low abundant species. This variation can be explained by the reduced ionization efficiencies as the molecular weight of the glycans increase.[172] Additionally, the labile nature of fucose residues during ESI can also influence ionization efficiencies.[173]

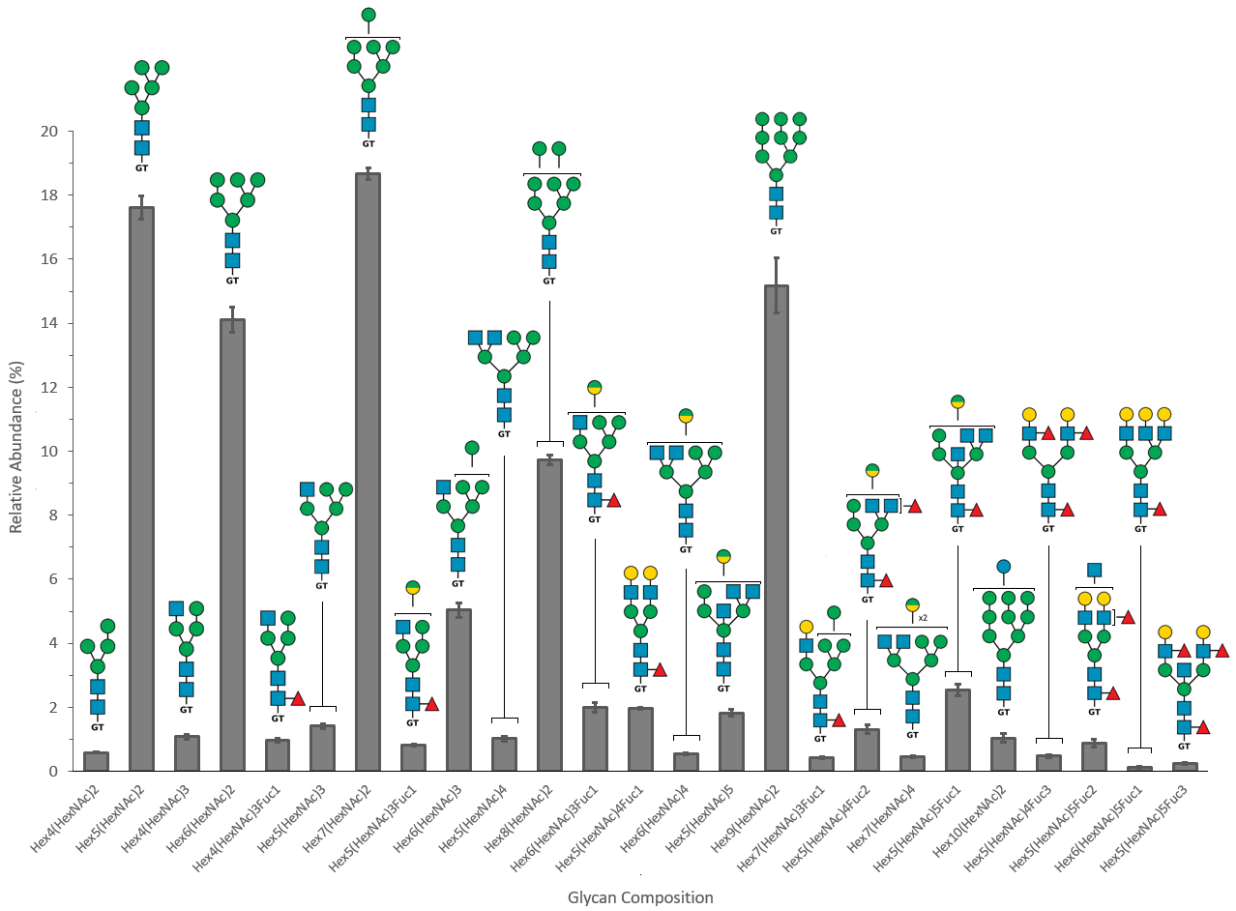

Figure 5.11. Relative abundances of 25 H3N2 A/Kansas/14/2017 glycoforms determined by CESI-MS. Three HA1 collections (10 µg) were performed via RP-HPLC followed by FASP GT-labeling and subsequent CESI-MS analysis for the evaluation of method repeatability.

Table 5.2. Theoretical *m/z*, average relative abundances (%) and calculated relative standard deviations (%) for the 25 H3N2 A/Kansas/14/2017 GT-labeled N-glycans determined by sheathless CESI-MS.

Glycan Composition	Theoretical *m/z* $[M+H]^{2+}$	Average Relative Abundance (%)	Relative Standard Deviation (%)
$Hex_4(HexNAc)_2$	593.75	0.58	1.00
$Hex_5(HexNAc)_2$	674.77	17.62	1.85
$Hex_4(HexNAc)_3$	695.29	1.08	1.84
$Hex_6(HexNAc)_2$	755.80	14.11	2.67
$Hex_4(HexNAc)_3Fuc_1$	768.31	0.96	4.97
$Hex_5(HexNAc)_3$	776.31	1.41	2.02
$Hex_7(HexNAc)_2$	836.83	18.67	0.89
$Hex_5(HexNAc)_3Fuc_1$	849.34	0.81	2.23

$Hex_6(HexNAc)_3$	857.34	5.04	5.38
$Hex_5(HexNAc)_4$	877.85	1.02	6.50
$Hex_8(HexNAc)_2$	917.85	9.73	1.37
$Hex_6(HexNAc)_3Fuc_1$	930.37	1.99	7.44
$Hex_5(HexNAc)_4Fuc_1$	950.88	1.96	2.06
$Hex_6(HexNAc)_4$	958.88	0.54	4.32
$Hex_5(HexNAc)_5$	979.39	1.83	5.77
$Hex_9(HexNAc)_2$	998.88	15.18	5.70
$Hex_7(HexNAc)_3Fuc_1$	1011.39	0.43	6.95
$Hex_5(HexNAc)_4Fuc_2$	1023.91	1.31	11.12
$Hex_7(HexNAc)_4$	1039.90	0.45	4.28
$Hex_5(HexNAc)_5Fuc_1$	1052.42	2.54	7.08
$Hex_{10}(HexNAc)_2$	1079.90	1.04	12.30
$Hex_5(HexNAc)_4Fuc_3$	1096.94	0.47	10.74
$Hex_5(HexNAc)_5Fuc_2$	1125.45	0.87	13.41
$Hex_6(HexNAc)_5Fuc_1$	1133.45	0.13	28.17
$Hex_5(HexNAc)_5Fuc_3$	1198.48	0.23	13.85

With these results, this method proved to be well suited for the analysis of enzymatically released neutral N-glycans. For this particular set of samples, the vaccine monovalent bulks contained material derived from purified whole influenza virus particles. Therefore, the viral sialidase NA was present in varying degrees, which consequently cleaves off accessible sialic acid residues on HA leaving predominantly neutrally charged N-glycans. However, when beginning to factor in acidic, negatively charged residues including sialic acid, upon labeling with a positive tag (i.e. GT) the resultant molecule would be neutrally charged which is no longer analyzable via positive ion mode CESI-MS. Therefore, further derivatization was required to broaden the applicability of the described method to enable the analysis and structural characterization of sialic acid bearing N-glycans.

Chapter 6: Dual Hydrazide Derivatization for the Analysis of Sialic-Acid Bearing N-Glycans via Sheathless CESI-MS

6.1 Sialic Acid Derivatization Strategies

The GT-labeling and CESI-MS method described thus far is well suited for the analysis of enzymatically released neutral influenza HA derived N-glycans that do not contain any acidic monosaccharide residues (i.e. sialic acid). However, HA produced through recombinant DNA technology as well as other expression systems can retain sialic acid residues because of the absence of the viral sialidase, NA.

Various derivatization strategies can be used to neutralize the negatively charged carboxylate moiety of sialic acid residues. Amidation, esterification, and acetohydrazide (AH) derivatization are among a few common techniques used in MS-based glycomics (Figure 6.1).[174] Sialic acid linkage specific derivatization to distinguish between α2,3- and α2,6-linkage isomers is also possible.[175-176] Although important for HA binding specificity on host cell receptors, the effect that different sialic acid linkage isomers have on other HA properties is not well understood. Therefore, for the purpose of this study, non-linkage specific sialic acid derivatization strategies were explored. In the sample preparation protocol adapted from Van Cott and coworkers described in section 4.2, [161, 177] a filter-aided approach for sialic acid derivatization with AH was used. After reduction and alkylation, sialic acid derivatization with AH is performed before enzymatic digestion with PNGase F while the N-glycans are still covalently attached to the glycoprotein backbone (Figure 6.2).

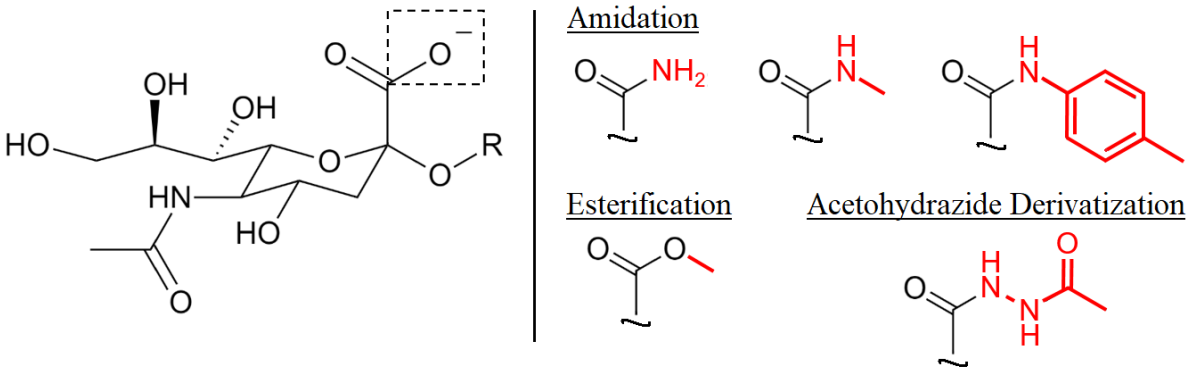

Figure 6.1. Various derivatization strategies for the neutralization and stabilization of sialic acid residues.

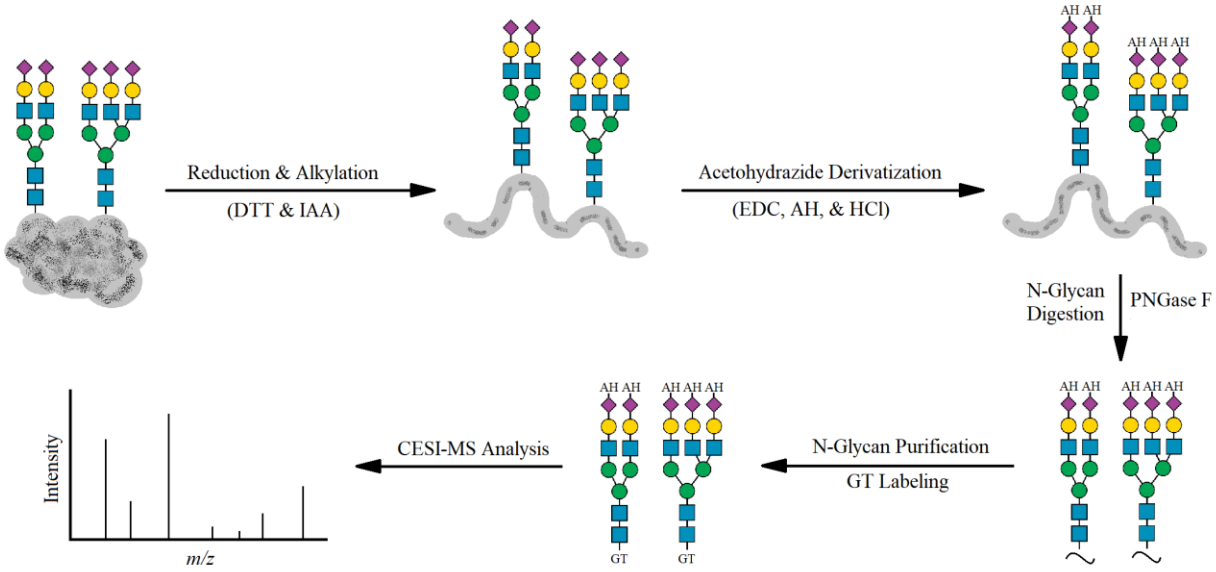

Figure 6.2. CESI-MS sample preparation scheme for AH-GT N-glycan derivatization. Adapted from Gil *et al.* 2010[161]

In this reaction, 1-ethyl-3-(3-dimethylaminopropyl)carbodiimide (EDC) reacts with the carboxylic acid group on sialic acid residues forming an intermediate o-acylisourea active ester that readily undergoes nucleophilic attack from the primary amine on AH (Figure 6.3). Since GT is used in this study for labeling the reducing end of enzymatically released N-glycans, after sialic acid derivatization, residual AH must be removed. If present in the sample prior to GT-labeling it can result in the partial neutral derivatization of the N-glycans reducing end by AH. However,

since the reaction takes place in a centrifugal filter unit, several buffer exchange steps are performed after sialic acid derivatization to remove unreacted AH prior to cationic labeling with GT.

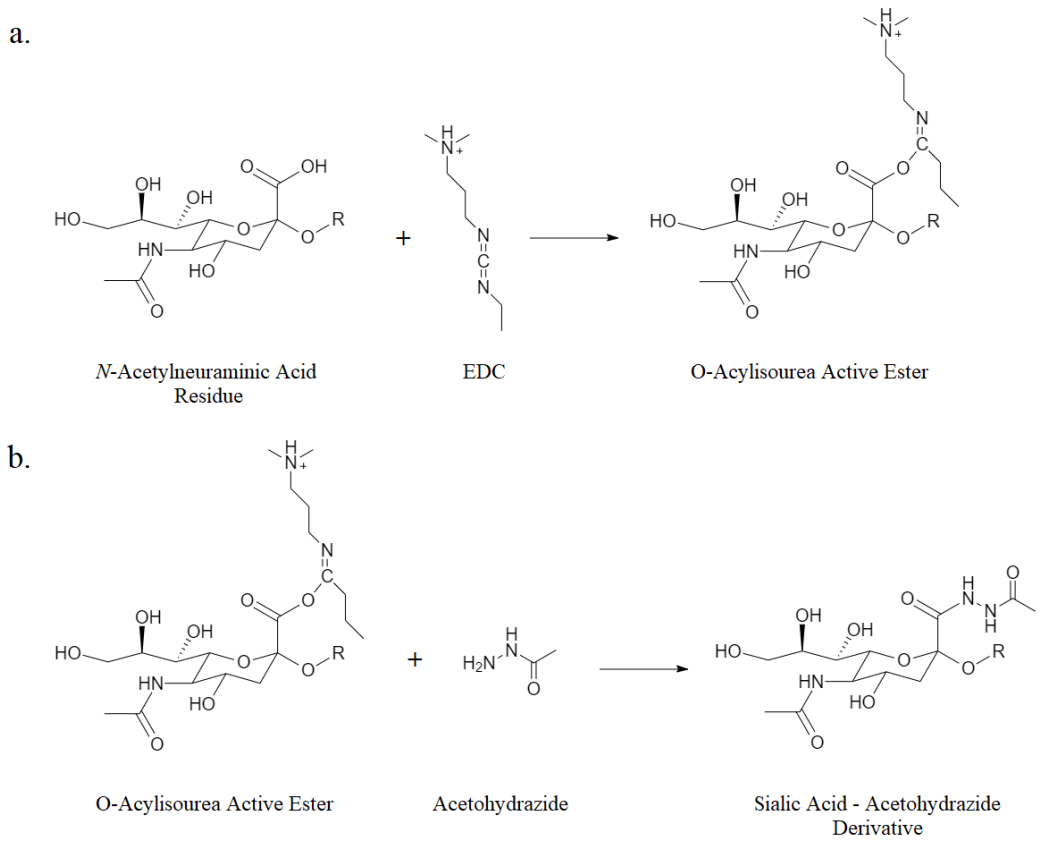

Figure 6.3. Reaction mechanism for the derivatization of sialic acids carboxyl group via acetohydrazide. (a) Reaction of sialic acid carboxyl group with EDC to form intermediate o-acylisourea active ester, (b) Nucleophilic attack of intermediate o-acylisourea active ester with acetohydrazide to form a sialic acid – acetohydrazide derivative.

CESI-MS/MS analysis of enzymatically released AH-GT-derivatized N-glycans yielded similar fragmentation patterns as observed in Section 4.5. However, some additional fragment ions were present that aided in the identification of sialic acid containing N-glycans. For example, the oxonium ion of a sialic acid residue labeled with AH was indicated by the fragment ion at *m/z* 348.14^{1+}. This is close to the *m/z* of the Hex-HexNAc oxonium ion (366.14^{1+}) with a single dehydration (348.13^{1+}). The resolution required to distinguish between these two ions is greater

than 30,000 (FWHM), however the product ion scan in the IDA method was operating in high sensitivity mode. Therefore, the resolution was diminished making these two species indistinguishable. However, the dehydrated ion is typically less than 10% of the intensity of the intact oxonium ion (366.14^{1+}). Therefore, in the example spectrum depicted in Figure 6.4a the almost equal intensities of *m/z* 366.14^{1+} and 348.14^{1+} indicate the presence of predominantly the AH-labeled sialic acid oxonium ion. Additionally, the presence of the fragment ion at *m/z* 330.13^{1+}, which represents the single dehydration of *m/z* 348.14^{1+}, provides further confidence in the identification of AH-labeled sialic acid residues (Figure 6.4a). Similar to the MS/MS fragmentation of GT-labeled N-glycans, the sequential fragmentation from the terminal end of AH-GT-labeled N-glycans resulted in the neutral loss of 162.05, 203.08, 146.06, and 347.13 Da, which corresponds to the monoisotopic mass of mannose/galactose, GlcNAc, fucose and AH-labeled sialic acid monosaccharide residues, respectively (Figure 6.4b).

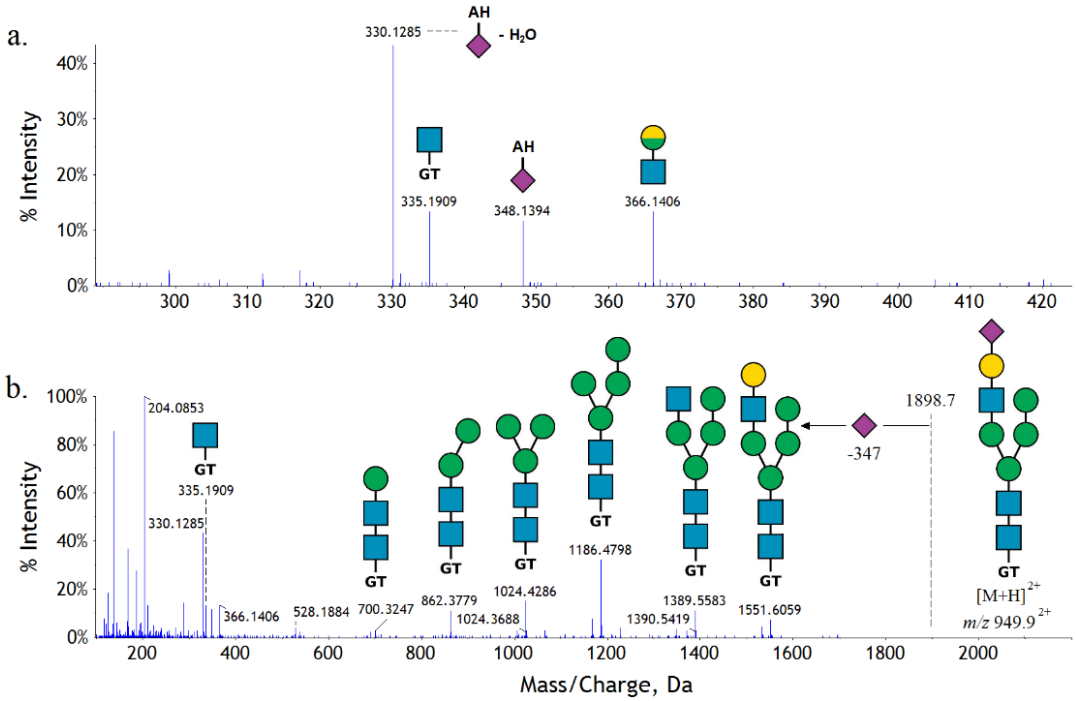

Figure 6.4. CESI-MS/MS spectrum of an AH-GT derivatized N-glycan derived from a 10 µg PNGase F digest of freestyle 293 expressed SARS-CoV-2 spike protein. Common b- and y-series oxonium ion fragments (a) and the structural elucidation of precursor ion with *m/z* 949.9^{2+} (b).

The use of this dual hydrazide labeling strategy has never been demonstrated for the profiling of enzymatically released N-glycan of sialic acid bearing glycoproteins in sheathless CESI-MS applications, therefore its utility was explored and outlined in this chapter.

6.2 Dual Hydrazide Labeling and Sheathless CESI-MS Analysis of SARS-CoV-2 Spike Protein Derived N-Glycans

The spike protein of severe acute respiratory syndrome coronavirus 2 (SARS-CoV-2) is a highly glycosylated trimeric protein located on the surface of these viruses. Due to the absence of membrane bound viral sialidases, SARS-CoV-2 glycoproteins retain sialic acid residues on their N-glycans. Glycosylation profiles of proteins produced by recombinant DNA technology are highly influenced by many factors including pH, temperature, O_2 concentration, and culture supplementation.[66, 178] Altering the ammonia concentration via ammonium chloride (NH_4Cl) supplementation can influence the degree of sialylation of recombinant glycoproteins.[66] To test the applicability of this dual hydrazide labeling approach and to see if the sheathless CESI-MS method was sensitive enough to capture differences in the degree of sialylation, the SARS-CoV-2 spike protein was expressed using the freestyle-293 expression system under two different culturing conditions. In the first sample, NH_4Cl was supplemented into the cell culture media at a final concentration of 10mM and the second was expressed under unaltered conditions to act as a control.

Enzymatically released N-glycans derived from 10 µg of SARS-CoV-2 spike protein expressed under each culture condition were AH-GT-labeled and analyzed via CESI-MS following the sample preparation protocol and analysis method outlined in section 2.3 and 2.5.2, respectively. A total of 46 N-glycan were identified using CESI-MS/MS and their relative abundances for each

sample were calculated as a fraction of the total abundance and arranged from left to right in order of increasing molecular weight (Figure 6.6).

As expected, after media supplementation with NH_4Cl an overall decrease in the degree of sialylation was observed and is likely explained by NH_4Cl's ability to inhibit of sialyltransferase and galactosyltransferase activities. 9.4% of the observed N-glycan subtypes in the freestyle-293 expressed SARS-CoV-2 spike protein control were complex-sialylated compared to 2.4% when NH_4Cl was supplemented into the cell culture media (Figure 6.5). As a means of comparison, enzymatically released native N-glycans from both spike samples were analyzed by HPAEC-PAD (Figure 6.7). Interestingly, some similarities between the two analytical methods were observed and are highlighted with dashed boxes in Figure 6.6 and 6.7.

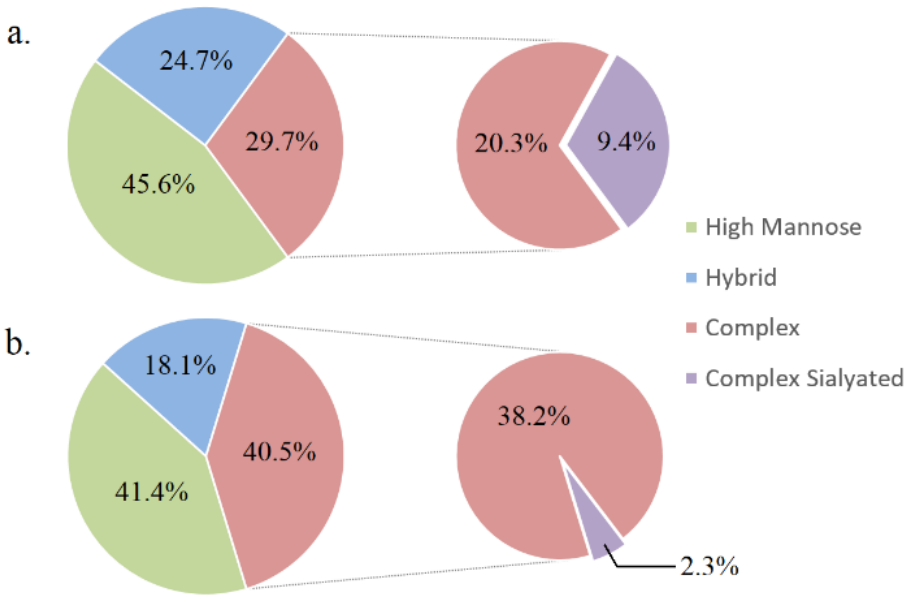

Figure 6.5. Relative abundances of freestyle-293 expressed SARS-CoV-2 spike protein N-glycan subtypes determined by CESI-MS. (a) Control and (b) NH_4Cl supplemented

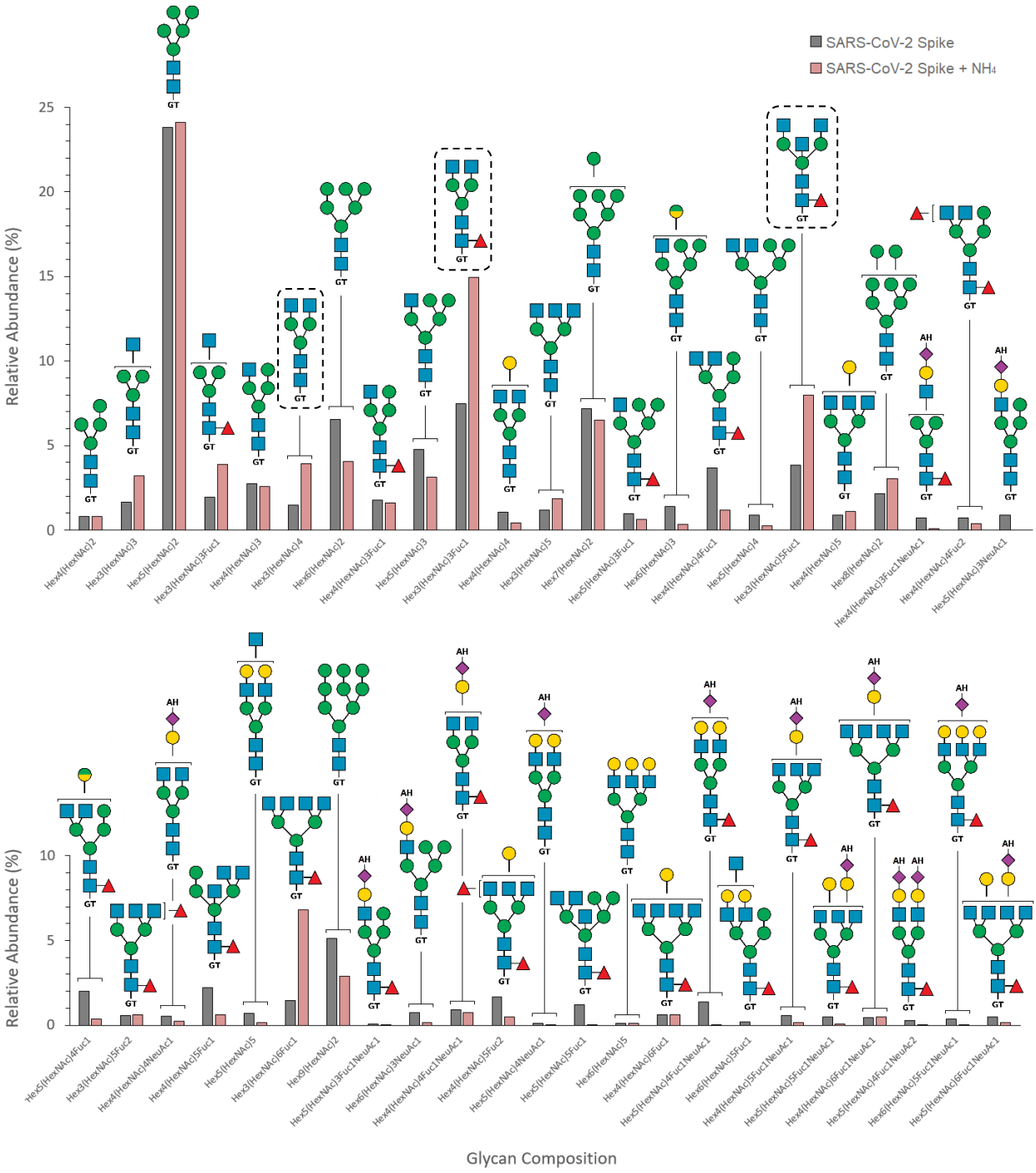

Figure 6.6. Relative abundances of 46 SARS-CoV-2 spike protein glycoforms identified by CESI-MS. Comparison between freestyle-293 expressed control versus NH_4Cl supplementation. Glycan subtypes highlighted with dashed box show similar results obtained by HPAEC-PAD (Figure 6.7).

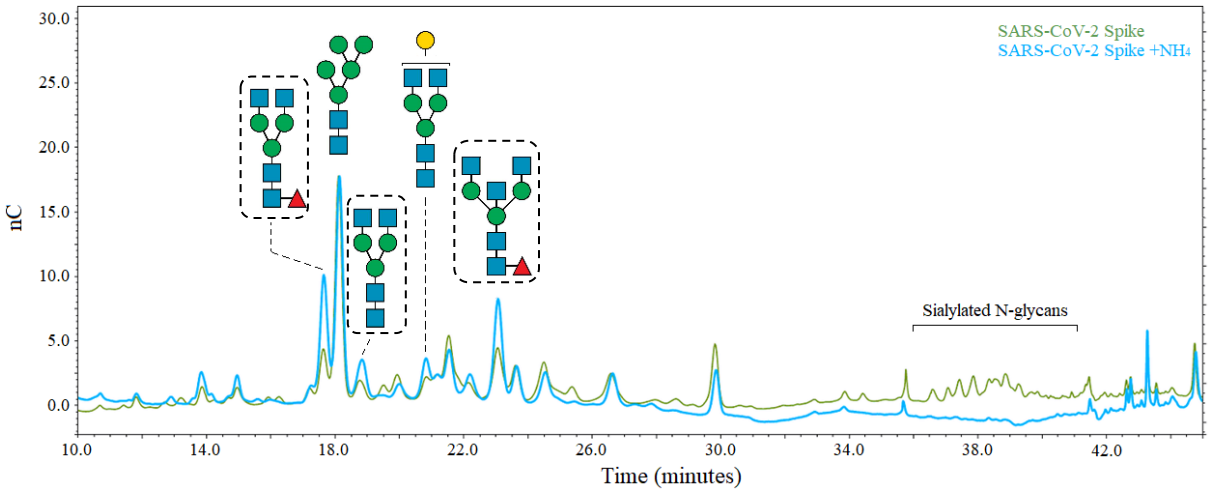

Figure 6.7. HPAEC-PAD chromatogram displaying N-glycan profiles for SARS-CoV-2 spike control versus with NH_4Cl media supplementation. Glycan subtypes highlighted with dashed box show similar results obtained by CESI-MS (Figure 6.5). Analysis was performed by the Regulatory Research Division Glycobiology Laboratory.

Additional experiments are required in order to determine method repeatability and sialic acid AH-labeling efficiencies. Van Cott and coworkers reported >90% AH-labeling efficiencies determined by NP-HPLC in their study but would need further verification for the following sheathless CESI-MS application.[177] Regardless, the sheathless CESI-MS experiments yielded promising results and indicated that the neutral derivatization of sialic acid bearing N-glycans enzymatically released from the SARS-CoV-2 spike protein was achievable. Additionally, these preliminary experiments indicate that the method was capable of capturing differences in the degree of sialylation induced by varying culture conditions.

Chapter 7: Concluding Remarks

Protein N-glycosylation is a complex and dynamic post-translational modification that plays major roles in many biological processes. N-glycan complexity is highly dependent on the expression system and can be influenced by many environmental factors including temperature, pH, dissolved oxygen, and ammonia concentration. Glycosylation of biotherapeutics including mAbs has implications on product stability, safety and efficacy, and therefore is a tightly controlled critical quality attribute. However, due to knowledge gaps and assay limitations not all biologic products implement the same level of control, such as influenza vaccines. Currently, the majority of manufactured influenza vaccines are egg-derived IIVs and, although well established, there are some limitations with the efficiency of their production methods. During manufacturing, egg-adaptive mutations can result in altered glycosylation characteristics of vaccine antigens and in recent years has been linked to low vaccine efficacy. There is increasing evidence suggesting not only site occupancy is important but also N-glycan subtype and complexity has immunogenicity implications. However, current IIV potency evaluation methods including the SRID are not sensitive to glycosylation and the lack of standardized assays for analyzing vaccine glycosylation pose problems with the quality control and regulation of these products. Therefore, methods that can accurately separate, assess and identify influenza vaccine N-glycan signatures during the manufacturing process are required.

Capillary zone electrophoresis with laser-induced fluorescence detection or coupled to high-resolution mass spectrometry are promising and powerful techniques that may aid in bridging the gap. In this study, the implementation and modification of a magnetic bead-based N-glycan labeling and purification approach along with the development of a CZE-LIF enabled the qualitative profiling of enzymatically released N-glycans derived from influenza vaccines. The

method offered some unique advantages over traditional CGE-LIF methodologies making it an attractive and potential alternative for N-glycan profiling in high throughput settings such as vaccine manufacturing. Glycan identification via CZE-LIF is challenging and therefore was addressed using a sheathless CESI-MS method that demonstrated acceptable repeatability using a filter-aided sample preparation approach for mass confirmation and structural determination. Separation performance and subsequent MS/MS spectral quality was enhanced through the sample preparation and IDA switch criteria optimization, which increased the structural elucidation accuracy of low abundance N-glycan species. The sheathless CESI-MS method was particularly suitable for the analysis of neutral egg-derived IIV N-glycans however could not be applied for the analysis of negatively charged N-glycans. Influenza vaccine antigens produced using various expression systems as well as recombinant DNA technology are alternative strategies becoming increasing popular. However, recombinant HA poses additional analytical challenges, as the lack of viral sialidases will result in N-glycans with retained sialic acid residues. Therefore, in order to broaden the applicability of the method, a dual-hydrazide labeling strategy was developed, which enabled the derivatization and analysis of sialic acid bearing N-glycans via sheathless CESI-MS. Both methods were used for the assessment of enzymatically released N-glycan profiles of three manufacturers egg-derived influenza vaccine monovalent bulks. Twenty-five N-glycan structures were identified via sheathless CESI-MS/MS and were in accordance with current literature on egg-based vaccine N-glycosylation.

Influenza continues to be a major threat to public health and vaccination is the most effective strategy against IFVs. However, in addition to egg-adaptive mutation susceptibility and associated allergies, rapid production and ability to adapt to circulating strains using the traditional egg-based vaccine-manufacturing platform is hindered by current potency evaluation method

timelines. Therefore, there is consistent pressure to transition to alternative means of production including other expression systems, recombinant DNA technology, and recently mRNA technology, which allows for large-scale rapid production of efficient vaccines. There is a clear link between influenza vaccine N-glycosylation and immunogenicity; therefore, there is a need for alternative potency evaluation strategies that are not only sensitive to glycosylation but also are not limited by reagent and reference material production timelines. The preliminary results obtained in this study are encouraging and with further optimization and validation, the implementation of capillary electrophoresis-based methods during in-process manufacturing and at the Drug Substance and Drug Product stage can help address current regulatory challenges and knowledge-gaps surrounding influenza vaccine N-glycosylation, ensuring the production of efficient and quality prophylactic measures against influenza.

References

[1] A. Mummert, E. Esche, J. Robinson and G. J. Armelagos, *Econ Hum Biol* **2011**, *9*, 284-301.

[2] J. M. Pearce-Duvet, *Biol Rev Camb Philos Soc* **2006**, *81*, 369-382.

[3] A. P. Dobson and E. R. Carper, *BioScience* **1996**, *46*, 115-126.

[4] W. N. Harrington, C. M. Kackos and R. J. Webby, *Exp Mol Med* **2021**, *53*, 737-749.

[5] A. D. Iuliano, K. M. Roguski, H. H. Chang, D. J. Muscatello, R. Palekar, S. Tempia, C. Cohen, J. M. Gran, D. Schanzer, B. J. Cowling, P. Wu, J. Kyncl, L. W. Ang, M. Park, M. Redlberger-Fritz, H. Yu, L. Espenhain, A. Krishnan, G. Emukule, L. van Asten, S. Pereira da Silva, S. Aungkulanon, U. Buchholz, M.-A. Widdowson, J. S. Bresee, E. Azziz-Baumgartner, P.-Y. Cheng, F. Dawood, I. Foppa, S. Olsen, M. Haber, C. Jeffers, C. R. MacIntyre, A. T. Newall, J. G. Wood, M. Kundi, T. Popow-Kraupp, M. Ahmed, M. Rahman, F. Marinho, C. V. Sotomayor Proschle, N. Vergara Mallegas, F. Luzhao, L. Sa, J. Barbosa-Ramírez, D. M. Sanchez, L. A. Gomez, X. B. Vargas, a. Acosta Herrera, M. J. Llanés, T. K. Fischer, T. G. Krause, K. Mølbak, J. Nielsen, R. Trebbien, A. Bruno, J. Ojeda, H. Ramos, M. an der Heiden, L. del Carmen Castillo Signor, C. E. Serrano, R. Bhardwaj, M. Chadha, V. Narayan, S. Kosen, M. Bromberg, A. Glatman-Freedman, Z. Kaufman, Y. Arima, K. Oishi, S. Chaves, B. Nyawanda, R. A. Al-Jarallah, P. A. Kuri-Morales, C. R. Matus, M. E. J. Corona, A. Burmaa, O. Darmaa, M. Obtel, I. Cherkaoui, C. C. van den Wijngaard, W. van der Hoek, M. Baker, D. Bandaranayake, A. Bissielo, S. Huang, L. Lopez, C. Newbern, E. Flem, G. M. Grøneng, S. Hauge, F. G. de Cosío, Y. de Moltó, L. M. Castillo, M. A. Cabello, M. von Horoch, J. Medina Osis, A. Machado, B. Nunes, A. P. Rodrigues, E. Rodrigues, C. Calomfirescu, E. Lupulescu, R. Popescu, O. Popovici, D. Bogdanovic, M. Kostic, K. Lazarevic, Z. Milosevic, B. Tiodorovic, M. Chen, J. Cutter, V. Lee, R. Lin, S. Ma, A. L. Cohen, F. Treurnicht, W. J. Kim, C. Delgado-Sanz, S. de mateo Ontañón, A. Larrauri, I. L. León, F. Vallejo, R. Born,

C. Junker, D. Koch, J.-H. Chuang, W.-T. Huang, H.-W. Kuo, Y.-C. Tsai, K. Bundhamcharoen, M. Chittaganpitch, H. K. Green, R. Pebody, N. Goñi, H. Chiparelli, L. Brammer and D. Mustaquim, *The Lancet* **2018**, *391*, 1285-1300.

[6] J. Paget, P. Spreeuwenberg, V. Charu, R. J. Taylor, A. D. Iuliano, J. Bresee, L. Simonsen, C. Viboud, N. Global Seasonal Influenza-associated Mortality Collaborator and G. L. C. Teams*, *J Glob Health* **2019**, *9*, 020421.

[7] W. Putri, D. J. Muscatello, M. S. Stockwell and A. T. Newall, *Vaccine* **2018**, *36*, 3960-3966.

[8] N. A. Molinari, I. R. Ortega-Sanchez, M. L. Messonnier, W. W. Thompson, P. M. Wortley, E. Weintraub and C. B. Bridges, *Vaccine* **2007**, *25*, 5086-5096.

[9] U. Arbeitskreis Blut, *Transfus Med Hemother* **2009**, *36*, 32-39.

[10] C. Peteranderl, S. Herold and C. Schmoldt, *Semin Respir Crit Care Med* **2016**, *37*, 487-500.

[11] N. M. Bouvier and P. Palese, *Vaccine* **2008**, *26*, 49-53.

[12] J. Chen, J. Wang, J. Zhang and H. Ly, *Front Immunol* **2021**, *12*, 711997.

[13] D. Dou, R. Revol, H. Ostbye, H. Wang and R. Daniels, *Front Immunol* **2018**, *9*, 1581.

[14] C. M. Mair, K. Ludwig, A. Herrmann and C. Sieben, *Biochim Biophys Acta* **2014**, *1838*, 1153-1168.

[15] I. Kass and I. T. Arkin, *Structure* **2005**, *13*, 1789-1798.

[16] J. L. McAuley, B. P. Gilbertson, S. Trifkovic, L. E. Brown and J. L. McKimm-Breschkin, *Front Microbiol* **2019**, *10*, 39.

[17] S. Herold, C. Becker, K. M. Ridge and G. R. Budinger, *Eur Respir J* **2015**, *45*, 1463-1478.

[18] N. Sriwilaijaroen and Y. Suzuki, *Proc Jpn Acad Ser B Phys Biol Sci* **2012**, *88*, 226-249.

[19] D. J. Benton, A. Nans, L. J. Calder, J. Turner, U. Neu, Y. P. Lin, E. Ketelaars, N. L. Kallewaard, D. Corti, A. Lanzavecchia, S. J. Gamblin, P. B. Rosenthal and J. J. Skehel, *Proc Natl Acad Sci U S A* **2018**, *115*, 10112-10117.

[20] M. Lazniewski, W. K. Dawson, T. Szczepinska and D. Plewczynski, *Brief Funct Genomics* **2018**, *17*, 415-427.

[21] N. C. Wu and I. A. Wilson, *Viruses* **2020**, *12*.

[22] J. L. McAuley, L. Corcilius, H. X. Tan, R. J. Payne, M. A. McGuckin and L. E. Brown, *Mucosal Immunol* **2017**, *10*, 1581-1593.

[23] A. Gaymard, N. Le Briand, E. Frobert, B. Lina and V. Escuret, *Clin Microbiol Infect* **2016**, *22*, 975-983.

[24] Y. A.Shtyrya, L. V. Mochalova and N. V. Bovin, *Acta Naturae* **2009**, *1*, 26-32.

[25] Q. Zhuang, S. Wang, S. Liu, G. Hou, J. Li, W. Jiang, K. Wang, C. Peng, D. Liu, A. Guo and J. Chen, *Virol J* **2019**, *16*, 85.

[26] Centers for Disease Control and Prevention in *Types of Influenza Viruses*, *Vol.* **2021**.

[27] V. N. Petrova and C. A. Russell, *Nat Rev Microbiol* **2018**, *16*, 47-60.

[28] N. Lei, H. B. Wang, Y. S. Zhang, J. H. Zhao, Y. Zhong, Y. J. Wang, L. Y. Huang, J. X. Ma, Q. Sun, L. Yang, Y. L. Shu, S. M. Li and L. L. Sun, *Sci Rep* **2019**, *9*, 2432.

[29] J. D. Allen and T. M. Ross, *Hum Vaccin Immunother* **2018**, *14*, 1840-1847.

[30] C. Biondo, G. Lentini, C. Beninati and G. Teti, *Biomed J* **2019**, *42*, 8-18.

[31] X. Chen, S. Liu, M. U. Goraya, M. Maarouf, S. Huang and J. L. Chen, *Front Immunol* **2018**, *9*, 320.

[32] L. Somerville, A. Cardani and T. J. Braciale, *Infect Dis Ther (San Antonio)* **2020**, *1*.

[33] J. Waithman and J. D. Mintern, *Virulence* **2012**, *3*, 603-608.

[34] M. M. Hufford, T. S. Kim, J. Sun and T. J. Braciale, *Curr Top Microbiol Immunol* **2015**, *386*, 423-455.

[35] F. Krammer, *Nat Rev Immunol* **2019**, *19*, 383-397.

[36] B. P. Blackburne, A. J. Hay and R. A. Goldstein, *PLoS Pathog* **2008**, *4*, e1000058.

[37] J. Fierer, D. Looney, M. Kok and J.-C. Pechère in *Nature and pathogenicity of micro-organisms*, **2010**, pp. 3-29.

[38] J. L. Myers, K. S. Wetzel, S. L. Linderman, Y. Li, C. B. Sullivan and S. E. Hensley, *J Virol* **2013**, *87*, 11168-11172.

[39] R. G. Webster and E. A. Govorkova, *Ann N Y Acad Sci* **2014**, *1323*, 115-139.

[40] S. Rockman, K. L. Laurie, S. Parkes, A. Wheatley and I. G. Barr, *Microorganisms* **2020**, *8*.

[41] Y. H. Kim, K. J. Hong, H. Kim and J. H. Nam, *Rev Med Virol* **2022**, *32*, e2243.

[42] A. Sabbaghi, S. M. Miri, M. Keshavarz, M. Zargar and A. Ghaemi, *Rev Med Virol* **2019**, *29*, e2074.

[43] L. Besnard, V. Fabre, M. Fettig, E. Gousseinov, Y. Kawakami, N. Laroudie, C. Scanlan and P. Pattnaik, *Biotechnol Adv* **2016**, *34*, 1-13.

[44] T. C. Kon, A. Onu, L. Berbecila, E. Lupulescu, A. Ghiorgisor, G. F. Kersten, Y. Q. Cui, J. P. Amorij and L. Van der Pol, *PLoS One* **2016**, *11*, e0150700.

[45] K. Subbarao, *Cold Spring Harb Perspect Med* **2021**, *11*.

[46] H. S. Izurieta, P. Haber, R. P. Wise, J. Iskander, D. Pratt, C. Mink, S. Chang, M. Braun and R. Ball, *Journal of the American Medical Association* **2005**, *294*, 2720-2725.

[47] World-Health-Organization in *WHO Information Meeting on the Composition of Influenza Virus Vaccines for Use in the 2022-2023 Northern Hemisphere Influenza Season*, *Vol. 2022* **2022**.

[48] Health-Canada in *Guidance Document: Annual update of seasonal influenza vaccines*, *Vol.* (Ed. H. Canada), **2016**.

[49] J. M. Wood, G. C. Schild, R. W. Newman and V. Seagroatt, *Journal of Biological Standardization* **1977**, *5*, 237-247.

[50] P. D. Minor, *Vaccines (Basel)* **2015**, *3*, 90-104.

[51] J. M. Wood and J. P. Weir, *Influenza Other Respir Viruses* **2018**, *12*, 195-201.

[52] B. Lorbetskie, A. M. Cunningham, M. Lemieux, L. Durno, A. Farnsworth, J. Wang, C. Li, X. Li, M. Gilbert, S. Sauve and M. Girard, *Anal Chem* **2019**, *91*, 8908-8917.

[53] Y. Wen, G. Palladino, Y. Xie, A. Ferrari and E. C. Settembre, *Vaccine* **2018**, *36*, 3010-3017.

[54] N. B. Ustinov, E. G. Zavyalova, I. G. Smirnova and A. M. Kopylov, *Biochemistry (Mosc)* **2017**, *82*, 1234-1248.

[55] Y. An, L. M. Parsons, E. Jankowska, D. Melnyk, M. Joshi and J. F. Cipollo, *Journal of Virology* **2019**, *93*.

[56] S. Ramazi and J. Zahiri, *Database (Oxford)* **2021**, *2021*.

[57] R. Wada, M. Matsui and N. Kawasaki, *MAbs* **2019**, *11*, 350-372.

[58] J. Zaia, *Chem Biol* **2008**, *15*, 881-892.

[59] A. Varki, *Glycobiology* **2017**, *27*, 3-49.

[60] A. Varki and J. B. Lowe, *Essentials of Glycobiology* **2009**, 75-88

[61] J. K. Liu, *Ann Med Surg (Lond)* **2014**, *3*, 113-116.

[62] S. L. Smith, *Journal of Transplant Coordination* **1996**, *6*, 109-119.

[63] S. Boune, P. Hu, A. L. Epstein and L. A. Khawli, *Antibodies (Basel)* **2020**, *9*.

[64] F. Cymer, H. Beck, A. Rohde and D. Reusch, *Biologicals* **2018**, *52*, 1-11.

[65] R. J. Keizer, A. D. R. Huitema, J. H. M. Schellens and J. H. Beijnen, *Clinical Pharmacokinetics* **2010**, *49*, 493-507.

[66] M. Yang and M. Butler, *Biotechnology and bioengineering* **2000**, *68*, 370-380.

[67] D. J. Falconer, G. P. Subedi, A. M. Marcella and A. W. Barb, *ACS Chem Biol* **2018**, *13*, 2179-2189.

[68] J. Hodoniczky, Y. Z. Zheng and D. C. James, *Biotechnology Progress* **2005**, *21*, 1644-1652.

[69] T. S. Raju, *Curr Opin Immunol* **2008**, *20*, 471-478.

[70] M. Bas, A. Terrier, E. Jacque, A. Dehenne, V. Pochet-Beghin, C. Beghin, A. S. Dezetter, G. Dupont, A. Engrand, B. Beaufils, P. Mondon, N. Fournier, C. de Romeuf, S. Jorieux, A. Fontayne, L. T. Mars and C. Monnet, *J Immunol* **2019**, *202*, 1582-1594.

[71] D. Reusch and M. L. Tejada, *Glycobiology* **2015**, *25*, 1325-1334.

[72] A. Zhu and R. Hurst, *Xenotransplantation* **2002**, *9*, 376-381.

[73] P. C. Roberts, W. Garten and H. Klenk, *Virology* **1993**, *67*, 3048-3060.

[74] Y. Yin, X. Zhang, Y. Qiao, X. Wang, Y. Su, S. Chen, T. Qin, D. Peng and X. Liu, *Vet Res* **2017**, *48*, 81.

[75] M. de Graaf and R. A. Fouchier, *EMBO J* **2014**, *33*, 823-841.

[76] M. Ohuchi, R. Ohuchi, A. Feldmann and H. Klenk, *Virology* **1997**, *71*, 8377-8384.

[77] F. X. Bosch, W. Garten, H. Klenk and R. Rott, *Virology* **1981**, *113*, 725-735.

[78] A. K. Maciola, M. A. Pietrzak, P. Kosson, M. Czarnocki-Cieciura, K. Smietanka, Z. Minta and E. Kopera, *Front Immunol* **2017**, *8*, 444.

[79] Y. Kobayashi and Y. Suzuki, *J Virol* **2012**, *86*, 3446-3451.

[80] M. D. Tate, E. R. Job, Y. M. Deng, V. Gunalan, S. Maurer-Stroh and P. C. Reading, *Viruses* **2014**, *6*, 1294-1316.

[81] M. T. Osterholm, N. S. Kelley, A. Sommer and E. A. Belongia, *The Lancet Infectious Diseases* **2012**, *12*, 36-44.

[82] S. J. Zost, K. Parkhouse, M. E. Gumina, K. Kim, S. Diaz Perez, P. C. Wilson, J. J. Treanor, A. J. Sant, S. Cobey and S. E. Hensley, *Proc Natl Acad Sci U S A* **2017**, *114*, 12578-12583.

[83] N. C. Wu, S. J. Zost, A. J. Thompson, D. Oyen, C. M. Nycholat, R. McBride, J. C. Paulson, S. E. Hensley and I. A. Wilson, *PLoS Pathog* **2017**, *13*, e1006682.

[84] D. M. Skowronski, N. Z. Janjua, G. De Serres, S. Sabaiduc, A. Eshaghi, J. A. Dickinson, K. Fonseca, A. L. Winter, J. B. Gubbay, M. Krajden, M. Petric, H. Charest, N. Bastien, T. L. Kwindt, S. M. Mahmud, P. Van Caeseele and Y. Li, *PLoS One* **2014**, *9*, e92153.

[85] A. B. Arunachalam, P. Post and D. Rudin, *NPJ Vaccines* **2021**, *6*, 144.

[86] J. R. Chen, Y. H. Yu, Y. C. Tseng, W. L. Chiang, M. F. Chiang, Y. A. Ko, Y. K. Chiu, H. H. Ma, C. Y. Wu, J. T. Jan, K. I. Lin, C. Ma and C. H. Wong, *Proc Natl Acad Sci U S A* **2014**, *111*, 2476-2481.

[87] Y. C. Tseng, C. Y. Wu, M. L. Liu, T. H. Chen, W. L. Chiang, Y. H. Yu, J. T. Jan, K. I. Lin, C. H. Wong and C. Ma, *Proc Natl Acad Sci U S A* **2019**, *116*, 4200-4205.

[88] J. R. Chen, Y. M. Liu, Y. C. Tseng and C. Ma, *J Biomed Sci* **2020**, *27*, 33.

[89] R. P. de Vries, C. H. Smit, E. de Bruin, A. Rigter, E. de Vries, L. A. Cornelissen, D. Eggink, N. P. Chung, J. P. Moore, R. W. Sanders, C. H. Hokke, M. Koopmans, P. J. Rottier and C. A. de Haan, *J Virol* **2012**, *86*, 11735-11744.

[90] S. C. Lin, J. T. Jan, B. Dionne, M. Butler, M. H. Huang, C. Y. Wu, C. H. Wong and S. C. Wu, *PLoS One* **2013**, *8*, e66719.

[91] C.-C. Wang, J.-R. Chen, Y.-C. Tseng, C.-H. Hsu, Y.-F. Hung, S.-W. Chen, C.-M. Chen, K.-H. Khoo, T.-J. Cheng, Y.-S. E. Cheng, J.-T. Jan, C.-Y. Wu, C. Ma and C.-H. Wong, *PNAS* **2009**, *106*, 18137-18142.

[92] S. Chun, C. Li, G. Van Domselaar, J. Wang, A. Farnsworth, X. Cui, H. Rode, T. D. Cyr, R. He and X. Li, *Vaccine* **2008**, *26*, 6068-6076.

[93] L. R. Kuck, R. Byrne-Nash, J. Gillis, K. Bueter, L. K. Couzens, M. C. Eichelberger and K. L. Rowlen, *Vaccine* **2018**, *36*, 2937-2945.

[94] L. R. Kuck, M. Sorensen, E. Matthews, I. Srivastava, M. M. Cox and K. L. Rowlen, *PLoS One* **2014**, *9*, e109616.

[95] B. Lorbetskie, J. Wang, C. Gravel, C. Allen, M. Walsh, A. Rinfret, X. Li and M. Girard, *Vaccine* **2011**, *29*, 3377-3389.

[96] B. Lorbetskie, N. Fortin, L. Durno, J. Wang, C. Li, X. Li, M. Girard and S. Sauve, *J Chromatogr A* **2017**, *1528*, 18-24.

[97] S. Hu and D. T. Wong, *Proteomics Clin Appl* **2009**, *3*, 148-154.

[98] M. Melmer, T. Stangler, M. Schiefermeier, W. Brunner, H. Toll, A. Rupprechter, W. Lindner and A. Premstaller, *Anal Bioanal Chem* **2010**, *398*, 905-914.

[99] C. T. Yuen, C. K. Gee and C. Jones, *Biomed Chromatogr* **2002**, *16*, 247-254.

[100] J. S. Rohrer, L. Basumallick and D. C. Hurum, *Glycobiology* **2016**, *26*, 582-591.

[101] X. Sun, L. Tao, L. Yi, Y. Ouyang, N. Xu, D. Li, R. J. Linhardt and Z. Zhang, *J Pharm Anal* **2017**, *7*, 87-94.

[102] L. R. Ruhaak, G. Zauner, C. Huhn, C. Bruggink, A. M. Deelder and M. Wuhrer, *Anal Bioanal Chem* **2010**, *397*, 3457-3481.

[103] N. J. Adamson and E. C. Reynolds, *Journal of Chromatography B* **1997**, *699*, 133-147.

[104] D. Corradini and L. Sprecacenere, *Chromatographia* **2003**, *58*, 587-596.

[105] G. d. Jong, *Detection in Capillary Electrophoresis - An Introduction*, **2016**, p. 368.

[106] D. M. Osbourn, D. J. Weiss and C. E. Lunte, *Electrophoresis* **2000**, *21*, 2768-2779.

[107] G. Lu, C. L. Crihfield, S. Gattu, L. M. Veltri and L. A. Holland, *Chem Rev* **2018**, *118*, 7867-7885.

[108] D. M. Goltz, S. Ahmadi, G. Absalan and D. B. Craig, *Journal of Liquid Chromatography & Related Technologies* **2012**, *35*, 2054-2065.

[109] N. G. S. Mogollon, C. D. Quiroz-Moreno, P. S. Prata, J. R. de Almeida, A. S. Cevallos, R. Torres-Guierrez and F. Augusto, *J Anal Methods Chem* **2018**, *2018*, 4142527.

[110] A. Macklin, S. Khan and T. Kislinger, *Clin Proteomics* **2020**, *17*, 17.

[111] K. F. Geoghegan and M. A. Kelly, *Mass Spectrom Rev* **2005**, *24*, 347-366.

[112] Y. Wang, J. Sun, J. Qiao, J. Ouyang and N. Na, *Anal Chem* **2018**, *90*, 14095-14099.

[113] S. Banerjee and S. Mazumdar, *Int J Anal Chem* **2012**, *2012*, 282574.

[114] C. Ho, C. Lam, M. Chan, R. Cheung, L. Law, L. Lit, K. Ng, M. Suen and H. Tai, *Clin Biochem Rev* **2003**, *24*.

[115] U. Boesl, *Mass Spectrom Rev* **2017**, *36*, 86-109.

[116] D. C. Harris, *Quantitative Chemical Analysis*, **2010**, p.

[117] R. Liu, Q. Li and L. M. Smith, *J Am Soc Mass Spectrom* **2014**, *25*, 1374-1383.

[118] O. B. Chassela, A. Grigoriev, A. Fedorov, N. André, E. Le Comte and J. Rouzaud, *CEAS Space Journal* **2019**, *11*, 597-605.

[119] H. Javaheri and B. B. Schneider, *J Am Soc Mass Spectrom* **2021**, *32*, 1945-1951.

[120] G. L. Andrews, B. L. Simons, J. B. Young, A. M. Hawkridge and D. C. Muddiman, *Anal Chem* **2011**, *83*, 5442-5446.

[121] D. N. Tabang, M. Ford and L. Li, *Front Chem* **2021**, *9*, 707387.

[122] H. Liu, N. Zhang, D. Wan, M. Cui, Z. Liu and S. Liu, *Clinical Proteomics* **2014**, *11*.

[123] M. Manea, G. Mezo, F. Hudecz and M. Przybylski, *J Pept Sci* **2007**, *13*, 227-236.

[124] G. Zhang, R. S. Annan, S. A. Carr and T. A. Neubert, *Curr Protoc Protein Sci* **2010**, *Chapter 16*, Unit16 11.

[125] T. Nishikaze, *Mass Spectrom (Tokyo)* **2017**, *6*, A0060.

[126] Y. Zhang, B. Wang, W. Jin, Y. Wen, L. Nan, M. Yang, R. Liu, Y. Zhu, C. Wang, L. Huang, X. Song and Z. Wang, *Anal Chim Acta* **2019**, *1048*, 105-114.

[127] Z. Zhang, J. Kuang and L. Li, *Analyst* **2013**, *138*, 6600-6606.

[128] S. Zhou, L. Veillon, X. Dong, Y. Huang and Y. Mechref, *Analyst* **2017**, *142*, 4446-4455.

[129] D. J. Harvey, W. B. Struwe, A. J. Behrens, S. Vasiljevic and M. Crispin, *Anal Bioanal Chem* **2021**, *413*, 7277-7294.

[130] J. A. Olivares, N. T. Nguyen, C. R. Yonker and R. D. Smith, *Analytical Chemical* **1987**, *59*, 1230-1232.

[131] P. M., B. S. C. and N. C., *Electrophoresis* **2012**, *33*, 1517-1530.

[132] C. Cruces-Blanco and A. M. García-Campaña, *TrAC Trends in Analytical Chemistry* **2012**, *31*, 85-95.

[133] R. Ramautar, G. W. Somsen and G. J. de Jong, *Electrophoresis* **2009**, *30*, 276-291.

[134] M. Moini, *Analytical Chemistry* **2007**, *79*, 4241-4246.

[135] R. Hennig, E. Rapp, R. Kottler, S. Cajic, M. Borowiak and U. Reichl, *Methods Mol Biol* **2015**, *1331*, 123-143.

[136] J. Hutter, J. V. Rodig, D. Hoper, P. H. Seeberger, U. Reichl, E. Rapp and B. Lepenies, *J Immunol* **2013**, *190*, 220-230.

[137] J. V. Roedig, E. Rapp, Y. Genzel and U. Reichl, *BMC Proceedings* **2011**, *5*, 113.

[138] J. V. Roedig, E. Rapp, D. Hoper, Y. Genzel and U. Reichl, *PLoS One* **2011**, *6*, e27989.

[139] J. Schwarzer, E. Rapp and U. Reichl, *Electrophoresis* **2008**, *29*, 4203-4214.

[140] H. Ahmadzadeh in *Instrumentation, capillary coating, and labeling chemistry for capillary electrophoresis with laser-induced fluorescence detection*, *Vol. Ph.D.* University of Alberta, **2000**, p. 474.

[141] N. Callewaert, S. Geysens, F. Molemans and R. Contreras, *Glycobiology* **2001**, *11*, 275-281.

[142] A. A. Chu, A. E. Saati, J. J. Scarcelli, R. J. Cornell and T. J. Porter, *Anal Biochem* **2018**, *546*, 23-27.

[143] G. Lu and L. A. Holland, *Anal Chem* **2019**, *91*, 1375-1383.

[144] S. Berensmeier, *Appl Microbiol Biotechnol* **2006**, *73*, 495-504.

[145] C. Varadi, C. Lew and A. Guttman, *Anal Chem* **2014**, *86*, 5682-5687.

[146] P. Kotidis and C. Kontoravdi, *Metab Eng Commun* **2020**, *10*, e00131.

[147] L. Xie, E. Zhang, Y. Xu, W. Gao, L. Wang, M. H. Xie, P. Qin, L. Lu, S. Li, P. Shen, W. Jiang and S. Liu, *BioDrugs* **2020**, *34*, 363-379.

[148] J. C. Reijenga, T. P. E. M. Verheggen, J. H. P. A. Martens and F. M. Everaerts, *Journal of Chromatography A* **1996**, *744*, 147-153.

[149] Y. Liu, O. Salas-Solano and L. A. Gennaro, *Analytical Chemistry* **2009**, *81*, 6823-6829.

[150] R. Haselberg, G. J. de Jong and G. W. Somsen, *Anal Chem* **2013**, *85*, 2289-2296.

[151] C. M. Snyder, X. Zhou, J. A. Karty, B. R. Fonslow, M. V. Novotny and S. C. Jacobson, *J Chromatogr A* **2017**, *1523*, 127-139.

[152] Y. Tian, L. M. Parsons, E. Jankowska and J. F. Cipollo, *Front Chem* **2021**, *9*, 767448.

[153] Y. Watanabe, J. D. Allen, D. Wrapp, J. S. McLellan and M. Crispin, *Science* **2020**, *369*, 330-333.

[154] J. Gobin, G. Muradia, J. Mehic, C. Westwood, L. Couvrette, A. Stalker, S. Bigelow, C. C. Luebbert, F. S. Bissonnette, M. J. W. Johnston, S. Sauve, R. Y. Tam, L. Wang, M. Rosu-Myles and J. R. Lavoie, *Stem Cell Res Ther* **2021**, *12*, 127.

[155] Z. Szabo, A. Guttman, T. Rejtar and B. L. Karger, *Electrophoresis* **2010**, *31*, 1389-1395.

[156] D. J. Harvey, *Mass Spectrom Rev* **2020**, *39*, 586-679.

[157] G. S. M. Lageveen-Kammeijer, N. de Haan, P. Mohaupt, S. Wagt, M. Filius, J. Nouta, D. Falck and M. Wuhrer, *Nat Commun* **2019**, *10*, 2137.

[158] J. Krenkova, F. Dusa and R. Cmelik, *Electrophoresis* **2020**, *41*, 684-690.

[159] R. L. Valk-Weeber, L. Dijkhuizen and S. S. van Leeuwen, *Carbohydr Res* **2019**, *479*, 13-22.

[160] S. Abdul Rahman, E. Bergstrom, C. J. Watson, K. M. Wilson, D. A. Ashford, J. R. Thomas, D. Ungar and J. E. Thomas-Oates, *J Proteome Res* **2014**, *13*, 1167-1176.

[161] G. C. Gil, B. Iliff, R. Cerny, W. H. Velander and K. E. Van Cott, *Anal Chem* **2010**, *82*, 6613-6620.

[162] E. S. Hecht, J. P. McCord and D. C. Muddiman, *J Vis Exp* **2016**.

[163] N. R. Novotny, E. N. Capley and A. C. Stenson, *J Mass Spectrom* **2014**, *49*, 316-326.

[164] M. Stefansson, P. J. R. Sjöberg and K. E. Markides, *Analytical Chemistry* **1996**, *68*, 1792-1797.

[165] P. Tuma, M. Bursova, B. Sommerova, R. Horsley, R. Cabala and T. Hlozek, *J Pharm Biomed Anal* **2018**, *160*, 368-373.

[166] J. Li, Y. Bi, L. Wang, F. Sun, Z. Chen, G. Xu and G. Fan, *J Pharm Biomed Anal* **2012**, *66*, 218-224.

[167] J. Sun, J. Feng, L. Shi, L. Liu, H. He, Y. Fan, S. Hu and S. Liu, *J Chromatogr A* **2016**, *1461*, 161-170.

[168] A. S. John, M. M. Sidek, L. Y. Thang, S. Sami, H. Y. Tey and H. H. See, *J Chromatogr A* **2021**, *1638*, 461868.

[169] A. Kruve and K. Kaupmees, *J Am Soc Mass Spectrom* **2017**, *28*, 887-894.

[170] N. C. Wu, H. Lv, A. J. Thompson, D. C. Wu, W. W. S. Ng, R. U. Kadam, C. W. Lin, C. M. Nycholat, R. McBride, W. Liang, J. C. Paulson, C. K. P. Mok and I. A. Wilson, *Cell Host Microbe* **2019**, *25*, 836-844 e835.

[171] A. J. Thompson, L. Cao, Y. Ma, X. Wang, J. K. Diedrich, C. Kikuchi, S. Willis, C. Worth, R. McBride, J. R. Yates, 3rd and J. C. Paulson, *Cell Host Microbe* **2020**, *27*, 725-735 e725.

[172] L. Han and C. E. Costello, *Biochemistry (Mosc)* **2013**, *78*, 710-720.

[173] Y. Wang, M. Santos and A. Guttman, *J Sep Sci* **2013**, *36*, 2862-2867.

[174] T. Nishikaze, *Proc Jpn Acad Ser B Phys Biol Sci* **2019**, *95*, 523-537.

[175] H. Hanamatsu, T. Nishikaze, N. Miura, J. Piao, K. Okada, S. Sekiya, S. Iwamoto, N. Sakamoto, K. Tanaka and J. I. Furukawa, *Anal Chem* **2018**, *90*, 13193-13199.

[176] K. R. Reiding, D. Blank, D. M. Kuijper, A. M. Deelder and M. Wuhrer, *Anal Chem* **2014**, *86*, 5784-5793.

[177] M. Toyoda, H. Ito, Y.-k. Matsuno, H. Narimatsu and A. Kameyama, *Analytical Chemistry* **2008**, *80*, 5211-5218.

[178] A. M. Lewis, W. D. Croughan, N. Aranibar, A. G. Lee, B. Warrack, N. R. Abu-Absi, R. Patel, B. Drew, M. C. Borys, M. D. Reily and Z. J. Li, *PLoS One* **2016**, *11*, e0157111.